Nanoscale

REVIEW

View Article Online
View Journal | View Issue

Cite this: *Nanoscale*, 2025, **17**, 4854

Bioactive surface-functionalized MXenes for biomedicine

Ting Li,[a] Weipeng Qiang[a] and Bo Lei *[a,b,c]

Received 15th October 2024,
Accepted 22nd December 2024

DOI: 10.1039/d4nr04260c

rsc.li/nanoscale

MXenes, with their good biocompatibility, excellent photovoltaic properties, excellent physicochemical properties, and desirable bioactivity, have broad application prospects in the field of tissue regeneration. MXenes have been used in a wide range of applications including biosensing, bioimaging, tumour/infection therapy, bone regeneration and wound repair. By applying bioactive materials to modify the surface of MXenes, a series of multifunctional MXene-based nanomaterials can be designed for different biomedical applications to achieve better therapeutic effects or more desirable biological functions. This paper reviews the existing studies on MXene-based bioactivities, surface modification strategies and biomedical applications. Finally, the challenges, trends and prospects of MXene nanomaterials are discussed. We expect that more and more well-designed MXene-based biomaterials will have a wider range of biomedical applications, thus providing favourable information for the clinical translation of nanomedicine.

1. Introduction

The rapid development of tissue engineering and regenerative medicine has placed higher demands on nanomaterials, requiring nanoparticles with excellent cytocompatibility, mechanical, electrical, optical and magnetic properties.[1] Two-dimensional (2D) nanomaterials are a new class of nanomaterials with sheet-like structures with lateral dimensions greater than 100 nm and thicknesses typically less than 5 nm.[2] With the vigorous development of nanoengineering materials and nanofabrication technology, various 2D nanomaterials such as graphene, graphene oxide, layered double hydroxide (LDH), and ultrathin black phosphorus (BP) nanosheets have emerged and have become a hot spot for research.[3–6] 2D nanomaterials are of interest in biomedical fields such as drug delivery, combination therapy, bioimaging, tissue engineering and biosensing due to their ultrathin structure, high specific surface area, unique optoelectronic properties and extraordinary mechanical properties.[3,7,8]

MXene is a novel multifunctional 2D lamellar material developed by Naguib *et al.*[9] It contains transition metal carbides, nitrides and carbon-nitrides with metallic conductivity and hydrophilicity, with the structural formula $M_{n+1}X_nT_x$ (M = transition metal, X = carbons or nitrides, T = terminal group (*e.g.* –O, –OH or –F)).[10] Compared with other 2D nanomaterials, MXenes' rich functional groups and high reactivity, excellent mechanical properties, electronic properties, electrical conductivity and hydrophilicity, antioxidant properties, and biological properties make them fascinatingly attractive in biomedical fields; they have broadband absorption and light-harvesting properties in the near-infrared (NIR) region, covering both the first and second NIR biological windows, as well as strong photothermal conversion capabilities, with great potential for photothermal therapy (PTT) and photoacoustic imaging (PA).[11,12] In addition, the high specific surface area of MXenes and the abundant functional groups on the surface can provide opportunities for surface modification of MXenes, which is very conducive to expanding the biological functions of MXenes.[13,14] So far, the cutting-edge research on MXene-based biomaterials with various attractive physicochemical properties and biological functions has attracted increasing attention from the nanomedical science community.[15,16]

In this review, we will firstly introduce the properties possessed by MXene-based biomaterials in the field of regenerative medicine, including biocompatibility, antioxidant, anti-inflammatory, optical, and antimicrobial properties, and tissue regeneration-promoting properties. Then, we will discuss the existing studies on the bioactive surface-modification strategies of MXenes, which are specifically classified into small molecules, macromolecules, nanoparticles, and surface polymerisation modification strategies. Afterwards, we will present the latest research advances in MXene-based biomaterials for applications in bioimaging, cancer therapy, infection treatment, wound repair, bone regeneration and other biomedical fields. Finally, we will summarise the challenges

[a]*Frontier Institute of Science and Technology, Xi'an Jiaotong University, Xi'an 710054, China. E-mail: rayboo@xjtu.edu.cn*
[b]*Department of Respiratory and Critical Care Medicine, The Second Affiliated Hospital of Xi'an Jiaotong University, Xi'an, 710004, China*
[c]*Department of Orthopedics, The First Affiliated Hospital of Xi'an Jiaotong University, Xi'an, P. R. 710061, China*

and future prospects related to MXene-based biomaterials in the biomedical field. Overall, by gaining a deeper understanding of the bioactivities, surface modification strategies, application potentials, and problematic challenges associated with 2D MXene nanosheets, we will be able to continue to facilitate clinical translation for the benefit of human health.

2. Bioactive properties for regenerative medicine

MXene-related biomaterials have the advantages of large specific surface area and abundant surface functional groups, as well as excellent electronic, optical, mechanical, and physicochemical properties, which give them considerable potential for a variety of biomedical applications. In this section, the properties exhibited by MXenes, such as biocompatibility, antioxidant, anti-inflammatory, photothermal, antimicrobial, and tissue regeneration-promoting properties, which are mainly applied in the fields of tissue repair, tumor therapy, bio-imaging, and drug delivery, will be described in detail.

2.1 Biocompatibility

Good biocompatibility is essential to ensure that MXenes can safely exert their therapeutic effects inside and on the surface of living organisms long term, so the biocompatibility of the designed MXene-based nanocomposites is crucial for their application in biomedical fields. Most MXenes exhibit concentration-dependent cytotoxicity, with good cytocompatibility at low concentrations and excessive concentrations leading to cytotoxic side effects. Our research team found that $Ti_3C_2T_x$ MXene exhibited good cytocompatibility with normal cells such as adipose stem cells (ADSC), mouse myoblasts (C2C12), mouse macrophages (RAW264.7), mouse fibroblasts (L929), and human umbilical venous endothelial cells (HUVECs), and maintained 90% of the cellular activity at a concentration of up to 200 μg mL^{-1}.[17,18] Interestingly, in a comparative *in vitro* cytotoxicity assay using MTT assay to investigate the *in vitro* cytotoxicity of layered $Ti_3C_2T_x$ MXene on two cancer cells (A549 and A375) and two normal cells (MRC-5 and HaCaT), MXenes were found to have a higher toxic effect on tumor cells than on normal cells.[19] This may be attributed to the fact that the production of reactive oxygen species (ROS) exceeds the threshold level of oxidative stress in cancer cells, leading to apoptosis. The cytotoxicity of MXenes is mainly related to two mechanisms: ROS generation and direct exposure.[20] The entry of MXenes into the cell results in the generation of ROS, which cause protein and DNA damage leading to cell death. Another mechanism of MXene toxicity is due to strong adhesion between MXenes and cell membranes, where MXenes and cell membranes interact directly through ionic interactions, hydrophobicity, van der Waals forces, and receptor–ligand binding, which leads to membrane instability and loss of cellular integrity. In addition, MXenes demonstrated superior blood compatibility of graphene oxide in whole-blood tests.[21] Current research advances suggest that MXenes exhibit a relatively favorable safety profile *in vivo*, with toxicity *in vivo* dependent on dose, treatment duration, and mode of administration. For example, in an *in vivo* study in which a mouse model was injected with 2 mg kg^{-1} of modified MXene (Ti_3C_2-DOX nanosheets), no liver or kidney damage, inflammatory response, or tissue necrosis was observed in experimental animal sections.[22] In a neurotoxicity and motility assay using a zebrafish embryo model, Ti_3C_2 was found to have almost negligible toxicological effects on muscle and neuronal activity in zebrafish embryos at a concentration of 50 μg mL^{-1}.[23] To further improve the biocompatibility and bioavailability of MXenes, researchers have modified the surface properties by coupling MXenes with biopolymers to reduce their toxicity. Studies have reported that modification of some biocompatible materials (*e.g.*, PEG, PLGA, PVP, chitosan, poly-L-lysine, sericin protein, polydopamine, *etc.*) on the surface of MXenes can effectively improve the biocompatibility of MXenes.[24] For example, after intravenous administration of 20 mg kg^{-1} of modified MXene (Nb_2C-PVP nanosheets) to 4T1 ruffled tumor-bearing mice, no significant weight loss or tissue damage was detected in any of the major organs, demonstrating that the Nb_2C-PVP nanosheets were safe and biocompatible at the doses tested *in vivo.*[11] However, there are limited studies on the toxicity of MXenes *in vivo*, very few of which involve animal models, and to date, toxicity studies of MXenes in human models and clinical trials remain unknown. MXene materials exhibit good biocompatibility in biomedical applications but need to be surface modified to reduce their toxicity to ensure their safety and efficacy.

2.2 Antioxidant property and biocatalysis

There exists an oxidative and antioxidant balance in biological organisms, but when subjected to adverse external stimuli this balance is disrupted in favor of an oxidative state, where excessive ROS are generated or accumulated within the organism, thereby exceeding the antioxidant capacity of the cells or tissues, resulting in a state of oxidative damage to biomolecules (*e.g.*, proteins, lipids, DNA, *etc.*), which may lead to a series of more serious diseases. Therefore, the antioxidant properties of biomaterials can add another highlight to their applications in biomedical fields. Currently, several studies have reported the excellent antioxidant capacity of MXenes, which exhibit superior antioxidant capacity than most artificial materials and natural compounds. For example, $Ti_3C_2T_x$ effectively scavenged $O_2^{\bullet-}$, $^{\bullet}OH$, 1,1-diphenyl-2-picrylhydrazyl radical ($DPPH^{\bullet}$) and 2,2′-azino-bis(3-ethylbenzothiazoline-6-sulfonic acid) radicals ($ABTS^{+}$).[25] Another study showed that $Ti_3C_2T_x$ effectively scavenged ROS in M1-type polarized macrophages.[17] For the treatment of oxidative stress-related diseases, researchers have proposed a therapeutic strategy of applying nano-enzymes (a new generation of man-made enzymes), which have the advantages of high catalytic activity, stability, cost-effectiveness, and ease of synthesis, *etc.*, and MXenes have also demonstrated their potential as nano-enzymes in a number of studies.[26] Feng *et al.* reported a two-dimensional

vanadium carbide (V_2C) MXene nano-enzyme (MXenzyme) that mimics up to six naturally occurring enzymes, including superoxide dismutase (SOD), catalase (CAT), peroxidase (POD), glutathione peroxidase (GPx), thiol peroxidase (TPx), and halogen peroxidase (HPO).[27] Based on these enzyme mimetic properties, the constructed V_2C MXenzyme was not only highly biocompatible but also effective in alleviating ROS-mediated inflammation and neurodegenerative diseases. In another study, it was reported that two-dimensional V_2C MXene could be used as a multi-enzyme mimetic for the treatment of ischemic stroke *in vivo*.[28] The antioxidant properties of MXenes are closely related to their unique structure, and the process of their function in the organism actually utilizes MXenes to catalyze the occurrence of redox reactions. The abundance of functional groups on the surface of MXenes, such as –F, –OH, –O, *etc*. not only increases their reactivity, but also the presence of these functional groups provides MXenes with an active site for interacting with biomolecules, which is essential for the initiation and conduct of catalytic reactions.[25] During biocatalysis, these functional groups can be used as intermediates of the reaction or be directly involved in the reaction, thus accelerating or modulating the reaction rate. The $M_{n+1}X_n$ layered structure in MXenes, which is formed by alternating weak van der Waals forces, gives them a unique advantage in biocatalysis.[25] This layered structure easily reacts with free radicals, similar to the interaction of the active center of an enzyme with a substrate, and can facilitate specific biochemical reactions. In biocatalysis, this structural property of MXenes can mimic the active site of enzymes in nature, thus effectively catalyzing specific biochemical reactions. In addition, MXene, as an electron-rich nanomaterial, can easily form pairs with electron-deficient free radicals, a property that is particularly important in biocatalysis. MXenes can react with free radicals through electron transfer, thus neutralizing the activity of free radicals and reducing the damage of biomolecules by oxidative stress. In summary, the biocatalytic mechanism of MXenes are closely related to their structural properties, which show great potential for mimicking enzyme activity, neutralizing free radicals and protecting biomolecules from oxidative damage in biocatalytic processes.

MXenes exhibit excellent antioxidant capacity and biocatalytic potential due to their unique structure and abundant functional groups, which can effectively neutralize free radicals and protect biomolecules from oxidative damage, providing a new strategy for the treatment of oxidative stress-related diseases.

2.3 Anti-inflammatory property

The excellent antioxidant properties of MXenes lays the foundation for their anti-inflammatory properties. Fewer studies have been reported on the performance of MXenes, mainly focusing on the $Ti_3C_2T_x$ type of MXene. Li *et al.* found that $Ti_3C_2T_x$ could down-regulate the expression of M1-type markers such as *IL-1β* and *TNF-α*, and further quantitative flow cytometry analysis showed that the MXene could effectively reduce the expression of CD86 protein, an M1-type macrophage marker.[17] Another study reported that MXene/HAP-coated surfaces with micro-fold morphology significantly affected macrophage polarization and promoted a shift in the macrophage to an anti-inflammatory, pro-healing M2 phenotype.[29] To further improve the anti-inflammatory properties of MXenes, researchers managed to improve the anti-inflammatory properties of MXenes by modifying a number of molecules with anti-inflammatory activity on MXene nanosheets. For example, researchers coated epigallocatechin gallate (EGCG)/Fe metal polyphenol nanodots on small-sized $Ti_3C_2T_x$ MXene nanosheets (MXene@EGCG); this is a naturally occurring polyphenol with anti-inflammatory properties, and the nanosheets showed good anti-inflammatory ability to reduce inflammation triggered by photothermal therapy (PTT).[30] Another work reported a method of loading rhizopodophyllin (Phl) onto MXene nanosheets, and the anti-inflammatory effects of Phl and MXene were able to eliminate inflammation induced by PTT scavenging of ROS.[31] In addition, a MXene@polydopamine-cryptotanshinone (MXene@PDA-CPT) nanosystem was developed.[32] After incubation of macrophages with MXene@PDA-CPT nanosheets, it was able to significantly increase the expression level of IL-10 and down-regulate the cellular level of TNF-α, and the loadability of cryptotanshinone further extended the mitigating inflammation effect of this system. However, the current research on the anti-inflammatory properties of MXenes is still mainly focused on $Ti_3C_2T_x$, with less research on the anti-inflammatory properties of other classes of MXene, and the research on the related anti-inflammatory mechanism needs to be further deepened. MXenes, especially $Ti_3C_2T_x$, exhibited significant anti-inflammatory effects due to their excellent antioxidant properties, which were further enhanced by binding anti-inflammatory molecules, but the anti-inflammatory potential and mechanisms of other types of MXenes still need to be explored in depth.

2.4 Optical property

As an emerging 2D material, MXenes have excellent optical properties (including light absorption, emission, and scattering) which play a critical role in their biomedical applications. MXenes exhibit strong absorption properties over a broad spectral range from UV-visible to near-infrared, allowing them to exhibit high absorption in the first (650–1000 nm) and second (1000–1350 nm) biological windows, which distinguishes them from conventional photothermal materials, and which is why they have unlimited potential for deep tissue photoacoustic imaging (PAI) and PTT.[33] MXenes' strong light absorption and localized surface plasmon resonance (LSPR) effect are the driving forces behind their photothermal conversion.[34,35] MXenes exhibit better photothermal performance than most materials, *e.g.*, gold nanorods have a photothermal efficiency of 21%,[36] graphene oxide has a photothermal efficiency of 24.6%,[37] and MXenes' superior photothermal conversion efficiency can reach about 50% under certain conditions.[22] As the first reported MXene-based photothermal agent, Ti_3C_2 nanosheets have shown considerable PTT efficacy *in vivo*. A study reported that the solution temperature of Ti_3C_2 can

reach 57 °C after irradiation for 6 min at a relatively low concentration (72 ppm) with a photothermal conversion efficiency of 30.6%, which suggests that Ti_3C_2 nanosheets can efficiently and rapidly convert near-infrared light into thermal energy, and could be used as a durable photothermal agent for cancer PTT.[38] The extinction coefficient of Ti_3C_2 nanosheets measured at 808 nm was 25.2 L g^{-1} cm^{-1}, which was higher than that of GO nanosheets (3.6 L g^{-1} cm^{-1}). Tantalum carbide (Ta_4C_3) is another MXene material with high photothermal conversion efficiency, which could also be used for PTT treatment of bacterial infected wounds. Ta_4C_3 nanosheets could be used for the treatment of diabetic wounds infected with drug-resistant bacteria as the temperature could be rapidly increased to 60–70 °C by irradiation at a concentration of 400 μg mL^{-1} for 10 min.[39] In addition, niobium carbide (Nb_2C), the latest MXene material, also has a very high photothermal conversion efficiency of 36.4% and 45.65% at 808 nm and 1064 nm, respectively, under near-infrared light.[40] Attractively, MXene-based quantum dots (QDs) can achieve a certain amount of luminescence under specific wavelengths of excitation (currently mainly UV-blue excitation), which is achieved by MXene QDs utilizing surface defects and size effects to induce quantum confinement.[41] Xue *et al.* prepared photoluminescent Ti_3C_2 MXene quantum dots (MQDs) by a simple hydrothermal method.[41] The photoluminescence excitation (PLE) spectra of MQDs showed two sharp peaks at 250 nm and 320 nm, and the MQDs were found to be readily taken up by the cells through the process of endocytosis after co-incubation with macrophage cells for 4 h, and their cell confocal images showed bright blue and green and red colors at 405, 488 and 543 nm excitation, respectively, demonstrating that MQDs have great potential as polychromatic cell imaging reagents. More and more researchers have found that MXene QDs have luminescence properties, such as Ti_2N, V_2N, Nb_2C, Ta_4C_3 and so on.[42–45] However, further studies on the emission color, luminescence efficiency and mechanism of MXenes are still needed. In general, the optical properties of MXenes mainly depend on the structure and type of M and X sites as well as the stoichiometry of the surface termination groups.[46] Therefore, we can prepare MXenes with different compositions, structures, and surface terminations as a means of modulating the optical properties, such as light absorption, emission, and scattering, and thus promote their diverse applications in biomedical fields.

MXenes show great potential in the fields of photothermal therapy, photoacoustic imaging, and polychromatic cellular imaging due to their excellent optical properties, but their luminescence mechanism and performance optimization still need to be further investigated.

2.5 Antibacterial activity

Bacterial infections are a major cause of global health issues and are becoming the second leading cause of death worldwide (after ischemic heart disease). Bacterial infections can be caused by the release of harmful substances (toxins), direct invasion of tissues, or a combination of both, which can further impede wound healing and cause great suffering to the patient, and the global misuse of antibiotics has led to severe bacterial resistance. Therefore, effective antimicrobial activity without bacterial resistance is the ideal target for the application of bioactive materials in the antimicrobial direction. Due to their structural characteristics and excellent photothermal properties, MXenes have become a hot research topic in the antibacterial field. Currently, researchers have summarized the antibacterial mechanism of MXenes as physical damage, induced oxidative stress, as well as photothermal and photodynamic therapy.[47] On the one hand, the hydrophilic and anionic nature of the MXene's surface enhances the interaction with the bacterial cell membrane, and the rough surface or sharp edges of MXenes cause physical damage to the bacterial membrane. In the study of Rasool *et al.* it was found that when *E. coli* and *B. subtilis* were treated with 100 μg mL^{-1} of $Ti_3C_2T_x$ for 4 h, SEM observed severe membrane rupture and cytoplasmic leakage in both bacteria, and the antibacterial rate was 97.70 ± 2.87% and 97.04 ± 2.91%, respectively.[48] Pandey *et al.* found that $Nb_2C_2T_x$ and $Nb_4C_3T_x$ nanosheets could kill more than 90% of *E. coli* and *S. aureus* at 120 μg mL^{-1}.[49] SEM and TEM images clearly showed that the nanosheets caused pore formation and partial disruption of the cell wall/cytoplasmic membrane upon entering the cells, which led to the efflux of the contents of the cells, resulting in the death of the bacteria. Interestingly, this antimicrobial capacity of MXenes shows a dependence on nanosheet size and treatment time, with smaller sized nanosheets tending to enter the bacteria more readily and disrupt cytoplasmic components by physical penetration or endocytosis.[50] On the other hand, MXenes induce oxidative stress by inducing the production of ROS, which can cause damage to bacterial proteins, lipids, DNA and RNA. MXenes typically have a negative zeta potential, excellent electrical conductivity, and an abundance of electronic properties, which contributes to their affinity for cell surfaces and ease of formation of chemical reactions, and MXenes can form conductive bridges with lipid bilayers to cause ROS production, leading to bacterial death.[48] Zheng *et al.* found that the MXene group produced 1.8-fold higher ROS than the control group, and further performed a lipid peroxidation assay and found that the MXene group was able to oxidize the bacterial membranes at a rate 1.3-fold higher than the control group.[51] The results of this study suggested that MXene could induce oxidative stress through the production of ROS, which could cause damage to bacterial membranes. In most studies, MXenes tended to enhance their photocatalytic activity by preventing electron/hole recombination through the available surface-terminal groups and excellent electrical conductivity. For example, few-layer $Ti_3C_2T_x$ generated much higher ROS compared with multi-layer $Ti_3C_2T_x$ nanosheets.[52] However, the most attractive strategies for MXene antimicrobials are PTT and photodynamic therapy (PDT), which are innovative approaches against drug-resistant bacteria and are highly dependent on the excellent photoactivation properties of MXenes. MXenes have excellent photothermal properties, converting light energy into heat and causing membrane

rupture, protein denaturation and irreversible damage in bacteria. Qu *et al.* found that 50 μg mL^{-1} of MXene irradiated with 808 nm laser for 10 min (0.75 W cm^{-2}) showed strong antibacterial activity against *E. coli*, *S. aureus*, and MRSA, with an antibacterial rate of more than 99%.[18] On the other hand, MXenes also possess photodynamic antibacterial properties, which can transfer energy to the surrounding oxygen molecules after receiving light, generating ROS and thus destroying the internal structure of bacteria. In a study using 1,3-diphenylisobenzofuran (DPBF) as a ROS-trapping agent, after irradiation with a 532 nm laser (20 mW) for 30 min, a decrease in absorbance at 417 nm was found in the MXene group, demonstrating that it produced singlet oxygen ($^1O_2$).[53] After irradiation with a xenon lamp (150 mW cm^{-2}), it showed good antibacterial activity against *E. coli* and *S. aureus*. This good antibacterial activity was attributed to the synergistic effect of the MXene's photothermal and photodynamic forces.

MXenes have shown strong potential in the antibacterial field due to their unique physical and chemical properties, providing a new strategy for antibacterial therapy by effectively combating bacteria, especially drug-resistant bacteria, through a variety of mechanisms such as physical damage, induced oxidative stress, as well as photothermal and photodynamic therapy.

2.6 Surface structure and promotion of tissue regeneration

MXenes have a large surface area and porosity, which can promote cell adhesion, proliferation and infiltration, which makes them also show infinite potential in promoting tissue regeneration, and more and more studies have reported that MXenes can promote the regeneration of tissues such as blood vessels, muscles, bones, skin and nerves.[15,54] Compared with other 2D nanomaterials, the unique surface chemical groups –OH and –O of the MXene family endow them with high hydrophilicity as well as reactivity, providing more potential for surface functionalization. Compared with graphene's smoother surface, their rough surface microstructure and interlayer spacing promote adhesion and delivery of proteins and nutrients, properties that greatly increase the chances of cell adhesion and ultimately affect tissue repair and regeneration.[55] In addition, the conductive properties of MXenes enable electrical stimulation, which shows promise in enhancing the soft tissue healing process.[56] For example, Li *et al.* reported that MXene, which has electrical conductivity properties, promotes vascular and skeletal muscle regeneration through the upregulation of myosin heavy chain (*MHC*) and vascular endothelial growth factor (*VEGF*) expression.[17] In another study, it was reported that the conductive MXene-PCL nerve-guiding catheter delivered physiological neuroelectric signals, induced angiogenesis, and stimulated nerve regeneration.[57] MXene-based scaffold materials can provide a favorable microenvironment for osteoblast attachment, proliferation and differentiation. For example, it has been reported that photoactivation of MXene can also regulate the osteogenic differentiation of adipose-derived stem cells (ADSC) through the ERK signaling pathway by activating heat shock protein 70 (HSP70) and enhancing bone tissue repair.[18] However, the current research on MXenes promoting tissue regeneration remains at a superficial level, and future work is expected to explore the mechanism of action of MXenes promoting tissue regeneration in depth.

Due to their unique surface structure and physicochemical properties, MXenes have shown great potential in promoting the regeneration of various tissues such as blood vessels, muscles, bones, skin and nerves, but further in-depth studies are needed to reveal their specific mechanism of action in promoting tissue regeneration.

3. Bioactive surface strategies

As a new type of 2D nanomaterial, MXenes have many advantages over ordinary 2D nanomaterials, such as large specific surface area, extreme thinness, good biocompatibility, rich surface functional groups, and excellent electronic, mechanical, and physicochemical properties, *etc*. Numerous scientific researchers have carried out in-depth investigations on MXenes and realized the corresponding applications. However, MXenes still have some drawbacks *in vivo*, such as their slow degradation, poor dispersibility in water and the presence of some toxicity, and there are limitations to their excellent performance while meeting the requirements of various applications. Therefore, surface modification and functionalization of MXene-based materials are necessary to improve their performance and give them new functions.[58] Fortunately, MXene-based materials are rich in surface end-group functionalities that impart hydrophilicity to MXenes. By controlling the surface end groups, surface active initiators, small molecules, and polymers as active sites for covalent binding, we can achieve flexible surface modification, functionalization, and scalable processing of MXenes to enable new functionalities such as drug loading.[59] Regarding the chemical surface functionalization of MXenes, we next present aspects of bioactive small molecules, bioactive macromolecules, bioactive nanoparticles, and surface polymerization-induced bioactivity of modified MXenes and surface functionalization methods used to prepare them (Table 1).

3.1 Bioactive small molecules

By modifying the surface of MXenes with various small molecules, this method can effectively enhance their performance characteristics such as mechanical stability, electrical properties and solution stability, which are easy to manipulate and inexpensive. Among them, the coupling agent is an important choice to prevent the structural degradation caused by spontaneous oxidation of MXenes on one hand, and improve their dispersion and interfacial bonding with polymer matrix on the other.[60] Riazi *et al.* reported amine functionalization of the $Ti_3C_2T_x$ MXene surface with [3-(2-aminoethylamino)-propyl]trimethoxysilane (AEAPTMS), and the functionalization changed the MXene surface charge from −35 mV to +25 mV at neutral pH, which made it possible to prepare self-assembled mem-

Table 1 Summary of recent research on MXenes surface modification strategies for biomedical applications

Bioactive surface strategies	MXene composition	Functionalized components	Bioactive property	Applications	Ref.
Bioactive small molecules	$Ti_3C_2T_x$	[3-(2-Aminoethylamino)-propyl] trimethoxysilane (AEAPTMS)	Adsorbing or desorbing protons, pH responsive	Cross-linked conductive composites, dye adsorbents, membranes and drug carriers	61
	$Ti_3C_2T_x$	$C_{12}E_6$	Ion transport, thickness-independent electrochemical performances	Biosensing, catalysis, filtration	62
	Nb_2CT_x	Deionized water/ethanol-based solvothermal treatment	Electromagnetic wave (EMW) absorbing	EMW-absorbing material	64
	Ti_3C_2	3-Aminopropyltriethoxysilane (APTES)	Immobilized bio-receptor	Cancer biomarker, biosensor	65
	$Ti_3C_2T_x$	APTES	pH stability, thermal stability and reusability	Enzymes	94
	Ti_3AlC_2	Ethylenediamine	Detecting and showing for cellular imaging	Biocompatibility nanoprobe	66
	$Ti_3C_2T_x$	APTES, thioketal, DOX, and polydopamine (PDA)	Antibacterial activity, photothermal properties, sensitive ROS/pH response	Drug delivery, antibacterial materials	67
	$Ti_3C_2T_x$	Au, polyethylene glycol (PEG) and DOX	pH-Responsive drug release, photothermal stability, biosafety	Drug delivery platform and cancer treatment	14
	$Ti_3C_2T_x$	GOX, DOX and PEG	Photothermal capability, CAT-like activity	Anti-cancer system	95
Bioactive macromolecules	Nb_2C	Polyvinyl pyrrolidone (PVP)	Photothermal conversion, enzyme-responsive, low phototoxicity	PTT and cancer treatment	40
	$Ti_3C_2T_x$	Sodium alginate (SA)	High conductivity, easy processing, mechanical flexibility and high electromagnetic shielding performance	EMI shielding materials	71
	$Ti_3C_2T_x$	Soybean phospholipid (SP)	NIR absorption and high photothermal conversion efficiency	Tumor therapy	38
	$Ti_3C_2T_x$	Silk fibroin (SF) and polyacrylamide (PAM)	High tensile strength, excellent toughness, high electrical conductivity and self-adhesion	Flexible electronics	72
	$Ti_3C_2T_x$	Hyaluronic acid (HA) and hyperbranched polysiloxane (HSi)	Mechanical flexibility, good resistance to water/solvents and thermal camouflage	Reliable long-term infrared stealth	73
	Ti_3AlC_2	Polyimide (PI)	Superelastic, mechanical flexibility and electrical conductivity	Microwave absorption coating, flexible strain sensor	69
	$Ti_3C_2T_x$	Polydiallyldimethylammonium chloride (PDDA)/PVA	Flexible and have electrical conductivities	Wearable electronics, electrochemical actuators	70
	2D $W_{1.33}C_i$-MXene	BSA	pH response, photothermal conversion, rapid biodegradation and biocompatibility	CT and PA imaging and cancer therapy	74
Bioactive nanoparticles	Ta_4C_3	IONPs and SP	Photothermal-conversion capability, imaging capability, biosafety	MR/CT imaging, PTT and tumor therapy	76
	Ti_3C_2	MnO_x	MR imaging of tumors and photothermal-conversion performance	Tumor therapy, theranostic nanomedicine	77
	Ta_4C_3	MnO_x and SP	MR imaging capability, biosafety	PTT for tumor and PA imaging	78
	Ti_3C_2	GdW_{10}-based polyoxometalates (POMs)	Biocompatibility, diagnostic-imaging guidance, monitoring	Contrast agent, tumor hyperthermia nanotherapy	85
	$Ti_3C_2T_x$	AuNPs	Photothermal conversion efficiency, stability, antibacterial	Photothermal antibacterial	79
	Ti_3C_2	Au, PEGylation	Stability, biocompatibility, photothermal effect and biosafety	Cancer therapy	80
	$Ti_3C_2T_x$	Plasmonic Au	Oxygen evolution performance	Oxygen evolution reaction (OER)	81
	Ti_3C_2	Pt	POD-like activity	Glucose and glutathione assays	83
	Ti_3C_2	Natural glucose oxidase (GOD) and IONPs	Catalyze, biocompatibility and photothermal performance	Nanocatalytic cancer therapy	75
	$Ti_3C_2T_x$	Bi_2S_3	Photocatalytic activity, antibacterial infection and biocompatibility	Biocompatible photoelectrical devices	96
Surface polymerization-induced bioactivity	Ti_3AlC_2	Polydopamine (PDA)	Adsorption capacity, stability	Adsorbents	89
	V_2C	Poly(2-(dimethylamino)ethyl methacrylate) (PDMAEMA)	CO_2 and temperature dual-responsive properties, conductivity	Smart responsive MXene systems	93
	$Ti_3C_2T_x$	*N*-Isopropylacrylamide (NIPAM)	Photothermal conversion, photothermal stability and thermal responsive	NIR-controlled "smart" windows, fluidic valves and photodetectors	92
	$Ti_3C_2T_x$	Poly(diallyldimethylammonium chloride) (PDDA) and PVA	Excellent conductivities, controlled thicknesses, and excellent flexibility	Wearable energy storage devices, fillers for radiofrequency shielding	70
	$Ti_3C_2T_x$	Poly(lactic-*co*-glycolic acid) (PLGA) and SP	Photothermal absorption and high photothermal conversion efficiency	Tumor therapy	38

branes *in situ*, and also confirmed the presence of mixtures of differently oriented AEAPTMS and the presence of both protonated and free amine groups on the $Ti_3C_2T_x$ surface.[61] The availability of free amine groups on the surface enables the fabrication of cross-linked conductive MXene/epoxy composites, dye adsorbents, high-performance membranes and drug carriers. In order to improve molecular interactions and thus enhance the filling symmetry, Xia *et al.* introduced nonionic surfactant hexaethylene glycol monododecyl ether ($C_{12}E_6$) on the surface of Ti_3C_2 MXenes ($C_{12}E_6$@Ti_3C_2). In the $C_{12}E_6$@Ti_3C_2 composite, strong hydrogen bonds were formed between the –O or –F groups on the surface of MXene and the –OH groups of $C_{12}E_6$.[62] In addition, Lei *et al.* reported the one-step preparation of sulfonic acid-based functionalized MXene (named Ti_3C_2–SO_3H) by the direct reaction of diazonium salts with Ti_3C_2 flakes (Fig. 1A).[63] Due to the introduction of the anionic sulfonic acid group, this provides a new method for the preparation of functionalized MXenes and can be extended to the preparation of other functionalized MXenes with good design properties and performance. Nb_2CT_x MXene was further processed by a simple one-step solvothermal/hydrothermal method by Jin *et al.* Accordingly, the interlayer space and surface functional groups of Nb_2CT_x MXene were enhanced, which significantly improved the EM wave absorption performance.[64] The solvothermal/hydrothermal treatment of Nb_2CT_x MXene was carried out using the low-toxicity solvents ethanol (Et) or deionized water (DI) instead of *N*,*N*-dimethylformamide (DMF). The results showed that Nb_2CT_x treated with Et as solvent absorbed EMW better.

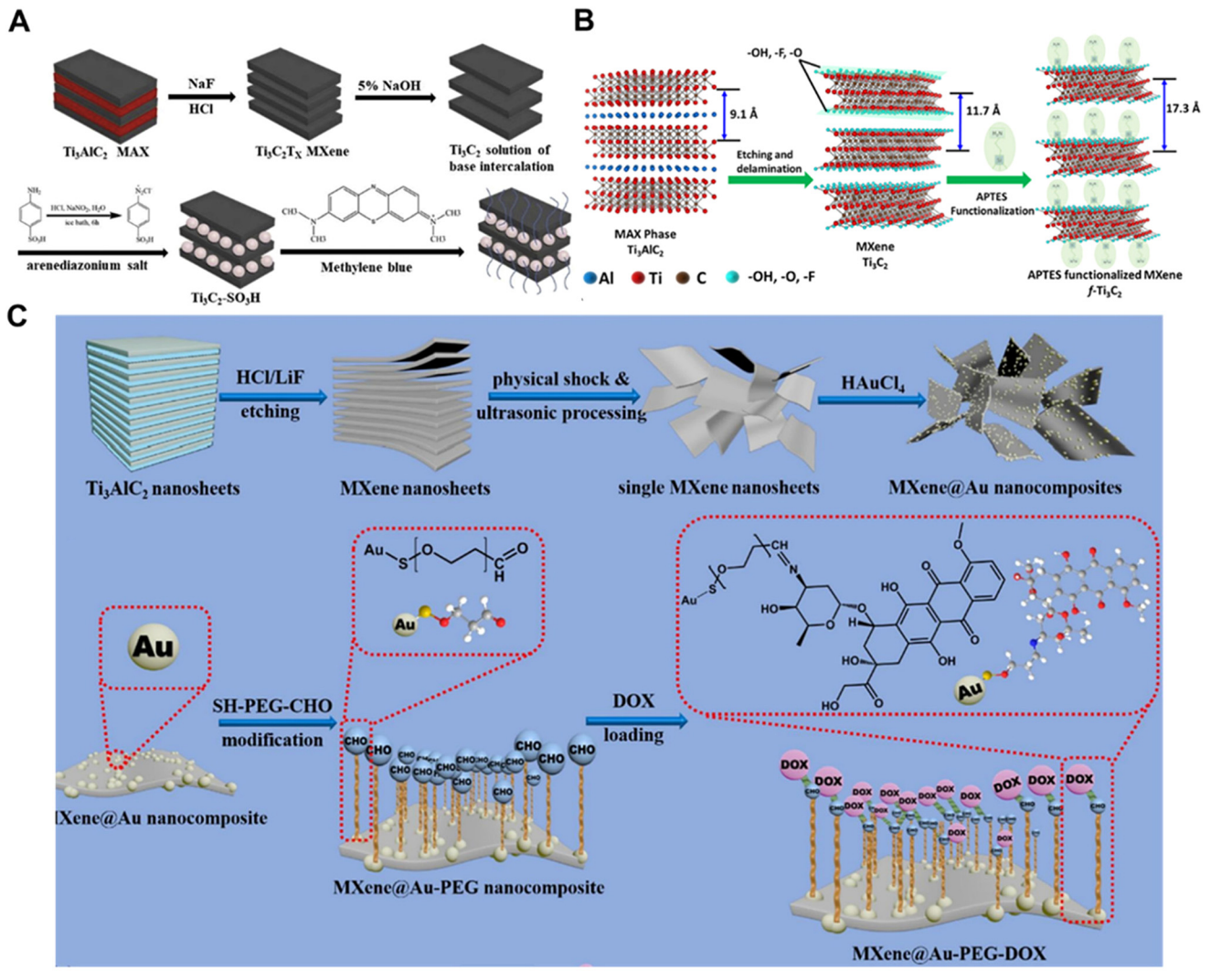

Fig. 1 Strategies for functionalizing MXenes with bioactive small molecules. (A) The scheme for the preparation of pristine Ti_3C_2 and Ti_3C_2-SO_3H.[63] Reproduced from ref. 63 with permission from Elsevier, copyright 2019. (B) Schematic representation of the functionalization of the Ti_3C_2-MXene surface using APTES.[65] Reproduced from ref. 65 with permission from Elsevier, copyright 2018. (C) Synthesis process for MXene and MXene@Au nanosheets and surface modification of MXene@Au using thiol polyethylene glycol aldehyde chains (SH-PEG-CHO), and the subsequent surface doxorubicin (DOX) loading.[14] Reproduced from ref. 14 with permission from Elsevier, copyright 2022.

Small molecules were chemically introduced on the surface of monolayer/multilayer MXene (Ti_3C_2) nanosheets with amino groups, and the resulting functionalized MXene nanosheets could be used as platforms for immobilization of different biomolecules. Kumar *et al.* synthesized ultrathin Ti_3C_2-MXene nanosheets by a minimally enhanced layer delamination method and homogeneously functionalized with aminosilane (F-Ti_3C_2-MXene) to provide covalent binding to immobilized bioreceptors (anti-CEA) for label-free, ultrasensitive cancer biomarker (carcinoembryonic antigen, CEA) detection (Fig. 1B).[65] They investigated the effects of different redox probes on the electrochemical behavior of F-Ti_3C_2-MXene and found that ammonium hexamine-mineral ($[Ru(NH_3)_6]^{3+}$) was a more ideal redox probe for biosensing. The prepared biofunctionalized Ti_3C_2-MXene opens a new window for the development of highly sensitive DNA, aptamer, enzyme, antibody, and cellular biosensors based on MXene, and can be further used for drug delivery applications. Meanwhile, MXenes have strong absorption of light in the wavelength range of 300–900 nm, which can burst the fluorescence of fluorescent groups by fluorescence resonance energy transfer (FRET) and can be used as highly efficient and broad-spectrum fluorescence bursting agents by combining with specific small molecules. Luo *et al.* investigated and prepared a biocompatible nanoprobe of N-Ti_3C_2 quantum dots (N-Ti_3C_2 QDs) based on MXene for the detection of intracellular glutathione.[66] Based on non-radiative electron–hole annihilation, N-Ti_3C_2 quantum dots acted as fluorescence reporters and iron (Fe^{3+}) acted as bursters. When N-Ti_3C_2 QDs/Fe^{3+} nanoprobes acted on cancer cells MCF-7, abundant GSH in the cancer cells could reduce Fe^{3+} to Fe^{2+}, thus restoring the fluorescence of N-Ti_3C_2 QDs, and the N-Ti_3C_2 quantum dots/Fe^{3+} nanoprobes might provide a new pathway for imaging-guided accurate cancer diagnosis.

There have also been numerous studies on DOX-functionalized MXenes for tumor therapy. Zhang *et al.* used hydrofluoric acid etching and TBAOH intercalation to obtain well-dispersed MXene with small lateral dimensions.[67] Functionalized MXene-TK-DOX@PDA nanoparticles have remarkable photothermal conversion properties and high photothermal stability, and exhibit sensitive ROS- and pH-responsive behaviors in the presence of H_2O_2 at pH = 5.5, which controls the local release of DOX and effectively reduces the premature release of the drug. The new MXene nanoparticles were designed for chemotherapeutic drug-targeted delivery with good antimicrobial activity, which provided a promising drug delivery strategy in the biomedical field and enriched the family of antimicrobial materials. In another study, Liu *et al.* reported the synthesis of an MXene@Au-PEG drug delivery platform for the highly loaded chemotherapeutic drug Adriamycin (DOX) with near-infrared (NIR) laser-triggered and pH-responsive drug release modes (Fig. 1C).[14] In *in vivo* and *in vitro* experiments, the MXene@Au-PEG-DOX system exhibited good photostability, thermal stability and histocompatibility. In addition, based on the good photothermal conversion ability of Au particles and MXene, this system had a synergistic effect of photothermal ablation and chemotherapy in tumor treatment. The passive targeted release property of MXene@Au-PEG delivery platform also enhanced the cellular uptake of DOX at the tumor site, thus improving the efficiency of the drug.

By modifying the surface of MXenes with small molecules, it is possible to significantly enhance their performance in terms of mechanical, electrical, and solution stability, and to expand their applications in biomedical fields such as drug delivery, biosensing, and tumor therapy.

3.2 Bioactive macromolecules

In the past decades, macromolecular surface modification technology has rapidly developed into a key driver of biomaterials innovation, and polyphenolic components, vitamins, alkaloids, proteins, peptides, and so on, have attracted much attention as material surface modification components due to their excellent bioactivities. Therefore, many studies have also been conducted to modify the surface of MXenes with bioactive macromolecules to further enhance their biological properties.

Some synthetic polymers, such as polyethylene glycol (PEG) and polyvinylpyrrolidone (PVP), are suitable for surface modification of MXenes.[68] PVP is often used for surface modification of MXene materials to improve their stability. Lin *et al.* explored a new ultrathin 2D niobium carbide (Nb_2C) MXene as a new type of phototherapeutic agent, and ultrathin transverse nano-Nb_2C nanosheets had excellent near-infrared photothermal properties with very high photothermal conversion efficiency and ideal photothermal stability. The Nb_2C nanosheets were further surface modified to prepare Nb_2C-PVP colloidal solutions, which greatly improved the biocompatibility and physiological stability of the nanosheets, with no significant toxicity *in vitro* and *in vivo*.[40] Liu *et al.* developed an interfacial enhancement strategy to construct versatile, superelastic and lightweight 3D MXene structures by bridging individual MXene sheets with polyimide macromolecules.[69] The resulting lightweight aerogels were superelastic with large reversible compressibility, excellent fatigue resistance (1000 cycles at 50% strain), 20% reversible stretchability and high electrical conductivity of $\approx$4.0 S m^{-1}. The excellent mechanical flexibility and electrical conductivity make the aerogel promising for applications in damping, microwave-absorbing coatings and flexible strain sensors. More interestingly, the material exhibited excellent microwave absorption properties at 9.59 GHz. Ling *et al.* prepared $Ti_3C_2T_x$/polymer composites by blending $Ti_3C_2T_x$ MXene with charged poly (dienyldimethylammonium chloride) (PDDA) or electrically neutral PVA. The prepared composites were flexible with high electrical conductivity.[70] The tensile strength of $Ti_3C_2T_x$/PVA composites was significantly improved compared with pure $Ti_3C_2T_x$ or PVA films. This study is the first step in exploring the potential of MXene in polymer-based multifunctional nanobiocomposites for applications such as wearable electronics, electrochemical actuators, and radio frequency shielding.

In addition, many natural macromolecules can also be used for MXene surface modification. Sodium alginate (SA) is a linear polysaccharide copolymer derived from seaweed. As a natural biomaterial, SA is potentially an ideal candidate for polymer matrices, being abundant, environmentally friendly and having excellent mechanical properties, while SA possesses oxygen-containing functional groups (–OH, –COO, and =O), which can potentially facilitate the formation and termination of hydrogen bonding with MXenes. Shahzad *et al.* employed SA to perform a 45 μm-thick $Ti_3C_2T_x$ thin film surface modification to show 92 dB EM shielding efficiency (>50 dB for 2.5 μm film), which is the highest EM shielding efficiency of any synthetic material of equivalent thickness produced to date.[71] In addition, the natural polymer soybean phospholipid (SP) has also been widely used for surface modification of MXenes as an economical modifier to improve the cycling stability of MXenes and enhance the material penetration. Lin *et al.* reported that MAX-ceramic biomaterials exhibited unique functionalities for cancer photothermal ablation after being stripped into atom-thick (MXene) ultrathin nanosheets (Fig. 2A).[38] The SP-modified Ti_3C_2 nanosheets showed good biocompatibility and may be of interest in exploring MXene-based ceramic biomaterials for biomedical applications. Silk fibroin (SF) is a natural fibrous protein composed of various amino acids such as tyrosine, glycine and alanine. It has both hydrophilic and hydrophobic blocks with abundant reactive groups and can form different secondary structures such as β-sheet and random curls through hydrogen bonding. Therefore, SF can form attractive interactions with MXenes through electrostatic interactions, hydrophobic interactions and hydrogen bonding. Li *et al.* prepared a novel electrically conductive MXene-based hydrogel by introducing SF-modified MXene (MXene-SF) into a polyacrylamide (PAM) network.[72] It was shown that the SF coating on the surface of MXene could greatly improve its stability, and also induce the formation of various noncovalent interactions between MXene-SF and PAM chains to enhance its adhesion properties. The high conformal adhesion and low interfacial impedance enabled the hydrogel bioelectrode to precisely monitor weak electrophysiological signals. Hyaluronic acid (HA) is a linear polysaccharide chain containing *N*-acetylglucosamine and glucuronic acid that is sensitive to ROS such as hydrogen peroxide, superoxide radicals and hydroxyl radicals. Its oxidative instability can be solved by using HA-modified MXene. Guo *et al.* designed and fabricated an MXene-based hybrid network containing hyaluronic acid (HA) and hyperbranched polysiloxane (HSi) molecules (Fig. 2B).[73] Notably, the presence of hyaluronic acid molecules limited the oxidation of MXene sheets without altering their infrared invisibility properties, which is superior to that of other water-soluble polymers, while HSi molecules could act as highly efficient cross-linking agents to produce strong interactions between MXene sheets and hyaluronic acid molecules. The optimized MXene/HA/HSi composites provided excellent mechanical flexibility, good water/solvent resistance and long-term stable thermal camouflage for reliable long-term infrared stealth. Another biocompatible natural macromolecule, bovine serum albumin (BSA), was attached to $W_{1.33}C_i$-MXenes through van der Waals forces and hydrogen bonding interactions to improve the colloidal stability of the nanosheets, and this work provides an example of i-MXenes being tailored for biomedical applications through combinatorial and structural design on atoms (Fig. 2C).[74]

Modification of the MXene surface by bioactive macromolecules not only enhances its biocompatibility and stability, but also expands the applications of MXenes in biomedical fields, such as drug delivery, tissue engineering, antimicrobial activity and biosensors.

3.3 Bioactive nanoparticles

MXenes have a unique two-dimensional planar structure that provides a suitable substrate for simple decoration of various 0D functional nanoparticles, resulting in versatile 0D/2D composites. To extend the versatility of MXenes, anchoring magnetic nanoparticles (*e.g.*, Fe_3O_4, MnO_x) on the surface of MXenes enables the integration of diagnostics and combination therapy. Liang *et al.* reported the triggering of Fenton-based nanocatalytic reactions on 2D titanium carbide (Ti_3C_2) MXenes nanosheets and as a photothermal conversion nanoagent to further synergistically improve the efficiency of nanocatalytic cancer cell killing.[75] The nano-enzymes Fe_3O_4 nanoparticles and natural glucose oxidase (GOD) were encapsulated on Ti_3C_2 MXenes as nanocarriers for composite nano-systems and as photothermal conversion nano-agents (Fig. 3A). The loaded GOD catalyzes the generation of a large number of hydrogen peroxide molecules from glucose phagocytosed by tumors, Fe_3O_4 nanoparticles further catalyze the generation of sufficient hydroxyl radicals to kill the cancer cells, and the Ti_3C_2 MXene substrate further enhances and accelerates this catalytic reaction under NIR-triggered photothermal conversion. Liu *et al.* reported the *in situ* growth of iron oxide nanoparticles (IONPs) on Ta_4C_3 MXenes by co-precipitation.[76] The obtained composite Ta_4C_3-IONPs combines the enhanced MR imaging capability of IONPs and the photothermal effect of Ta_4C_3 MXenes for efficient cancer therapy. Although MXenes have excellent hydrophilicity, they have insufficient colloidal stability due to severe aggregation and precipitation in complex physiological media. Dai *et al.* developed for the first time a versatile but highly efficient "redox-induced growth" (RH-IG) method for *in situ* growth of MnOx nanosheets (MnO_x/Ti_3C_2) on the two-dimensional Ti_3C_2 MXene surface, which can be used for effective tumor diagnosis and treatment.[77] They also proposed a surface engineering strategy based on using a two-dimensional tantalum carbide (Ta_4C_3) MXene for *in situ* growth of manganese oxide nanoparticles on the Ta_4C_3 MXene surface by triggering a redox reaction between the reducing MXene surface and the strongly oxidizing MnO_4-(MnO_x/Ta_4C_3) (Fig. 3B).[78] The integrated MnO_x component endows the composite MXenes nanosheets with tumor microenvironment (TME)-responsive *T*1-weighted MR imaging capability.

Various metal nanoparticle/MXene hybridizations have been reported many times, especially Au nanoparticles. Wen

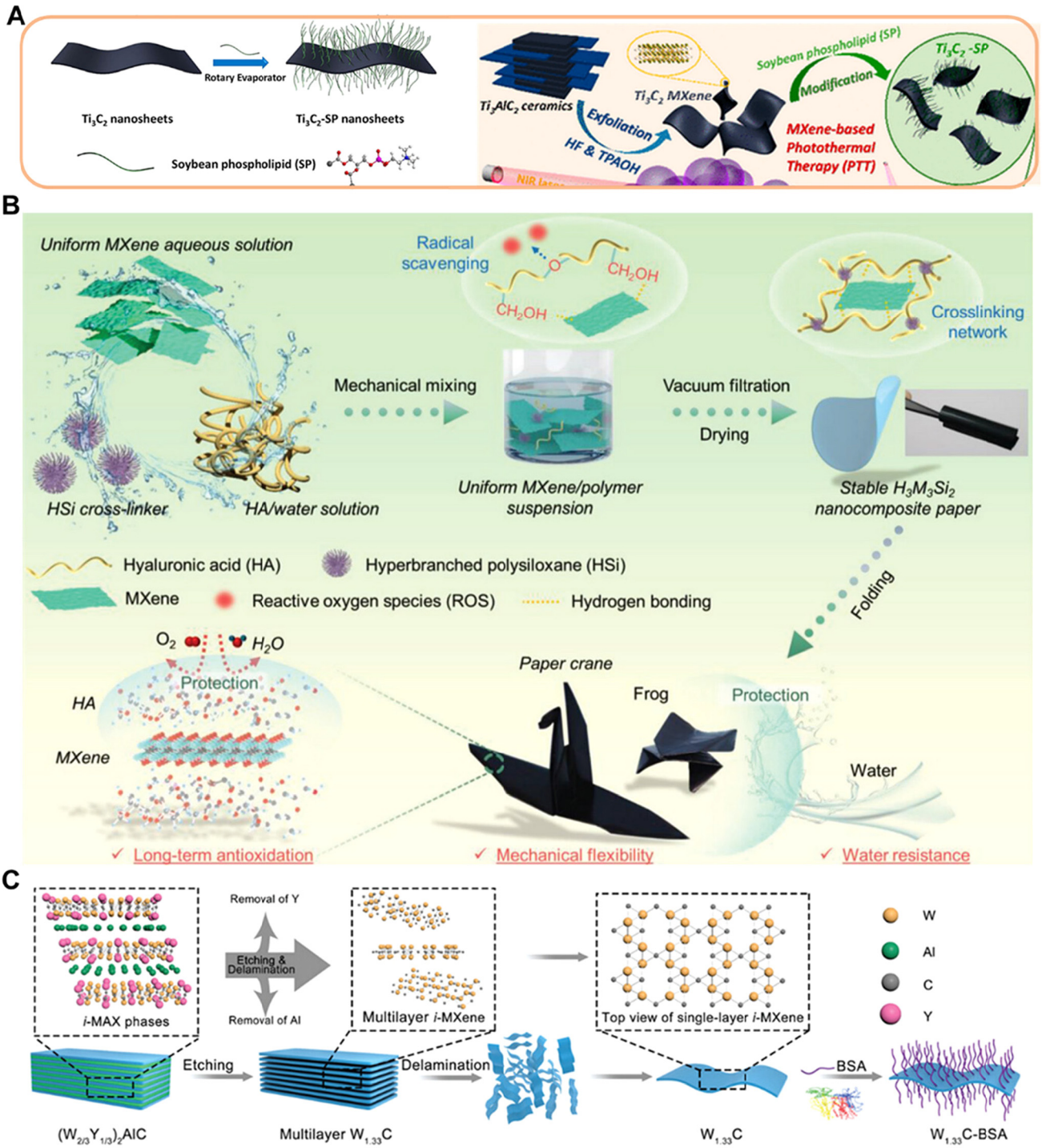

Fig. 2 Strategies for functionalizing MXenes with bioactive macromolecules. (A) Schematics of surface modification of exfoliated Ti_3C_2 nanosheets modified with soybean phospholipid and Ti_3C_2-SP use for photothermal therapy.[38] Reproduced from ref. 38 with permission from American Chemical Society, copyright 2016. (B) Schematic representation of the preparation process of polysiloxane-modified HA/MXene composite network and its application.[73] Reproduced from ref. 73 with permission from Wiley-VCH, copyright 2024. (C) Schematic illustration on the construction of 2D $W_{1.33}C_i$-BSA nanosheets as a 2D phototherapeutic agent.[74] Reproduced from ref. 74 with permission from Wiley-VCH, copyright 2021.

et al. reported a simple strategy to construct Au@$Ti_3C_2T_x$ heterostructures with enhanced photothermal antimicrobial effect by utilizing the reducing activity of $Ti_3C_2T_x$ NSs itself, and the *in situ* reduction of Au precursors on $Ti_3C_2T_x$ substrates.[79] A series of Au@$Ti_3C_2T_x$ nanocomposites was obtained by adjusting the Au/Ti feed ratio without adding any

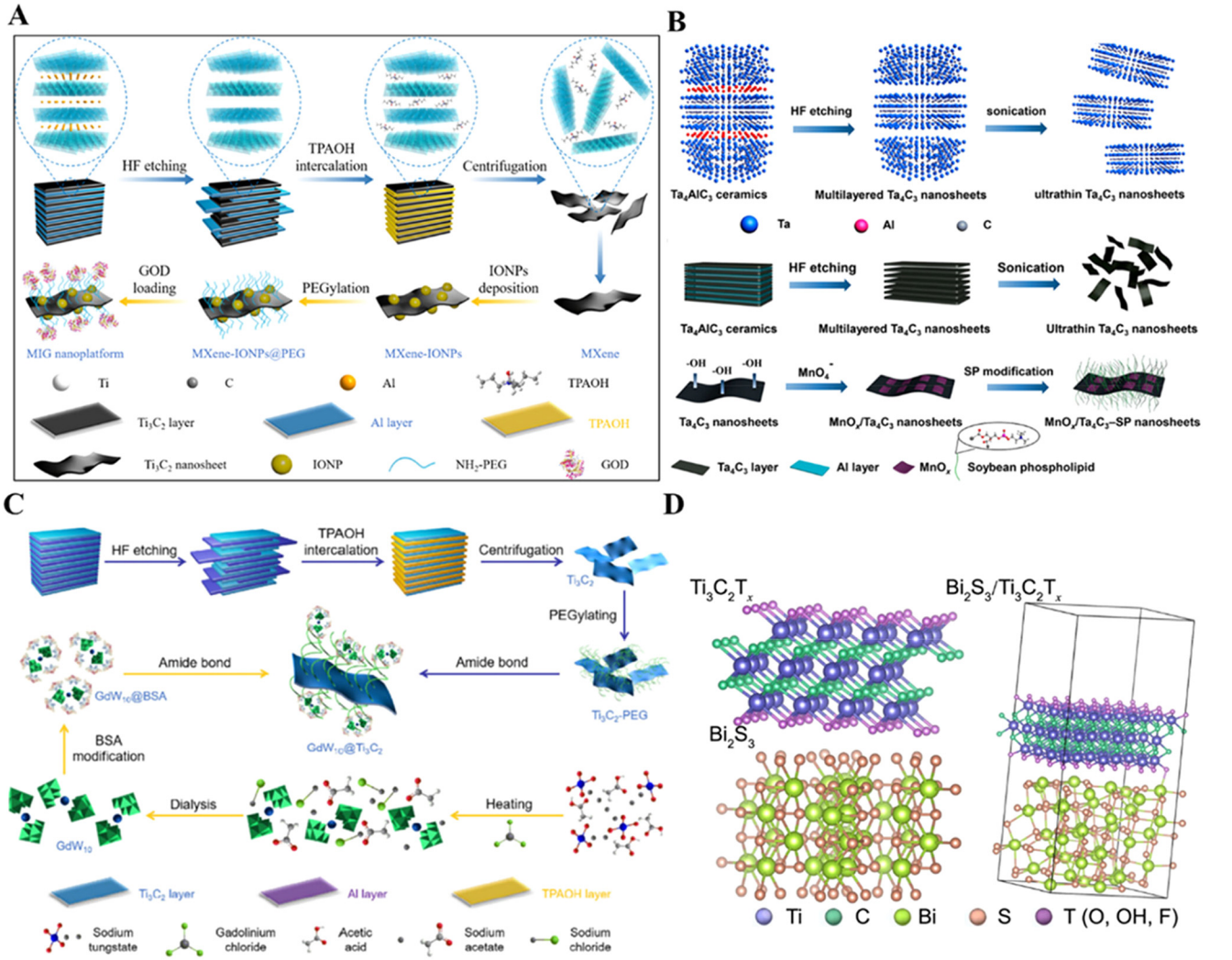

Fig. 3 Strategies for functionalizing MXenes with bioactive nanoparticles. (A) Schematic illustration of the successive synthetic procedures of 2D Ti_3C_2 MXene and MIG nanoplatforms for *in vivo* synergistic photothermal-enhanced nanocatalytic cancer therapy.[75] Reproduced from ref. 75 with permission from American Chemical Society, copyright 2019. (B) The scheme of the synthetic procedure for Ta_4C_3 and MnO_x/Ta_4C_3-SP composite nanosheets, including HF etching, sonication exfoliation, *in situ* redox reaction between Ta_4C_3 nanosheets and postintroduced $KMnO_4$, and subsequent surface SP modification.[78] Reproduced from ref. 78 with permission from American Chemical Society, copyright 2017. (C) Schematic illustration for the synthesis of $GdW_{10}@Ti_3C_2$ composite nanosheets, including chemical exfoliation of MAX-phase Ti_3AlC_2 ceramic to produce Ti_3C_2 MXene and further surface functionalization with GdW_{10} POM nanoclusters.[85] Reproduced from ref. 85 with permission from Tsinghua University Press, copyright 2018. (D) Crystal structure of $Ti_3C_2T_x$, Bi_2S_3 and $Ti_3C_2T_x/Bi_2S_3$ after structure optimization.[86] Reproduced from ref. 86 with permission from Springer Nature, copyright 2021.

surfactant. The photothermal conversion efficiency and stability of the composite were improved due to the LSPR effect of Au NPs' interaction. Under 660 nm laser irradiation, more than 99% of Gram-positive *S. aureus* and Gram-negative *E. coli* were efficiently killed due to the synergistic effect of intrinsic physical damage and photothermal ablation. This work presents the potential of multifunctional $Au@Ti_3C_2T_x$ heterostructures for fighting drug-resistant bacteria by photothermal treatment. Tang *et al.* synthesized multifunctional two-dimensional core–shell structures of Ti_2C_3@Au nanocomposites for imaging-guided cancer therapy *via* a seed-growth method.[80] The stability and biocompatibility of Ti_2C_3@Au nanocomposites were significantly enhanced and their optical absorbance in both NIR-I and NIR-II bio-windows were greatly enhanced. The nanocomposites were successfully applied in photothermally enhanced RT through mild photothermal effects and good synergistic effects were realized. Wang *et al.* successfully prepared MXene $Ti_3C_2T_x$ nanosheets mixed with Au nanoparticles ($AuNPs@Ti_3C_2T_x$) *via* electrostatic interactions and systematically investigated them for plasma-enhanced catalysis.[81] The experimental results showed that the plasma MXene-based heterostructure could further enhance the catalytic activity of MXene effectively. Au–TiO_2@Ti_2C was synthesized by Wojciechowski *et al.* using isopropanol as a reducing agent and $Ti(O_i\text{-}Pr)_4$ and Au^{3+} ions as precursors with stirring for 2 days.[82] Geng *et al.* constructed Ti_3C_2/Pt hybrids

with synergistically enhanced catalytic activity.[83] TEM images of Ti_3C_2 nanosheets and Ti_3C_2/Pt with different Pt loadings showed that the lateral sizes of the prepared layers of Ti_3C_2 were between 100 nm and 300 nm, and the particles dispersed on the Ti_3C_2 sheets could be clearly seen after the deposition of Pt NPs. Although Ti_3C_2 does not possess oxidase and peroxidase-like activities, it can greatly and selectively enhance the peroxidase-like activity of Pt nano-enzymes. NIR irradiation can further specifically enhance the peroxidase-like activity of Ti_3C_2/Pt. This catalytic enhancement is due to the combined effect of the strong interfacial electronic effect and the unique photothermal effect of Ti_3C_2, which provides an effective means for the introduction of ideal carriers to improve the catalytic activity and selectivity of the nano-enzymes, and has a certain value of reference for the design of efficient nano-enzymes. However, these methods typically involve a multi-step process, are lengthy, and use surface stabilizers/reducers.[84]

Polyoxometalates (POMs) can be used for MXene surface modification. In a study, Ti_3C_2 MXenes were functionalized by GdW_{10}-based POMs (Fig. 3C).[85] The hybrid Ti_3C_2 MXenes had the enhanced CT/MR imaging capability of POM in multimodal imaging-guided PTT. Bi_2S_3 nanorods were grown *in situ* on the surface of $Ti_3C_2T_x$ nanosheets.[86] The results showed that the combination of $Ti_3C_2T_x$ with n-type Bi_2S_3 promoted the separation and transfer of photogenerated charges, which accelerated the interfacial charge transfer in the photocatalytic process, increased the ROS yield, and was effective in eliminating bacterial infections (Fig. 3D). In addition, mesoporous silica nanoparticles (MSN), CeO_2 nanoparticles, *etc*. can also be used for MXene modification.[87,88]

MXenes, as a unique two-dimensional material, form multifunctional 0D/2D composites by combining with 0D functional nanoparticles, and exhibit a wide range of potential applications in biomedical fields, especially in diagnostics, therapeutics, and photothermal conversion.

3.4 Surface polymerization-induced bioactivity

The hydroxyl (–OH), fluorine (–F) and many other reactive functional groups on the surface of MXenes allow the polymers to undergo non-*in situ* or *in situ* polymerization.

The first is the *in situ* polymerization between polymers and MXenes with the help of hydrogen bonding, electrostatic interactions, ε-spin and *in situ* polymerization with monomers such as pyrroles, which effectively enhances their physicochemical properties and biological activities. Dopamine is formed by surface polymerization to form polydopamine (PDA), which is rich in amino and catechol groups in its main chain and is firmly bound to organic and inorganic surfaces through the formation of non-covalent and covalent interactions, and the surface bioactivity is significantly enhanced by it. For example, Qing *et al.* produced MXene/PDA composites by *in situ* polymerization of PDA first in MXene solution.[89] In the work, it was found that PDA nanoparticles promoted the stripping of MXene by different adsorption measurements and had a strong synergistic effect in the removal of Cr(VI), and the stability was greatly improved, and the work suggested that MXene/PDA composites can be used as an alternative adsorbent (Fig. 4A). In addition, in the research of Lin *et al.*, Ti_3C_2 was further modified using poly(lactic-*co*-glycolic acid) (PLGA) for intratumoral implantation.[38] The high PTT efficiency *in vivo* on tumor xenografts successfully demonstrated the efficacy of PLGA/Ti_3C_2 for tumor therapy, expanding the possibilities of MXene nanosheets for biomedical applications, especially in anti-cancer applications. Ling *et al.* selected Ti_3AlC_2 as the MAX precursor and prepared $Ti_3C_2T_x$/PDDA composite films and $Ti_3C_2T_x$/PVA composite films by surface polymerization of two polymers: poly(dienyldimethylammonium chloride) (PDDA) and PVA, which have excellent flexibility, impressive electrical conductivity and hydrophilic surface (Fig. 4B).[70] However, most of the MXene complexes synthesized by surface *in situ* polymerization are unstable and more complicated to operate, and thus can be limited in practical biomedical applications.

Unlike common polymerization methods, self-initiated photografting and photopolymerization (SIPGP) eliminates the need for an anchoring layer, a self-assembled monolayer (SAM), and an initiator, and requires only a one-step reaction under UV irradiation at room temperature, which occurs directly on the surface of the material.[90] SIPGP has been successfully applied to graphene, carbon nanotubes, *etc*., and is a simple method for polymerization.[91] Recently, MXene prepared by Tao *et al.* could generate hydroxyl radicals and act as initiators for the free radical polymerization of a series of acrylic monomers.[92] PNIPAM-based nanocomposite hydrogels were prepared by simply mixing *N*-isopropylacrylamide (NIPAM) with p-$Ti_3C_2T_x$ nanosheets under deoxygenated conditions. The nanocomposite hydrogels had better photothermal stability than pristine $Ti_3C_2T_x$ and were thermoresponsive (Fig. 4C). In addition, Chen *et al.* reported a powerful strategy by grafting poly(2-(dimethylamino)ethyl methacrylate) (PDMAEMA) brushes on the surface of MXenes. V_2C MXene was prepared by soaking V_2AlC powder in hydrofluoric acid at room temperature. Then, they utilized the hydroxyl group on the surface as a photoactive site for further growth and amplification of the polymer brushes by SIPGP. Finally, the CO_2 and temperature dual-response properties of the V_2C@PDMAEMA hybridized materials were further explored (Fig. 4D).[93] SIPGP is a promising strategy to improve the raw performance of MXene, which could be tailored for biological applications.

The reactive functional groups on the surface of MXenes can be enhanced by a variety of polymerization methods to enhance their physicochemical properties and bioactivity, but stability and handling complexity remain major challenges for their biomedical applications.

MXenes will have more excellent physicochemical properties after surface modification and functionalization. Surface functionalization makes MXene materials suitable for electrochemical biosensors, catalysis, antimicrobial coatings, and drug delivery, *etc*., which have been widely explored in biomedical applications.

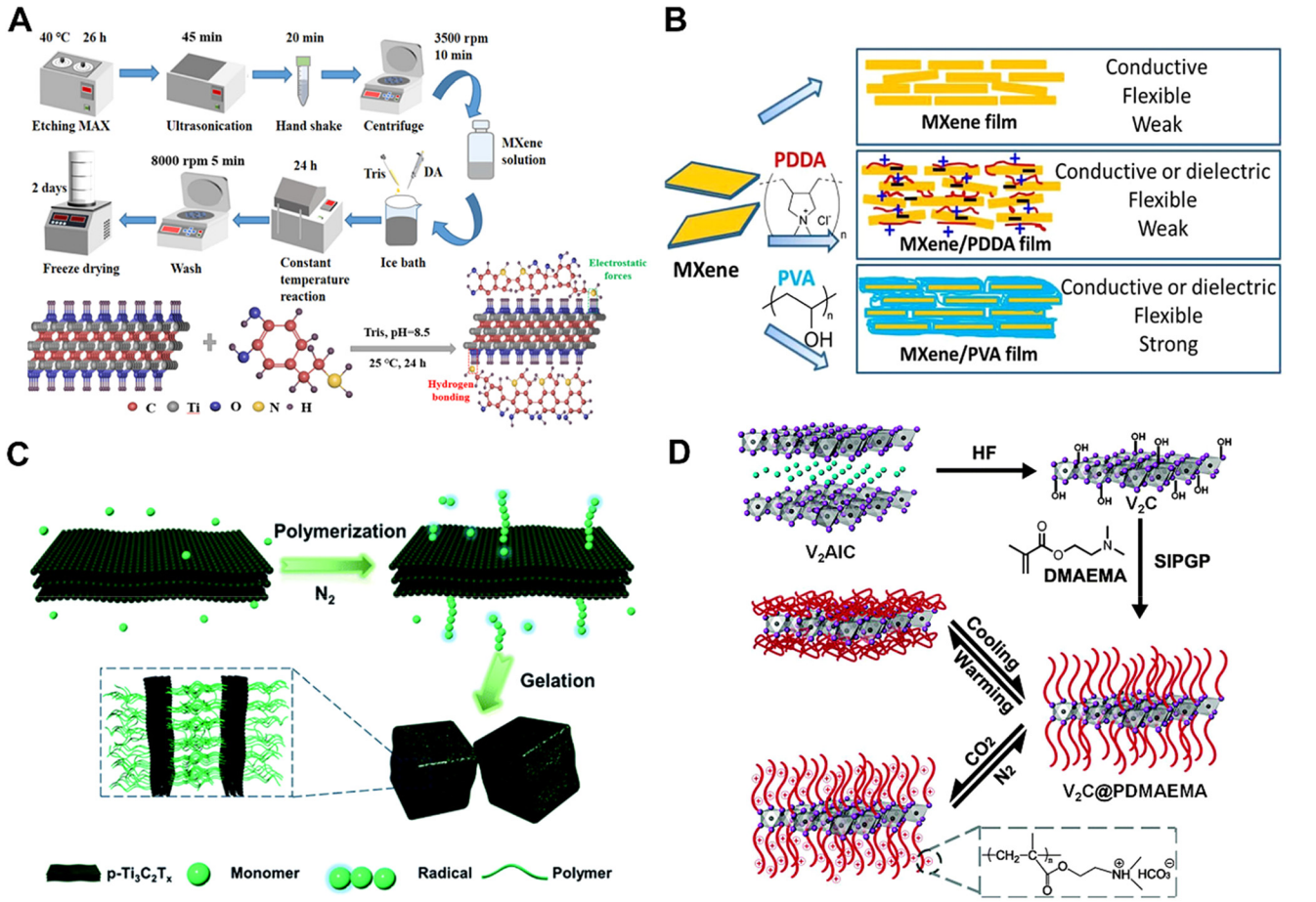

Fig. 4 Strategies for functionalizing MXenes with surface polymerization-induced bioactivity. (A) Schematic illustrations showing the preparation processes of the MXene/PDA composite particles and stacking of PDA macromolecules on the nanosheet of MXene.[89] Reproduced from ref. 89 with permission from American Chemical Society, copyright 2023. (B) A schematic illustration of MXene-based functional films with adjustable properties.[70] Reproduced from ref. 70 with permission from National Academy of Sciences of America, copyright 2014. (C) Schematic illustration of p-$Ti_3C_2T_x$-initiated polymerization and subsequent gelation.[92] Reproduced from ref. 92 with permission from the Royal Society of Chemistry, copyright 2019. (D) Schematic representation of preparing V_2C@PDMAEMA smart hybrid systems. The C atoms are denoted by off-white color, the V atoms are denoted by purple color which occupy every other elemental atomic plane, the Al atoms are denoted by blue color, and occupy every third plane.[93] Reproduced from ref. 93 with permission from the Royal Society of Chemistry, copyright 2015.

4. Regenerative medicine applications

The unique physicochemical and biological properties of 2D MXene materials offer new solutions for the diagnosis and treatment of clinically significant diseases. Novel 2D MXene materials have been extensively investigated in the biomedical field due to their diverse chemistry and structure as well as tunable physicochemical properties, including MXenes in bioimaging, cancer therapy, infection treatment, skin repair, bone regeneration, and other fields. This section highlights recent advances in MXene-based biomaterials for biomedical applications.

4.1 Bioimaging

With the rapid development of nanotechnology in recent years, MXenes and MXene-based composites have attracted increasing attention from researchers due to their special structural, light- and heat-absorbing properties as well as surface multifunctionality; those that have the ability to satisfy the quantum size effect for fluorescence imaging, the intrinsic photothermal properties for photoacoustic imaging (PAI), the elemental enhancement of contrast for X-ray computerized tomography (CT) imaging, and the effective loading of functional contrast agents for magnetic resonance imaging (MRI) with payloads of functional contrast agents, have emerged as the most promising alternative candidates for bioimaging (Table 2).[97]

Compared with conventional organic fluorophores, MXenes and their corresponding QDs show interesting fluorescence properties in bioimaging, such as tunable wavelength, high photostability, and desirable quantum yields. Xue and coworkers reported that photoluminescent Ti_3C_2 MXene quantum dots (MQDs) can be prepared by a facile hydrothermal method, and that they exhibit excitation-dependent

Table 2 Summary of recent research on MXene-based nanomaterials for bioimaging applications

MXene composition	Synthesis strategy	Description	Applications	Ref.
Ti_3C_2 QDs	HF etching and hydrothermal treatment	Displays excitation-dependent photoluminescence spectra with quantum yields up to ≈10%	Fluorescent imaging and Zinc ion Sensor	41
$Ti_3C_2T_x$-derived GQDs	Dimethylformamide (DMF) heat treatment	Tunable photoluminescence, low cytotoxicity, good photostability and chemical inertness	Fluorescent inks, luminescent composites and fluorescent imaging	98
Ti_3C_2 QDs	HF etching and oleylamine heat treatment	Exhibits white photoluminescence and two-photon fluorescence properties	—	99
N-Ti_3C_2 QDs/Fe^{3+}	HF etching and hydrothermal treatment	Uniform size, excellent optical properties, biocompatible	Detection of glutathione in living cells and fluorescence imaging	66
Nb_2C QDs	Pulsed ultrasound-assisted physicochemical stripping in TPAOH	Excellent chemical stability, biocompatibility, photobleaching resistance and enzyme responsive biodegradability	Metal ion sensing and fluorescence imaging	110
Nb_2C QDs	Hydrothermal treatment	Exhibit excellent green fluorescence and exhibit excitation-dependent photoluminescence, anti-photobleaching and dispersion stability	Cu^{2+} sensing and cellular imaging	44
$Ti_3C_2T_x$-Pt-PEG	LiF and HCl etching methods	With POD-like activity, and shows desirable photothermal effects, generating high temperatures that enhance the catalytic activity of the nano-enzymes	PAI and the integration of diagnostic and therapeutic oncology	111
$Ti_3C_2T_x$@Dox	Layer less ionic liquid (IL) stripping technology	Exhibits high drug loading and pH/photosensitivity, good biosafety, excellent photoacoustic imaging	PAI and tumor PTT/PDT	112
Ti_3C_2/Cu_2O	—	Generation of $^{\bullet}OH$ *via* Fenton-like reactions for CDT in acidic tumor environments	PAI and tumor PTT/PDT	113
Ta_4C_3	Combination of HF etching and probe sonication	Reasonable extinction coefficient and very high photothermal conversion efficiency (44.7%), and good photothermal stability	PAI, CT imaging and tumor therapy	105
V_4C_3	HF etching and TPAOH intercalation and ultrasound-assisted processing	Capable of triggering Fenton-like reactions, photothermal ablation, and ROS generation to convert cold tumors to hot tumors (macrophages: M2 → M1)	PAI, CT imaging, and tumor PTT/PDT	106
Ti_3C_2@Au	HF etching and TPAOH stripping	Good biosafety, significantly enhanced absorbance in NIR-I and NIR-II windows, improves tumor oxygenation	PAI, CT imaging and tumor therapy	80
$Ti_3C_2T_x$-Gd	HF etching and sonication	Capture of Gd^{3+} ions leads to change of initial anti-magnetic behavior to paramagnetic with high stability and cytocompatibility	MRI and PTT	109
MnOx/Ta_4C_3 composite nanosheets	HF etching and sonication	Highly biocompatible and biosafe, multiple imaging-guided photothermal thermotherapy significantly inhibits tumor growth	PAI, MRI, CT imaging and tumor therapy	78
Fe-Ti_3C_2	LiF and HCI etching and sonication	NIR irradiation stores and releases ferrous ions and produces ROS through the synergistic action of the Fenton reaction and GSH reduction	MRI and tumor PTT/PDT	114
V_2C	Using algal extraction to embed and layer V_2AlC produces V_2C	High absorption in the NIR region, with photothermal conversion efficiencies up to 48%	PAI, MRI, and PTT for Cancer	115

PL behaviors with high quantum yields of as high as up to 9.9%.[41] The application of MQDs as a multicolor cell imaging reagent was demonstrated by labeling the RAW264.7 cell line, which suggests that MXene-based QDs have great potential for applications in optical, biomedical and cellular imaging. As another example, Zhou *et al.* reported an unprecedented method to synthesize amphiphilic carbide-derived graphene quantum dots (GQDs) from layered $Ti_3C_2T_x$ MXene by solvothermal treatment of the lamellar $Ti_3C_2T_x$ MXene in dimethylformamide (DMF); the GQDs exhibited bright and tunable photoluminescence.[98] Breast cancer cells (MCF-7) were incubated with GQD aqueous dispersions (20 μg mL^{-1}) for 2 h, and strong green and blue fluorescence of MCF-7 cells was observed by laser excitation at 488 nm and 364 nm, respectively, which demonstrated that the GQDs could be internalized efficiently by MCF-7 cells, and the results indicated that GQDs could be used as fluorescent probes for cell imaging applications (Fig. 5A). Most of the MXene QDs (MQDs) reported so far show blue fluorescence emission, and Lu *et al.* have unprecedentedly devised a facile and high-yield method to prepare Ti_3C_2 MQDs with direct white photoluminescence (photoluminescence quantum yield, 9.36%) and two-photon fluorescence (TPFL).[99]

PAI is a new non-invasive and non-ionizing biomedical imaging method developed in recent years that uses non-ionizing laser pulses to irradiate biological tissue. When the tissue absorbs light and converts it to heat, the released heat causes a localized temperature increase and thermal expansion of the tissue, which results in the emission of ultrasound waves (the photoacoustic effect).[100] The photoacoustic signals generated

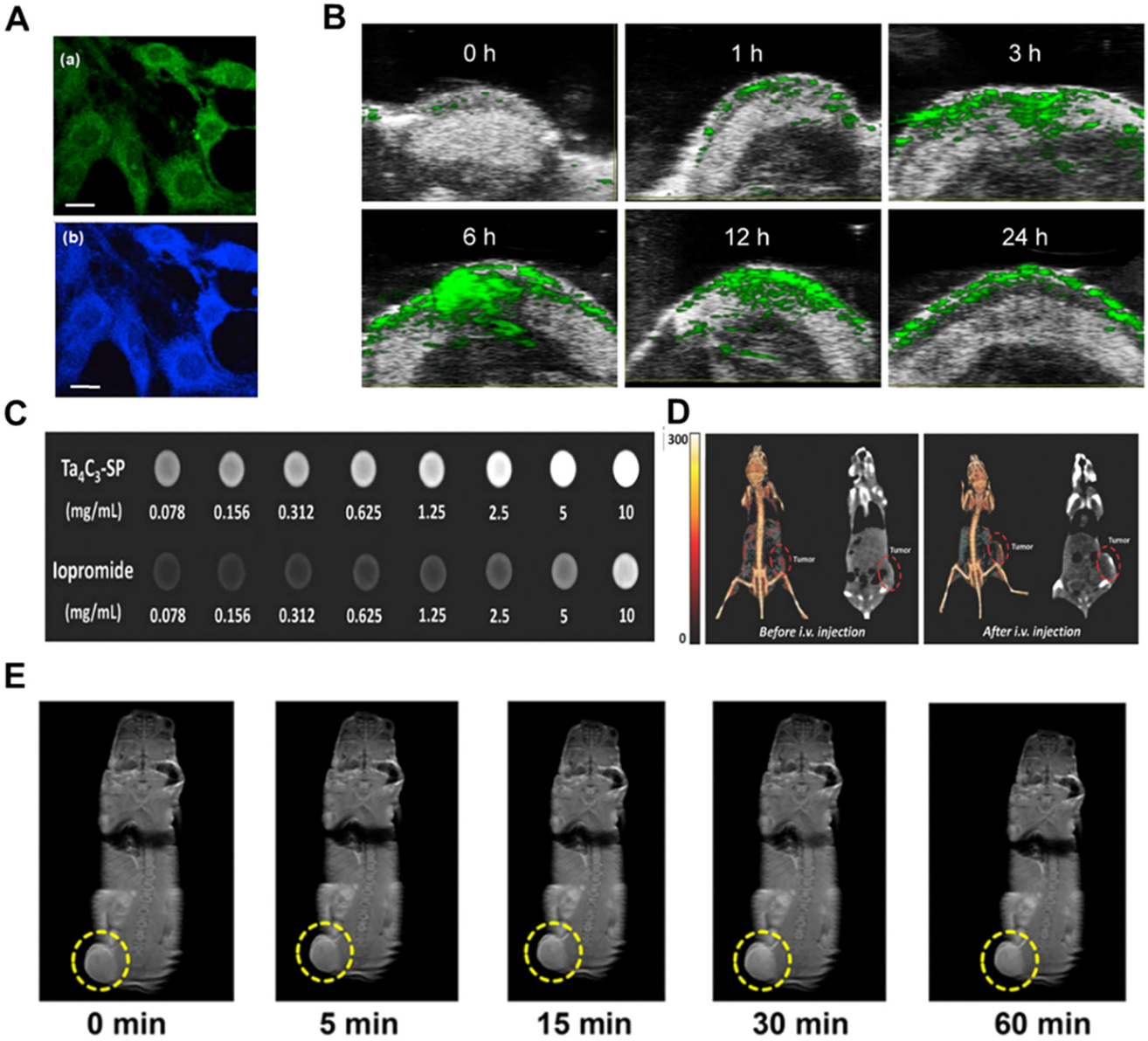

Fig. 5 MXene-based bioimaging applications. (A) CLSM images of MCF-7 cells incubated with GQD for 2 h by excitation at 488 nm (a), 364 nm (b). The scale bar is 20 μm.[98] Reproduced from ref. 98 with permission from Elsevier, copyright 2017. (B) *In vivo* PA images of tumor sites after intravenous injection of $Ti_3C_2T_x$-Pt-PEG at different time intervals.[103] Reproduced from ref. 103 with permission from American Chemical Society, copyright 2022. (C) CT images of Ta_4C_3-SP nanosheet solution (top) and iodine bromide solution (bottom) at different concentrations.[105] Reproduced from ref. 105 with permission from Wiley-VCH, copyright 2018. (D) *In vivo* CT contrast images (right panel) and 3D reconstructed CT images (left panel) of mice before and after intravenous injection of Ta_4C_3-SP nanosheet solution (10 mg mL^{-1}, 200 μL) for 24 h.[105] Reproduced from ref. 105 with permission from Wiley-VCH, copyright 2018. (J) *T*1-Weighted imaging of 4T1 tumor-bearing mice after prolonged intravenous injection of MnO_x/Ta_4C_3-SP composite nanosheets.[78] Reproduced from ref. 78 with permission from American Chemical Society, copyright 2017.

by the photoacoustic effect at biological tissue sites carry information about the light-absorption properties of the tissue that can be further converted into light-absorption distribution images.[101] The excellent photothermal conversion properties of MXene-based materials allow for potential PAI capabilities.[102] For example, Zhu *et al.* reported a $Ti_3C_2T_x$-Pt-PEG nanocomposite with unique NIR-II absorbance and good photothermal conversion efficiency (31.78%), making it a good contrast-enhanced PA imaging nanomaterial.[103] The PA images *in vitro* based on $Ti_3C_2T_x$-Pt-PEG nanocomposites showed unique PA signals, and the intensity of PA signals was concentration-dependent, with PA signals increasing significantly with the increase of sample concentration. After $Ti_3C_2T_x$-Pt-PEG (10 mg kg^{-1}, 100 μL) was intravenously injected into 4T1 tumor-bearing female BALB/c mice, PA images were obtained at different time intervals, and the results showed that the PA signal intensity at the tumor site gradually increased with the increase of time and reached the maximum at 6 h due to the

accumulation of $Ti_3C_2T_x$-Pt-PEG nanocomposites at the tumor site (Fig. 5B).

CT imaging uses X-rays to penetrate different tissues of the body with different attenuation coefficients.[104] It measures the intensity of X-rays through a certain thickness of the object to be measured and converts the X-ray intensity from black to white to grayscale. CT imaging has a high spatial resolution and deep tissue penetration and is used for 3D tomography of anatomical structures based on the difference in X-ray absorption between lesions and tissues, and is therefore widely used mainly for medical diagnostics. Since the X-ray attenuation coefficient increases with increasing atomic number, nanomaterials containing high atomic number (Z) elements are often explored as contrast agents (CAs) for CT imaging. In this regard, tantalum (Ta)-based MXenes (Ta_4C_3) can undoubtedly be used as CA for CT imaging because of the high atomic number of tantalum (Z = 73) and the large attenuation coefficient of X-rays.[105] For example, Lin and his colleagues reported that CT images of different concentrations of biocompatible soybean phospholipid (SP)-modified Ta_4C_3 (Ta_4C_3-SP) in xanthan gum showed a dramatic enhancement of the signal as the concentration of Ta_4C_3-SP increased, and the signal intensity was stronger than that of commercial iodine-based CT CAs (Fig. 5C). Ta_4C_3-SP (20 mg kg^{-1}) was intravenously injected into mice carrying 4T1 tumors for *in vivo* CT imaging, and the CT images obtained 24 hours after injection showed significant tumor contrast, which demonstrated that Ta_4C_3 MXene can be used as a promising CAs for CT imaging of tumors (Fig. 5D). In addition, Feng *et al.* reported a V_4C_3 MXene nanosheet with excellent photothermal and X-ray absorption properties for dual-modality PA/CT imaging.[106]

MRI has been widely used for clinical diagnostic imaging due to its high spatial resolution, excellent three-dimensional soft tissue contrast difference, and noninvasive properties.[107] During MRI, the body is placed in a static magnetic field and certain radiofrequency (RF) pulses are used to excite the nucleus of a hydrogen atom and indicate the presence of protons (^{1}H). When the RF pulses are stopped, the protons return to an equilibrium state in the magnetic field and produce weak energy (MRI signals) during the relaxation process. When these signals are received, magnetic resonance images can be obtained by processing them with spatial resolution and image reconstruction. The intensity of the MR signal is mainly dependent on the relaxation time of the hydrogen protons. The utilization of MXenes in MRI is limited by their usual antimagnetism; however, it is possible to functionalize the MXene with ferromagnetic or paramagnetic compounds and nanoparticles, which can be effective in increasing the difference in tissue MRI signals to improve imaging contrast and clarity, provide information about the directional location of tumors, and guide photothermal ablation and chemotherapy of tumors.[108] In a study, Gd was utilized to chelate with $Ti_3C_2T_x$ to obtain MXene-Gd, which can be used as a CA for MRI.[109] The investigators found that the relaxation value of pristine MXene was close to zero due to the diamagnetic nature of the electronic degrees of freedom in the pristine flakes, and the relaxation ($r1$) increased significantly to 5.87 s^{-1}/mM (at a 0.5 T magnetic field) after entrapment of Gd^{3+} ions. Dai *et al.* proposed another surface engineering strategy to grow manganese oxide nanoparticles *in situ* onto the surface of Ta_4C_3 MXene, and after further surface organic modification with soybean phospholipids (SP), the MnO_x/Ta_4C_3-SP composite nanosheet system was obtained, which can be used for multiplexed imaging-guided photothermal tumor ablation.[78] Among them, the Mn^{2+} released from the MnO_x/Ta_4C_3-SP composite nanosheets could effectively enhance the relaxation of hydrogen protons, indicating its performance as an MRI CA *in vivo*. During the test period of 60 min after intravenous injection of MnO_x/Ta_4C_3-SP composite nanosheets (20 mg kg^{-1}, 100 μL) into 4T1 tumor-bearing mice *in vivo*, MRI signal enhancement of the tumor tissues and their corresponding enlargement of the $T1$-weighted MR images could be clearly observed (Fig. 5E).

Currently, most of the research on MXene bioimaging focuses on $Ti_3C_2T_x$, a class of MXene, and more luminescent nanomaterials based on other MXenes are expected to be developed for bioimaging applications in the future.

4.2 Cancer therapy

With excellent optical/electrical properties, biocompatibility, ease of functionalization and enzyme immobilization, MXenes can be used to enhance the biocompatibility, tumor-targeting ability, and anti-tumor effects of the resulting therapeutic platforms through elemental doping, surface oxidation, nanohybridization, or surface encapsulation to cope with the complex tumor microenvironment. MXenes and MXene-based nanomaterials are capable of inhibiting tumors through various therapeutic mechanisms, including PTT, chemodynamic therapy (CDT), PDT, and sonodynamic therapy (SDT), and have made significant advances in being used in various cancer models and therapeutic strategies (Table 3).

As a typical non-invasive treatment method, PTT ablates tumors with the help of heat generated by light excitation, which has the advantages of high selectivity, non-invasiveness, low toxicity, low cost and strong targeting. However, the application of traditional anti-tumor PTT is often hampered by the limited depth of light penetration and the insufficient efficiency of material photothermal conversion. In recent years, MXenes have shown great potential in the treatment of deep-seated tumors due to their strong absorption in the NIR region and good photothermal conversion efficiency, and have become an excellent candidate for anti-tumor PTT under NIR-I and NIR-II windows. Tang *et al.* optimized the well-known electronic structure and NIR-II absorption of Ti_3C_2 using an anionic solid solution with the help of lattice N modulation and associated additional electron injection, which enhanced the response in the NIR-II region (Fig. 6A).[116] Among them, $Ti_3C_{1.23}N_{0.77}$ showed a high photothermal conversion efficiency of 12.0% at 1064 nm at a low concentration of 5 ppm, and exhibited efficient NIR-II PTT ablation of tumors both *in vitro* and *in vivo*. The results suggest that ideas for optimizing low-dose tumor photothermal therapy can be provided

Table 3 Summary of recent research on MXene-based nanomaterials for cancer therapy applications

MXene composition	Synthesis strategy	Animal models	Treatment strategy	Ref.
Ti_3C_2-based anionic solid solutions	HF etch-assisted sonication	4T1 tumor model in BALB/c mice	PTT	116
Ti_3CN	HF etch-assisted sonication	The homograft 4 T1 tumor model	PTT	117
V_4C_3/ATO@BSA	HF/tetrapropylammonium hydroxide (TPAOH) method	4T1 tumor-bearing mice model	Nanozyme catalytic/PTT	118
n-HA/g-C_3N_4/MXene scaffold ($Ti_3C_2T_x$)	HF etching and DMF ultrasonication	Saos-2 tumor-bearing mouse model	PTT/PDT	124
A wearable biological electrothermal patch based on $Ti_3C_2T_x$	HF etch-assisted sonication	B16F10 tumor-bearing C57BL/6J mice model	PTT	125
Mo_2C-PVA	LiF/HCl and HF/TBAOH method	4T1 tumor-bearing mice model	PTT	11
NMQDs-$Ti_3C_2T_x$	HF etching and micro-explosive methods	BALB/c nude mice bearing HeLa tumor xenograft model	CDT	119
FA@MXene/CuO_2/GA (Ti_3C_2 MXene)	HF etch-assisted sonication	4T1 tumor model in BALB/c mice	PTT/CDT	120
$Cu_2O/Ti_3C_2T_x$	HF etching-assisted ultrasonic stripping method	The xenograft model of 4 T1 cells	PTT/CDT	126
$Ti_3C_2T_x$-GOx/DOX-PEG	LiF etching and TPAOH intercalation	4T1 tumor-bearing BALB/c mice model	Chemo/starvation/ photothermal combination therapy	95
CoPc-Mn/$Ti_3C_2T_x$	HF etching	B16-tumor-bearing mice model	PTT/CDT/PDT	127
BTO@Nb_2C-PEG	HF etching and TPAOH intercalation	4T1 tumor-bearing mice model	PTT/PDT	121
Ti_3C_2-DOX	LiF etching and TPAOH intercalation	HCT-116 tumor-bearing mice model	PTT/PDT/chemo therapy	22
H-Ti_3C_2 NSs	Chemical exfoliation and high-temperature treatment	4T1 tumor-bearing mice model	PTT/SDT	122
Ti_3C_2/CuO_2@BSA	HF etching and TPAOH intercalation	The U87 tumor-bearing BALB/c nude mice model	SDT/CDT	123

by modulating the anions in the MXene. Liu *et al.* successfully developed a unique metal–carbon nitride (d-Ti_3CN) MXene with excellent photothermal properties for efficient photothermal therapy of tumors both *in vitro* and *in vivo*, and tumor-free treatment could be achieved at 1064 nm irradiation with minimal side effects.[117] Although MXene exhibits better PTT performance than other photothermal nanomaterials in tumor therapy, researchers have found that surface modification of MXene can further enhance its photothermal effect. For example, by modifying the nanosystem (V_4C_3/ATO@BSA, VAB) obtained by modifying bovine albumin (BSA) and Atovaquone (ATO) on V_4C_3, Zhao *et al.* calculated that the photothermal conversion efficiency of VAB was as high as 61%, which was higher than that of V_2C (48%), and the nanoplatform could exhibit significant anti-tumor effects by disrupting redox homeostasis as well as PTT in tumor cells.[118]

CDT utilizes metal ions (*e.g.*, Fe^{2+}, Cu^{2+}, Mn^{2+}, Ti^{3+}, and Nb^{2+}) to catalyze a Fenton or Fenton-like reaction of H_2O_2 to produce cytotoxic $^{\bullet}OH$ to kill tumors. However, there are challenges such as low catalytic efficiency, poor biocompatibility and even potential toxicity. Based on the excellent biocompatibility of MXene, it has become an emerging hot nanomaterial for researchers to implement effective and safe anti-tumor CDT. Li *et al.* proposed a $Ti_3C_2T_x$ quantum dot with excellent biocompatibility that could generate a large amount of $^{\bullet}OH$ through Fenton-like reaction when combined with H_2O_2, and it could inhibit tumors up to 91.9% without damaging normal tissues.[119] To further enhance the application of MXene in tumor CDT, researchers have attempted to dope various metal ions (with CDT catalytic activity) into the structure of MXene nanosheets for synergistic PTT and CDT treatment of tumors. For example, Xiong *et al.* developed a near-infrared (NIR)-light-triggered MXene nanocomposite (FA@MXene/CuO_2/GA), in which the photothermal effect of MXene significantly accelerated the CuO_2-catalyzed conversion of $^{\bullet}OH$, resulting in an excellent synergistic PTT/CDT anticancer therapeutic effect (Fig. 6B).[120]

PDT has the advantage of being non-invasive and spatiotemporally specific to kill cancer cells with the help of localized ROS generation under light irradiation. However, the therapeutic efficacy of PDT is greatly reduced by the limited reactive oxygen species (ROS) generation due to the hypoxic tumor microenvironment and the rapid electron–hole pair complex mediated by light irradiation. MXene-based nanomaterials have excellent photothermal effects, and the heat generated by laser irradiation promotes electron–hole space separation, which reacts with the surrounding O_2 and H_2O molecules to produce toxic ROS, making them popular research materials for implementing PTT/PDT synergistic therapies. Zhang *et al.* rationally developed a multifunctional therapeutic nano-heterojunction in which two-dimensional niobium carbide (Nb_2C) MXene was grown *in situ* with barium

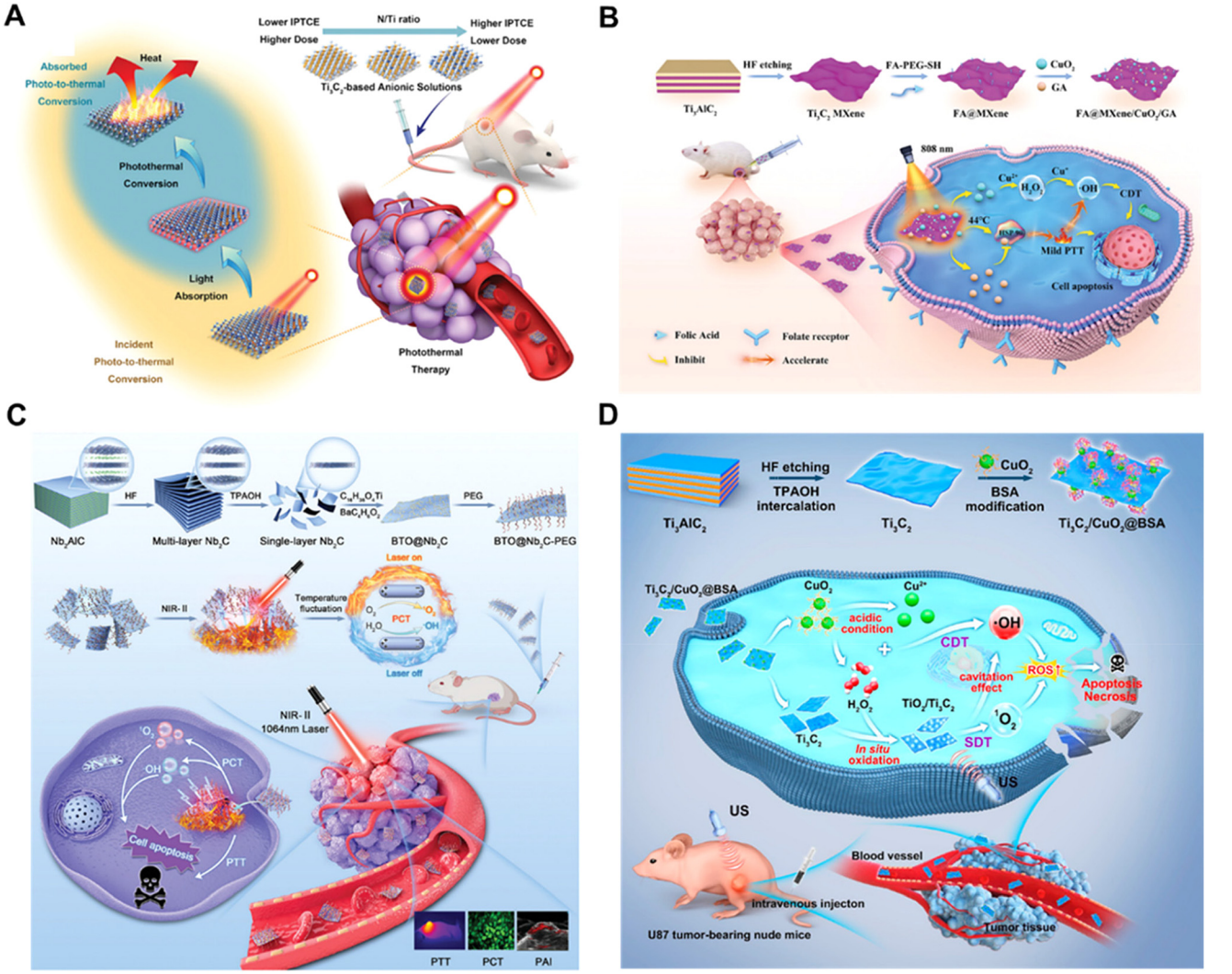

Fig. 6 MXene-based applications in cancer therapy. (A) Schematic illustration of Ti_3C_2-based anionic solid solutions for NIR-II photothermal therapy *in vivo*.[116] Reproduced from ref. 116 with permission from Wiley-VCH, copyright 2023. (B) Schematic illustration of FA@MXene/CuO_2/GA nanocomposite: synthesis and therapeutic mechanism.[120] Reproduced from ref. 120 with permission from Wiley-VCH, copyright 2024. (C) Schematic illustration of the pyroelectric nanocatalysts BTO@Nb_2C-PEG for PTT and PCT-augmented cancer therapy.[121] Reproduced from ref. 121 with permission from Wiley-VCH, copyright 2023. (D) Schematic illustration of 2D MXene-originated *in situ* nanosonosensitizer generation for augmented and synergistic sonodynamic tumor nanotherapy.[123] Reproduced from ref. 123 with permission from American Chemical Society, copyright 2022.

titanate (BTO) to generate a robust photogenerated pyroelectric catalyst called BTO@Nb_2C nanosheets, which could enhance the ROS generation and achieve a synergistic effect of combining the materials' PTT and PDT with tumor inhibition rate of 94.9% *in vivo* (Fig. 6C).[121] As another example, Liu *et al.* synthesized a multifunctional nanoplatform (Ti_3C_2-DOX) that exhibited excellent photothermal conversion efficiency (~58.3%) and effective single-linear oxygen generation ($^1O_2$) under 808 nm laser irradiation.[22] *In vitro* and *in vivo* experiments demonstrated that Ti_3C_2-DOX showed enhanced biocompatibility, tumor-specific accumulation, and stimuli-responsive drug release behaviors, and achieved effective cancer cell killing and tumor tissue destruction *via* photothermal/photodynamic/chemotherapeutic synergistic therapy.

SDT has attracted wide interest in biomedicine for its novel noninvasive therapeutic approach triggered by ultrasound (US). Despite the advantages of high tissue penetration depth, absence of ionizing radiation and low cost, SDT still suffers from low ROS quantum yield, limited delivery efficiency and potential toxicity of acoustic sensitizers. Researchers have designed various MXene-based nanosystems to perform effective antitumor SDT. For example, Li *et al.* developed Ti_3C_2 MXene nanosheets (H-Ti_3C_2 NSs) with good acoustic sensitizer properties by a two-step method of chemical stripping and high-temperature treatment, and by high-temperature treatment, the oxygen defects of H-Ti_3C_2 NSs greatly increased.[122] The electrons (e^-) and holes (h) generated by US could be separated faster due to the increased oxidation, and then H-Ti_3C_2

NSs could take advantage of the abundant oxygen defects to prevent the recombination of e^- and h under the irradiation of US, greatly improving the acoustic kinetic efficiency. The *in vivo* study further showed that the increased blood supply resulting from the mild photothermal effect significantly alleviated the hypoxic condition in the tumor microenvironment, showing that PTT enhanced the effect of SDT. In another study, a nanoacoustic sensitizer/nanocatalyst (Ti_3C_2/CuO_2@BSA) was reported to achieve high-performance and synergistic acoustic/chemodynamic tumor therapy by generating nanoacoustic sensitizers *in situ* in response to the tumor microenvironment.[123] Integration of CuO_2 nanoparticles on 2D Ti_3C_2 MXene allowed *in situ* generation of H_2O_2 and oxidation of Ti_3C_2 to generate TiO_2 nanosensitizers for acoustic sensitization in an acidic tumor microenvironment, while the oxidized carbon matrix enhanced the separation of e^- and h, which further improved the efficacy of SDT (Fig. 6D). Ultrasound irradiation during the sonodynamic process also enhanced the copper-triggered Fenton-like reaction to generate more ROS, thus synergizing the SDT.

MXene-based nanomaterials exhibit multimodal therapeutic potential in cancer therapy, including PTT, CDT, PDT, and SDT, due to their excellent optical/electrical properties and biocompatibility, enhanced therapeutic efficacy and biocompatibility through different strategies and surface modifications, and due to responding effectively to the complex tumor microenvironment.

4.3 Infection therapy

Infectious diseases refer to a group of diseases caused by pathogens such as bacteria, fungi, viruses, and parasites that infect the human body, and are still the second leading cause of death in humans. When the body is attacked by an infection, it triggers intense oxidative stress and significant inflammatory responses that may impede the healing process of the disease. Especially for wounds damaged by multidrug-resistant bacteria, conventional antibiotics are powerless. In recent years, MXene-based materials have become an effective option for the treatment of infectious diseases due to their excellent antioxidant and anti-inflammatory properties, photothermal/photodynamic antimicrobial performance, and low bacterial resistance (Table 4).

Table 4 Summary of recent research on MXene-based nanomaterials for infection therapy

MXene composition	Synthesis strategy	Description	Animal models	Ref.
Pt@V_2C	HF etching and TPAOH intercalation	Effective in the removal of bacteria and bacterial biofilms and may modulate inflammation through the NOD-like receptor signaling pathway and the IL-17 signaling pathway	A subcutaneous abscess model in mice infected with MRSA, the MRSA-infected keratitis model	128
Ti_3C_2 MXene/Fe-MOFs composite (MXM)	LiF/HCl etching and ultrasonication	The photothermal conversion efficiency is close to 51.9% and exhibits NIR-enhanced POD-like activity	The MRSA infected burn wound model	129
HNTM/Ti_3C_2 hybrid nanomaterials (HN-Ti_3C_2)	HF etching and DFM heat treatment	Effective killing of MRSA by SDT and promotion of bone regeneration through activation of calcium, Wnt, and TGF-β signaling pathways	A MRSA-infected rat tibial osteomyelitis model	130
Nb_2C@TP	HF etching and TPAOH intercalation	Significantly down-regulates energy metabolism-related pathways and activates Agr in bacteria, which fundamentally kills bacteria, inhibits biofilm formation and promotes biofilm separation	A mouse subcutaneous infection model	131
GA/OKGM/MT hydrogel (MT: Ti_3C_2@TiO_2)	HF etch-assisted sonication	PTT effectively destroys bacteria and eliminates excess ROS, thereby facilitating the transition from the inflammatory to the proliferative phase	The *S. aureus*-infected wound model in SD rats	133
Monolayer high-entropy (HE) MXenes	Selectively etched through a high-entropy MAX phase (HE MAX)	NIR-II-enhanced endogenous oxidase mimetic activity, excellent photothermal conversion efficiency and very high biocatalytic activity	Bacterial keratitis (BK) and subcutaneous abscess infections model induced by MRSA	134
VS_4/Ti_3C_2 (VSM)	LiF/HCl etching and ultrasonication	Schottky junction, POD-like activity and acoustic dynamics	A tibial plateau MRSA-infected bone defect model	135
CuS/$Ti_3C_2T_x$@VMP	HF etch-assisted sonication	Significantly promotes skin rejuvenation through pathogen elimination, angiogenesis promotion and collagen deposition	Full-thickness wounds infected by *S. aureus*	136
V_2N	HF etching and TPAOH intercalation	Excellent OXD and POD catalytic activity, ideal photothermal conversion efficiency, abundant ROS generation	A mice subcutaneous abscess model in BALB/c mice	137
PLGA-$Ti_3C_2T_x$/Ag_2S@LOx	LiF/HCl etch-assisted sonication	Promotes wound healing by killing bacteria, stopping bleeding, promoting epithelialization/collagen deposition in the wound bed and angiogenesis	An *S. aureus*-infected mouse skin wound model on the dorsal sites of mice	138
$Ti_3C_2T_x$, $Ta_4C_3T_x$, $Mo_2Ti_2C_3T_x$ and $Nb_4C_3T_x$	HF etching and TPAOH intercalation	$Ti_3C_2T_x$ and $Mo_2Ti_2C_3T_x$ MXene showed antiviral activity against SARS-CoV-2	—	132

MXene-based nanomaterials with strong biocompatibility and photothermal conversion efficiency can be used for PTT antimicrobial treatment of bacterial infectious diseases. The laser irradiation range of the V_2C MXene is limited to the near-infrared I region (NIR-I), which restricts its penetration into tissues and makes it difficult to achieve complete bacterial eradication with single-acting therapeutic strategies. To address this issue, He *et al.* attached platinum nanoparticles (Pt NPs) to V_2C to form an artificial nanoplatform (Pt@V_2C).[128] Due to the localized surface plasmon resonance (LSPR) effect of Pt NPs and V_2C, Pt@V_2C exhibited enhanced photothermal conversion efficiency (59.6%) and longer irradiation lasing (NIR-II). Notably, Pt@V_2C possessed CDT- and NIR-II-enhanced oxidase (OXD), POD-like activities. In an *in vivo* animal model, Pt@V_2C effectively cleared MRSA from deep tissues in the setting of subcutaneous abscesses and bacterial keratitis through the synergistic effect of PTT/CDT, down-regulated the expression of CD86 and IL-6 in the infected tissues, accelerated abscess regression, and facilitated the healing of wounds and corneas (Fig. 7A). In another study, Zhao *et al.* proposed a strategy for NIR plasmonic enhancement of the catalytic and photothermal properties of nanoenzymes for effective anti-infective and antibacterial applications.[129] A Ti_3C_2 MXene/Fe-MOFs composite (MXM) with NIR plasmonic-enhanced CDT and photothermal properties was successfully developed by loading metal–organic framework (MOF) nanoenzymes on Ti_3C_2 MXene. SEM images demonstrated the morphological changes of *E. coli*, MRSA, and *C. albicans* after treatment with NaAc buffer, H_2O_2, MXM, and MXM + H_2O_2 (100 μg mL^{-1}) irradiation with or without NIR (Fig. 7B). The cell membranes of Control and H_2O_2 groups remained intact, and the treatment effect was negligible. However, some wrinkles in the bacterial membrane were observed in the MXM + H_2O_2 or MXM + NIR groups, indicating significant CDT activity and excellent photothermal properties of MXM, respectively. The results of *in vivo* experiments showed that the LSPR-induced MXM system has outstanding antibacterial properties and promotes rapid healing of MRSA-infected burn wounds. SDT is a novel strategy for overcoming the problem of bacterial resistance to antibiotic therapy. For example, Wang and his colleagues developed a HNTM/Ti_3C_2 hybridized nanomaterial (HN-Ti_3C_2) with Schottky heterojunction for efficient SDT for osteomyelitis and bone regeneration.[130] Ti_3C_2 greatly improved the acoustic catalytic performance by rapidly transferring the carriers generated by HNTM under US irradiation and killed drug-resistant bacteria by generating a large amount of ROS, and it showed an excellent 99.75% antimicrobial effect against MRSA. In addition, the acoustic flow generated by HN-Ti_3C_2 at low intensity US could promote the proliferation of stem cells by regulating the cell cycle, DNA replication and apoptosis, thereby promoting the long-term repair of bone defects. In the MRSA-infected rat tibial osteomyelitis model, HN-Ti_3C_2 successfully eliminated the infection and significantly improved bone regeneration under US irradiation. The various synergistic effects generated based on MXenes hold great promise for the design and fabrication of novel and effective MXene nanocomposites to combat bacterial infections.

With the proliferation of indwelling devices and implants, the associated infections caused by invasive bacterial adhesion and biofilm formation on medical implant surfaces are increasingly recognized as an intractable global public health problem. MXene nanosheets are promising safe candidates for implant surface modification, bringing biofilm-resistant properties to implantable devices. For example, researchers have combined two-dimensional Nb_2C MXene nanosheets with medical titanium plates (TP) to craft a biofunctional Nb_2C@TP (NTP) therapeutic platform for multimodal infection control with bacterial clearance and tissue regeneration (Fig. 7C).[131] Confocal 3D images showed that the TP group was covered by live bacteria with dense stacked biofilm structures, while almost no dead and live bacteria biofilms were detected in the Nb_2C@TP group (Fig. 7C). Nb_2C@TP played a crucial role in inhibiting bacteria through multiple modes. In terms of biofilm elimination, Nb_2C@TP activated an auxiliary gene regulator (Agr) that prevented bacterial adhesion and promoted biofilm separation when bacteria attempted to invade the implant surface. In addition, Nb_2C@TP directly killed bacteria through metabolic pathways such as the downregulation of the tricarboxylic acid (TCA) cycle and the phosphotransferase system (PTS) pathway, leading to bacterial death. In terms of planktonic bacterial clearance, Nb_2C@TP sensitized bacteria to thermotherapy and killed them *via* NIR-responsive thermotherapy. In addition to excellent bacterial clearance, Nb_2C@TP attenuated excessive pro-inflammatory and oxidative stress *in vivo* and accelerated angiogenesis and tissue remodeling processes. Nb_2C@TP holds promise for treating cases of implant-associated infections with bacterial/biofilm clearance and tissue remodeling capabilities.

In addition to antimicrobial activity, several studies have demonstrated the potential application of 2D materials as antiviral agents. In one study, MXenes were found to possess antiviral activity, and have the potential to be used as therapeutic agents for viral infectious diseases in the future.[132] Using SARS-CoV-2 as a model, the researchers explored the antiviral properties and immune profiles of a large group of four highly stable and well-characterized MXenes ($Ti_3C_2T_x$, $Ta_4C_3T_x$, $Mo_2Ti_2C_3T_x$ and $Nb_4C_3T_x$). It was found that $Ti_3C_2T_x$ and $Mo_2Ti_2C_3T_x$ showed antiviral activity against SARS-CoV-2, with $Ti_3C_2T_x$ being the most effective material tested against SARS-CoV-2 particles, and did not produce cytotoxicity in any of the peripheral blood mononuclear cell populations. The authors described the mechanism of MXene-dependent antiviral activity by docking analysis, proteomics data, and comparison with SARS-CoV-2 protein interaction profiles (Fig. 7D). $Ti_3C_2T_x$ exerts its viral inhibitory activity not only on the cell surface but also through different signaling mechanisms including membrane trafficking, GPCR signaling, mitochondrial function, metabolic pathways and viral replication. The results indicated that host proteins such as GNG5, GRPEL1 and NUTF2 are important regulators of $Ti_3C_2T_x$-dependent antiviral activity. These host proteins interact with viral NSP7,

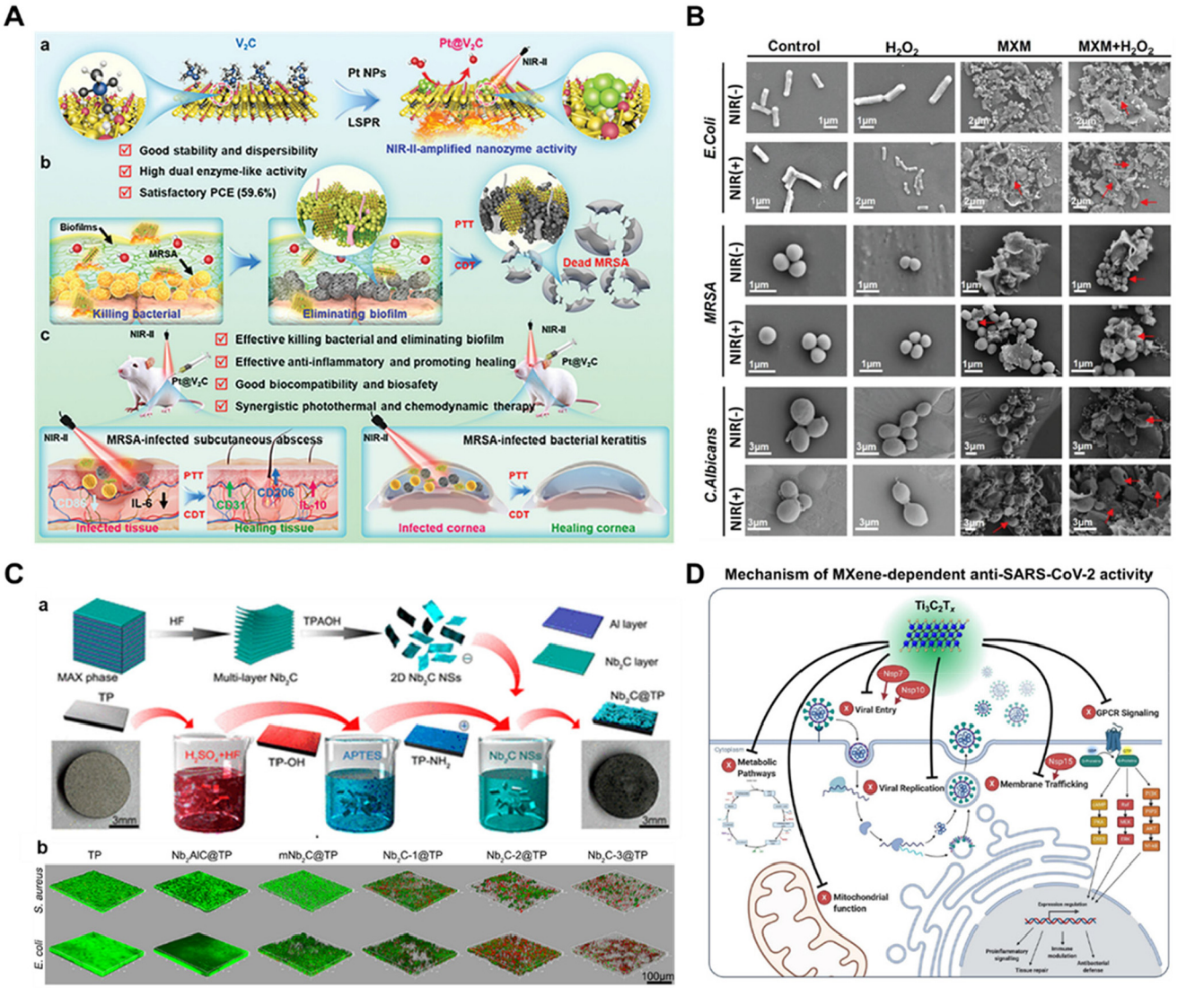

Fig. 7 MXene-based applications in infection therapy. (A) Schematic illustration of the construction, antibacterial, and anti-infective therapy of Pt@V_2C nanoplatforms with photothermal and chemodynamic therapy.[128] Reproduced from ref. 128 with permission from Wiley-VCH, copyright 2024. (B) SEM images of *E. coli*, MRSA and *C. albicans* exposed to different samples without and with NIR irradiation (808 nm laser, 1.25 W cm^{-2}). MXM concentration is 200 μg mL^{-1}. The concentration of *E. coli*, MRSA, and *C. albicans* is 1.0×10^8 CFU mL^{-1}, respectively. H_2O_2 concentration is 100 μM.[129] Reproduced from ref. 129 with permission from Wiley-VCH, copyright 2023. (C) (a) Preparation and characterization of Nb_2C@TP. (b) Confocal 3D images of biofilm. Green indicates live bacteria, and red indicates dead bacteria.[131] Reproduced from ref. 131 with permission from American Chemical Society, copyright 2020. (D) Overview of the mechanism of MXene-dependent viral inhibition.[132] Reproduced from ref. 132 with permission from Elsevier, copyright 2021.

NSP10 and NSP15 proteins, respectively. During SARS-CoV-2 infection, NSP7 plays an important role in membrane transport and G protein-coupled receptor (GPCR) signaling, and NSP15 is involved in vesicular and nuclear transport mechanisms. NSP7 and NSP10 are among the several proteins that can alter the endosomal membrane compartment to facilitate viral entry and replication. Thus, MXenes are able to exert their antiviral activity by modulating these viral proteins and pathways that are important for viral transmission. This study provides guidance for future research into the implementation of MXene nanomaterials in tools targeting viral infectious diseases as well as any immune system-related syndromes.

MXene-based nanomaterials show great potential in the field of infectious disease therapy due to their unique physicochemical properties. These materials not only possess excellent biocompatibility and photothermal conversion efficiency for effective PTT antimicrobial activity, but also synergize antimicrobial activity through multiple mechanisms such as CDT, PDT, and SDT. The surface functional groups of MXenes allow for easy functionalization, enhancing their prospects for application in antimicrobial and antiviral therapies, especially in

combating infections with multidrug-resistant bacteria. In addition, the antiviral activity of MXenes provides a new direction for the treatment of viral infectious diseases in the future. In summary, MXene-based nanomaterials have a wide range of applications in the treatment of infectious diseases and provide a powerful tool for the development of novel antibacterial and antiviral therapeutic strategies.

4.4 Wound healing

Wounds are breaks in the skin caused by various external injuries. The presence of a wound greatly increases the risk of infection, which often leads to deterioration of the wound condition, prolonged wound healing, a complicated healing process, and even death.[139] Wound healing is a complex process involving multiple cell types within the epidermis, dermis, and subcutaneous layers and consists of four highly integrated and overlapping phases: hemostasis, inflammation, proliferation, and tissue remodeling.[140] All of these steps must be performed precisely to successfully heal wounds. MXenes have antimicrobial, anti-inflammatory and antioxidant properties, promoting cell adhesion and proliferation as well as tissue regeneration, and the integration of MXenes with other bioactive materials to form multifunctional composites has emerged as a promising strategy for wound healing (Table 5).

Bacterial infections (persistent bacterial colonization, high oxidative stress and severe inflammation) are the first serious challenge for wound healing. MXenes have excellent antimicrobial properties; however, MXenes alone cannot meet the requirements for treating the complexity of bacterial-infected wounds. Biomedical hydrogels with good hydrophilicity, biocompatibility, extracellular matrix-like properties and customizable properties have attracted much attention from researchers in inducing skin wound repair.[141] Researchers have proposed improved strategies for introducing MXenes

Table 5 Summary of recent research on MXene-based nanomaterials for wound healing

MXene composition	Synthesis strategy	Characteristic	Animal models	Ref.
FPSa@$Ti_3C_2T_x$	LiF/HCl etch-assisted sonication	Injectable, rapid gelation, conductive, photothermal, antioxidant, anti-inflammatory and promotes vascular regeneration	A mouse full-thickness skin wound MRSA infection model and a burn wound model	142
F127-$Ti_3C_2T_x$-Exo (FM-Exo)	LiF/HCl etch-assisted sonication	Photothermal antimicrobial, promotes fibroblast proliferation, migration and angiogenic capacity of endothelial cells and overcomes high glucose-derived immunosuppression	The full-thickness cutaneous wound model	143
MNPs@MXene-hydrogel	LiF/HCl etch-assisted sonication	Antimicrobial resistance, photothermal properties, multi-stimulus responsiveness and controlled drug delivery capabilities	The full-thickness cutaneous wound and subcutaneous infected wound of the rat model	144
HA-DA/Ti_3C_2@PDA	HF etching and TPAOH intercalation	Hemostasis, O_2 release, scavenging of ROS as well as reactive nitrogen, promotion of proliferation and migration of HUVECs and modulation of macrophage phenotype	The full-thickness cutaneous wound model in infected diabetic mice	145
Ti_3C_2@TA/Fe-hydrogel	HF etching and TPAOH intercalation	POD/CAT-like activity, antioxidant, resistance to protein adsorption and bacterial adhesion, antimicrobial, promotion of granulation tissue regeneration, epithelial formation and collagen deposition	Burn wound model in SD rats	148
FGDN hydrogel (Nb_2C@PDA)	HF etching and TPAOH intercalation	Hemostatic, eradication of bacterial infections, anti-inflammatory and antioxidant, angiogenesis, promotion of granulation tissue production, collagen deposition and re-epithelialization	A mouse full-thickness cutaneous MRSA-infected wound model	149
$Ti_3C_2T_x$ composite fibers	—	Unidirectional thermal conductivity, photothermal properties, and the ability to effectively kill drug-resistant bacteria and residual cancer cells after surgery	Tumor recurrence models in NVSG mice and full-thickness skin wound in SD rats	150
MN-PGA-Ti_3C_2-GOx	—	Reduces local glucose and pH, antioxidant, induces mild hyperthermia, enhances catalytic activity of GOx, promotes cell proliferation, migration, angiogenesis and tissue remodeling	A diabetic mouse dorsal wound model	151
Fe_2O_3/Ti_3C_2-MXene@GOx (FMG)	HF etching and sonication	Excellent photothermal, photodynamic, and chemodynamic properties, induces bacterial iron death	A full-thickness skin defect model in diabetic SD rats with *S. aureus* infection	146
AgNPs/$Ti_3C_2T_x$/GG/Alg-PBA	—	Mechanical properties, excellent healing ability, reliable injectability, easy degradability, biocompatibility, antimicrobial capacity, ability to monitor body signals	A murine full-thickness wound model	147
$Ti_3C_2T_x$-based conductive composite ionogel patch	LiF/HCl etch-assisted sonication	Good photothermal effect to kill bacteria and prevent wound infection, on-demand electrical stimulation to promote wound healing by increasing the expression of growth factors, good transmittance for visualization and real-time monitoring of treatment effect	The infected skin wound model	152

into hydrogel systems, both to enhance the performance of the MXene and to stimulate new functionalities. For example, Ma *et al.* designed a hydrogel (FPSa@M) self-assembled from $Ti_3C_2T_x$ MXene and poly (salicylic acid)-Pluronic F127-poly (salicylic acid) (Fig. 8A).[142] FPSa@M exhibits injectability, rapid gelation, electrical conductivity, as well as beneficial antioxidant and photothermal effects. The photothermal temperature-tunable FPSa@M hydrogel effectively achieved complete photothermal eradication of high concentrations of multidrug-resistant bacteria and significantly promoted healing of complex wounds caused by MRSA infections or burns by remodeling the oxidative stress and inflammatory microenvironment of wound healing through the activation of heat shock protein 90 (HSP90), scavenging of ROS, and angiogenesis. In another study, a simple and effective nano-hydrogel composite (FM-Exo) of F127-MXene (FM) composite with M2 macrophage exosomes (Exo) was reported.[143] The effect of macrophage-conditioned medium obtained from the FM-Exo group on the behavior of HUVECs in a high-glucose microenvironment was investigated, and the results showed that high-glucose stimulation impaired the migratory and tube-forming abilities of HUVECs compared with those of the normal-glucose group, and that HUVECs treated with the FM-Exo-conditioned medium exhibited optimal migratory as well as tube-forming abilities. Yang *et al.* designed an MXene-based hydrogel based on multiple stimulus responses.[144] When exposed to NIR or AMF, the temperature of the MXene increased significantly, leading to the contraction of the hydrogel system, thus precisely controlling the release of therapeutic drug AgNPs and eliminating bacteria adhering to the wound depth. Wound images also demonstrated that this MXene-based hydrogel exhibited the best wound closure under NIR irradiation. In addition, another study found that the MXenes-based hydrogel treatment group could effectively reduce ROS levels in wounds, up-regulate the expression of epidermal growth factor (EGF) and vascular endothelial growth factor (VEGF), and down-regulate the expression of hypoxia-inducible factor-1 α (HIF-1α), which suggests that the MXene-based hydrogel could accelerate diabetic wound healing by advancing the formation of the epidermis, alleviating local hypoxia and neovascularization.[145]

Diabetes mellitus (DM) is an autoimmune metabolic disorder characterized by persistent high blood glucose levels,

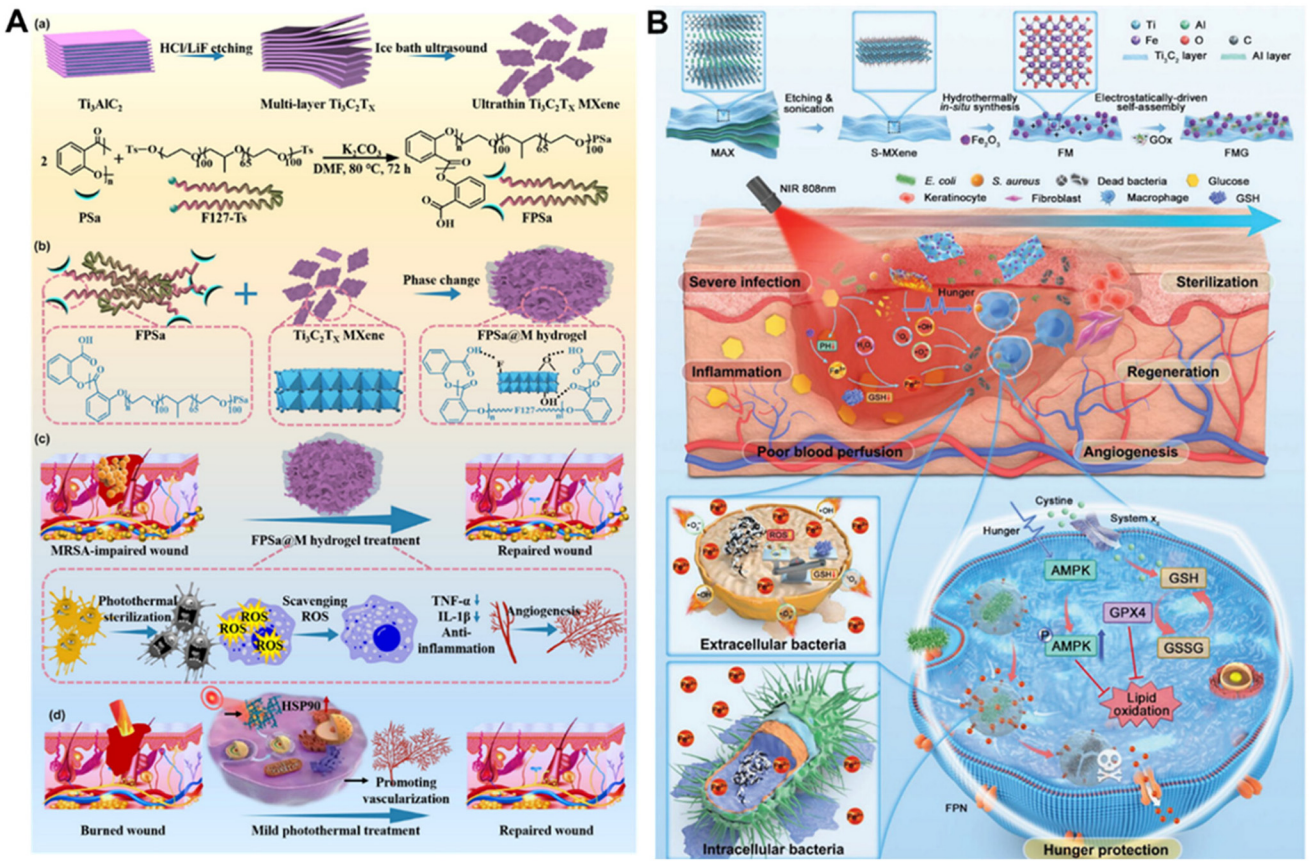

Fig. 8 MXene-based applications in wound healing. (A) Schematic diagram illustrating single platform of FPSa@M hydrogel integrated diverse capabilities to accelerate complete regeneration of MDR bacterial infected wounds and burn wounds.[142] Reproduced from ref. 142 with permission from Elsevier, copyright 2024. (B) Schematic diagram of ferroptosis bio-heterojunction (F-bio-HJs). Flowchart of the preparation steps and procedure for FMG bio-HJ and the mechanism of extra-intracellular bacteria-targeted ferroptosis and hunger-triggered cell protection induced by F-bio-HJ.[146] Reproduced from ref. 146 with permission from Wiley-VCH, copyright 2023.

elevated ROS, and excessive inflammation that poses a serious threat to human health. The diabetic hyperglycemic microenvironment prevents collagen deposition, granulation tissue formation and vascular maturation, leading to chronic diabetic wound formation. In response to the high complication and failure rate of intracellular bacterial infections in diabetic wounds, Dai *et al.* conceptualized and fabricated an innovative bacterial-targeted ferrite bio-hybrid junction (F-bio-HJ) composed of Fe_2O_3/Ti_3C_2-MXene and GOx (Fig. 8B).[146] Under NIR irradiation, Fe_2O_3/Ti_3C_2-MXene@GOx (FMG) catalyzed the production of large amounts of ROS, which attacked the extracellular bacterial membranes, facilitated the penetration of synchronously produced Fe^{2+}/Fe^{3+} into the bacteria, and led to the death of the planktonic bacteria through iron-leaping, Fe^{2+} overloading and lipid peroxidation. In addition, FMG promoted ferroptosis in intracellular bacteria by transporting Fe^{2+} to them *via* inward ferritin (FPN). When GOx is depleted of glucose, FMG exerts a starvation-protective effect, helping macrophages to escape from ferroptosis by activating the 5′-monophosphate (AMP) activated protein kinase (AMPK) pathway. The *in vivo* results demonstrated that FMG could induce extracellular bacterial-targeted iron oxidation and promote regeneration of infected diabetic skin without triggering ferroptosis in normal cells. This study provides a promising MXene-based approach for the treatment of diabetic infected wounds.

In recent years, various conductive hydrogel-based flexible epidermal sensors have been well developed for human healthcare monitoring but lack the comprehensive and efficient therapeutic capabilities for reliable and sensitive diagnostic healthcare sensing and timely treatment. MXene nanosheets are considered as attractive candidates for the preparation of conductive hydrogel epidermal sensors that can simultaneously achieve the ability to have reliable self-healing capabilities and significant sensing performance for wearable human–computer interaction and accelerated wound healing for subsequent medical treatment. For example, Li *et al.* introduced antimicrobial silver nanoparticle-coated MXene (AgNPs/MXene) nanosheet networks into guar gum (GG) and phenylboronic acid grafted sodium alginate (Alg-PBA) polymer networks, resulting in the facile preparation of healing, injectable, and antimicrobial MXene hydrogels (AgNPs/MXene/GG/Alg-PBA).[147] This MXene hydrogel can be used for wearable human–computer interaction and high-performance human health monitoring for potential rehabilitation and diagnosis of cardiovascular and muscle-related diseases, as well as highly effective wound therapies that significantly accelerate wound healing. Epidermal sensors based on MXene's flexible conductive hydrogels show unlimited potential, with the promise of integrating diagnosis, detection and therapy in the future.

4.5 Bone regeneration

Due to the poor self-healing ability of bone defects, the repair of bone defects remains one of the most challenging problems in clinical practice. Currently, the application of biomaterials and bio-scaffolds implanted into the defect site to promote the healing of bone defects is the main therapeutic approach for bone defect repair. In recent years, the emergence of two-dimensional materials has brought new opportunities for biomaterials. As a ceramic-based two-dimensional nanomaterial with unique physicochemical properties, such as electrical conductivity, hydrophilicity, antimicrobial, and photothermal effects, MXenes have a very broad application prospect in bone defect biomaterials (Table 6).[153]

The repair and regeneration of bone defects is a complex and continuous process involving various internal and external environmental factors. The work of Qu *et al.* revealed that photoactivated MXene ($Ti_3C_2T_x$) nanosheets had positive effects on promoting both bone and soft tissue regeneration, and further investigated the detailed effects and potential mechanisms of photoactivated MXene on tissue regeneration.[18] The photoactivated MXene exhibited good thermal effect and strong antibacterial activity, inhibited the expression of inflammatory factors and methicillin-resistant *Staphylococcus aureus* (MRSA) infection, and induced the expression of pro-angiogenic factors and soft tissue wound repair. Photoactivated MXene can also regulate osteogenic differentiation of adipose-derived stem cells (ADSCs) by activating heat shock protein 70 (HSP70) through the ERK signaling pathway to promote bone tissue repair. This work revealed the development of bioactive MXene photothermal activation as an effective strategy for the simultaneous regeneration of bone and soft tissue (Fig. 9A). Based on the above findings, a new idea based on MXene was provided for bone tissue repair. In order to further optimize the performance of MXene to enhance its osteogenic activity, the researchers sought to endow MXene with different functions through different modification strategies to cope with the complex pathological environment.

For larger bone defects, the application of MXene-based materials as biomaterial scaffolds in defect repair and bone regeneration has attracted much attention.[154] MXene (Ti_2AlN)/PCL composite bone repair scaffolds were successfully prepared using 3D printing technology for *in situ* maxillofacial bone defect repair.[155] The results of rat tibial bone defect repair experiments and rabbit maxillofacial bone defect repair experiments showed that the PCL@Ti_2AlN scaffolds promoted new bone formation, and the scaffolds could induce new bone formation and *in situ* regeneration of bone defects *in vivo*, with good clinical applications. Wang *et al.* constructed a multifunctional 3D mimetic bone scaffold by rationally integrating photon-responsive 2D ultrathin niobium carbide (Nb_2C) MXene nanosheets (NSs) into a 3d-printed bone mimetic scaffold (NBGS) for osteosarcoma treatment.[155] The integrated 2D Nb_2C-MXene NSs had a specific photon response in the NIR-II biological window with high tissue penetration depth to efficiently kill bone cancer cells, and calcium and phosphate released during scaffold degradation could promote the mineralization of new bone tissue. Huang *et al.* modified conventional β-tricalcium phosphate-based scaffolds by ultrathin MXene-Ti_3C_2 modification and Zn^{2+}/Sr^{2+} ion substitution, which resulted in excellent reactive oxygen species scavenging,

Table 6 Summary of recent research on MXene-based nanomaterials for bone regeneration

MXene composition	Application form	Bioactive property	Animal models	Ref.
(Ti_2AlN)/polycaprolactone	Scaffold	Hydrophilicity, cytocompatibility, mechanical properties, cell adhesion ability and osteogenic differentiation ability	Rat tibial bone defect model and rabbit maxillofacial bone defect model	164
Nb_2C, bioactive glass scaffolds (BGS)	Scaffold	Photothermal properties, inhibit tumor cell proliferation, promote vascular regeneration as well as bone regeneration	Bone malignancy model and bone defect model of SD rats	165
$Ti_3C_2T_x$, β-TCP, Zn and Sr ions	3D-printed scaffold	ROS scavenging ability, NIR responsivity, enhanced mechanical properties, supports new bone mineralization and bone regeneration	Rat cranial defect model	156
$Ti_3C_2T_x$, polycaprolactone (PCL)	Electrospinning PCL membranes scaffold	Conductivity, cell adhesion, antibacterial	—	166
Ti_3C_2, self-assembled silk fibroin methacrylate (SF-MA)	3D-printed theragenerative scaffolds	Photothermal anti-osteosarcoma ablation and bone regeneration	—	158
Nano-hydroxyapatite particles (n-HA), MXene nanosheets and g-C_3N_4	Scaffold	Photodynamic and photothermal effects, osteogenic differentiation and inhibits the proliferation of bone tumor cells	Saos-2 tumor-bearing mouse model	167
Ti_3C_2, bioactive glass (BG)	3D-printing scaffold	Photothermal conversion, bone-tumor killing and bone-tissue regeneration	Saos-2 bone tumor model in BALB/c nude mice	168
Ti_3C_2, hydroxyapatite and sodium alginate	Scaffold	High mechanical strength, biocompatibility, promoted mineralization, bone regeneration	Rat calvarial defect model	169
$Mo_2Ti_2C_3$ MXene, acrylamidemonomer, deacetylated chitosan, glacial acetic acid and gelatin	Hydrogel	Biocompatibility, electrical conductivity, viscosity enhancement and promotion of osteogenic differentiation	Calvarial bone defects mode of mice	155
Ti_3AlC_2, Regenerated silk fibroin (RSF)	Hydrogel	Re-establishment of the electrical microenvironment for bone regeneration	Calvarial defect model of SD rats	56
$Ti_3C_2T_x$, dexamethasone (Dex), poly(*N*-isopropylacrylamide)-*co*-*N*-(hydroxymethyl) acrylamide hydrogel	Hydrogel	Photothermal effect, drug release and anti-apoptosis of bone-derived mesenchymal stem cells	Calvarial defects of SD rats	160
GelMA/β-TCP/sodium alginate (Sr^{2+})/MXene (Ti_3C_2)	Hydrogel scaffolds	Photothermal antibacterial, bone regeneration	*S. aureus*-infected mandible defects of rats	170
Ti_3C_2 nanosheets, gelatin-based nanocomposite hydrogels	Hydrogel	Biodegradable, mechanical, ROS scavenging, and osteogenic inducing properties	Critical-sized calvarial defect repair of SD rats	171
$Ti_3C_2T_x$ Nanosheets	Nanosheet	Thermal effect, antibacterial activity, inhibit the expression of inflammation factors, induce the expression of pro-angiogenic factors	Skull defect model of rats	18
Poly(lactic acid) (PLA), $Ti_3C_2T_z$	Nanocomposite membranes	High mechanical strength, enhance the adhesion, proliferation, and osteogenic differentiation	—	161
Multilayered $Ti_3C_2T_x$	Nanosheets	Cytocompatible, osteoinductivity and bone regeneration activity	Calvarial defect model of rats	162
$Ti_3C_2T_x$, ultralong hydroxyapatite nanowires (UHAPNWs)	Nanocomposite membranes	Mechanical properties, biocompatibility and osteoinductivity	Calvarial defect mode of rat	163

near-infrared responsiveness, enhanced mechanical properties, and precise temporal immunomodulation of the bone healing process by the smart 3D scaffold-enhanced bone regeneration in the rat model of cranial bone defects (Fig. 9B).[156] In the work of Diedkova *et al.* biocompatible and biodegradable nanofibrous scaffolds were prepared from polycaprolactone (PCL) by electrostatic spinning, and the MXene coatings formed a suitable environment for cell attachment and proliferation, with a mild antimicrobial effect, and possessed good structural, chemical, electrical and biological properties.[157] A bifunctional thermally regenerative 3D aerogel composite scaffold was developed by hybridization of photocrosslinked silk fibroin (SF) biopolymers with MXene (Ti_3C_2) 2D nanosheets by Pektas *et al.* This scaffold could mediate the growth and proliferation of preosteogenic cell lines *in vitro*, and had a strong photothermal effect under remote irradiation with near-infrared laser light, while significantly stimulating bone mineral deposition on the surface of the scaffold.[158] By constructing specific biomaterial scaffolds according to the cause of bone defects and endowing them with more comprehensive biological properties, these scaffolds could reproduce the important features of bone and mimic the function of natural bone tissues, thus further accelerating the repair process of bone defects and regenerating damaged tissues.[159]

Various physical and chemical properties of MXenes, such as the osteogenic differentiation ability which promotes cell growth and bone regeneration in the damaged area after bone defects, and the good antimicrobial ability of MXene led by

Ti_3C_2, combined with the unique near-infrared thermal effect, can be introduced into the design of composites for the repair of bone defects as additive materials represented by the form of hydrogels. Hu *et al.* prepared an electroactive hydrogel based on regenerated silk fibroin (RSF) and bioencapsulated MXene to promote effective bone regeneration.[56] This MXene/RSF hydrogel could also be used as a piezoresistive pressure sensor, which activated Ca^{2+}/CALM signaling and promoted direct osteogenesis under electrical stimulation, modulating the immune microenvironment and neovascularization, thus re-establishing the electrical microenvironment for bone regeneration (Fig. 9C). Wang *et al.* added $Mo_2Ti_2C_3$ MXene to hydrogels to improve mechanical strength and electrical conductivity.[155] $Mo_2Ti_2C_3$ MXene hydrogels have properties such as biocompatibility, electrical conductivity, surface functionalization, chemical cross-linking, elastic modulus, and viscosity, and good osteogenic capacity, which promotes the osteogenic genes and osteogenic proteins *in vitro*. Animal models of cranial bone defects show that $Mo_2Ti_2C_3$ MXene hydrogel promotes osteogenesis and neurogenesis in bone defects *in vivo*. Chen *et al.* demonstrated superior osteogenic properties using a biocompatible dexamethasone (Dex)-loaded MXene-poly(*N*-isopropylacrylamide)-*co*-*N*-(hydroxymethyl) acrylamide hydrogel, which was capable of supersensitive release of Dex under NIR irradiation at ≈42 °C.[160] Mild heat and supersensitive release of Dex synergistically counteracted apoptosis of bone-derived mesenchymal stem cells and osteogenic differentiation. MXene-based hydrogels are incredible candidates for bone repair applications that hold significant promise for biomedical applications due to their unique properties, including large surface area, tunable chemistry, and compatibility with living organisms.

In addition, MXenes can exist in various forms such as thin films and nanocomposites, and the rich functional group structure on their surface gives them the potential to carry drugs, growth factors, further expanding their application prospects in bone defect repair.[153] In another work, Chen *et al.* prepared biocompatible $Ti_3C_2T_z$-reinforced polylactic acid (PLA) nanocomposite membranes with high biocompatibility, and the optimized nanocomposite membranes showed a 33% increase in ultimate tensile strength compared with the pure PLA membranes.[161] The incorporation of $Ti_3C_2T_z$ enhanced the biological properties of the membranes, and facilitated the adherence, proliferation, and osteogenic differentiation of mouse preosteoblasts *in vitro*. Zhang *et al.* used flexible free-standing $Ti_3C_2T_x$ MXene films to evaluate the cytocompatibility and osteoinductive capacity of $Ti_3C_2T_x$ MXene *in vitro* and investigated the host tissue response and guided bone regeneration capacity of the material *in vivo*.[162] In addition, Fu *et al.* prepared free-standing UHAPNWs/MXene nanocomposite membranes by introducing different weight ratios of ultra-long hydroxyapatite nanowires (UHAPNWs) into MXene to explore their potential in bone regeneration (Fig. 9D).[163] The incorporation of UHAPNWs improved mechanical properties and hydrophilicity, and enhanced cell adhesion, proliferation and osteogenic differentiation. Furthermore, UHAPNWs/MXene nanocomposite membrane quantitatively and qualitatively effectively enhanced bone tissue formation in rat cranial bone defects, a novel inorganic composite material for bone tissue regeneration.

In order to fully utilize MXene-based capabilities in the field of bone repair, further research is necessary to thoroughly evaluate its compatibility with biological systems, refine its manufacturing methods, design more sophisticated methods to enhance its functionality, and encourage collaboration between different disciplines to promote its practical application.

4.6 Other applications

Numerous studies have shown that MXene-based materials possess a range of favorable biological, physical and chemical properties. These properties include biocompatibility, antimicrobial properties, drug loading and antioxidant capacity, large specific surface area, tunable size, NIR absorption, metal conductivity and abundant surface functional groups. Based on these properties, MXenes also have potential applications in muscle tissue engineering, nerve regeneration, drug delivery, and biosensors, and related studies have emerged (Table 7).

Muscles are soft, elastic tissues attached to bones or internal organs that possess the ability to contract and play an important role in generating voluntary movement. Regeneration of muscle tissue following severe mechanical injuries and muscle-related diseases remains a challenge. It has been demonstrated that conductive nanocomposites can effectively modulate the formation of skeletal muscle tissues *in vivo* and promote their regeneration. MXenes have excellent electrical conductivity and have the potential to be applied in skeletal muscle regeneration. Li *et al.* found that $Ti_3C_2T_x$ could regulate the cellular microenvironment through anti-inflammatory and antioxidant activities, promoting angiogenesis, muscle fiber formation and skeletal muscle regeneration (Fig. 10A).[17] Muscle pictures and immunohistochemical staining results of myosin heavy chain (MHC) from animal experiments of rat tibialis anterior muscle defects showed the superior ability of MXene to promote skeletal muscle regeneration. It has also been found that Nb_2C MXene-functionalized hydrogel can restore skeletal muscle regeneration function by reducing ROS levels, attenuating inflammation, decreasing fibrosis, and promoting angiogenesis, neo-myotube formation and neurogenesis.[172] Song *et al.* designed an integrated $Ti_3C_2T_x$-based epidermal electrode for diagnostic muscle therapy, which could comfortably record electromyography (EMG) signals as well as enable electrical stimulation and electrothermal therapy for diagnostic muscle therapy.[173] In addition, based on MXene's excellent mechanical properties and metal conductivity, MXene can be engineered as an artificial muscle.[174] Myocardial infarction (MI) is the deadliest of all cardiovascular diseases and is usually caused by coronary artery blockage, which results in damage to heart muscle cells due to ischemia. This process usually results in the release of excess ROS, leading to excessive oxidative stress. One of the promising strategies for the treatment of MI is the design and

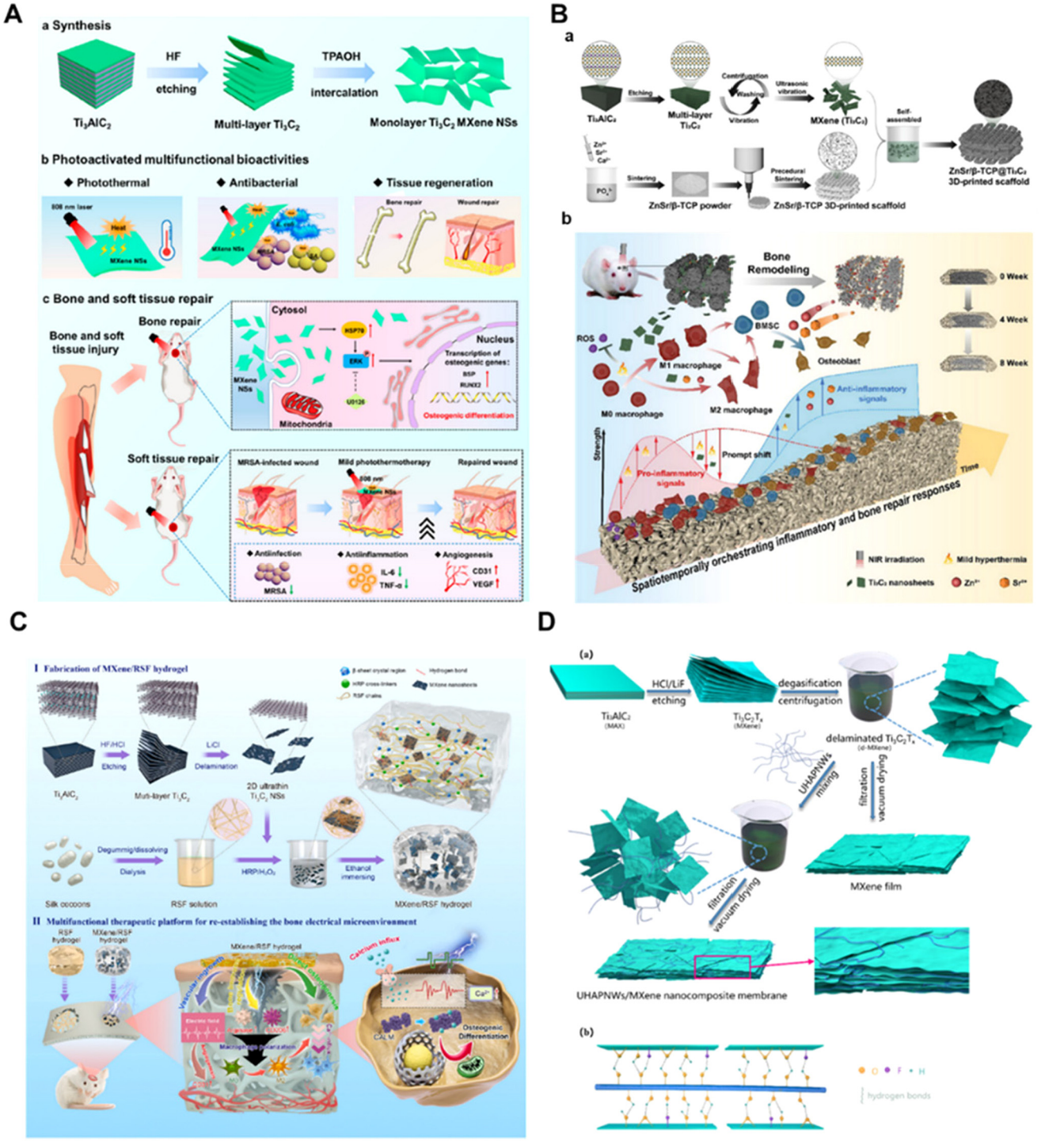

Fig. 9 MXene-based applications in bone regeneration. (A) Synthesis process, multifunctional bioactivities, and the application of photoactivated MXene nanosheets in bone and soft tissue regeneration.[18] Reproduced from ref. 18 with permission from American Chemical Society, copyright 2023. (B) Schematic illustration of the fabrication process (a) and their applications (enhance osteogenesis by spatiotemporally orchestrating inflammatory and bone repair responses) (b) of $Ti_3C_2T_x$ MXene-decorated 3D-printed ceramic scaffold.[156] Reproduced from ref. 156 with permission from Wiley-VCH, copyright 2024. (C) Schematic showing the fabrication and application of multifunctional electroactive hydrogels for the diversified treatment of bone defects.[56] Reproduced from ref. 56 with permission from KeAi, copyright 2022. (D) (a) Schematic illustration of the fabrication of the UHAPNWs/MXene nanocomposite membrane. (b) Schematic diagram of the interaction between UHAPNWs and MXene, involving the hydrogen bonds formed by terminated surface groups of MXene (–F, =O or –OH) and hydroxyl in UHAPNWs.[163] Reproduced from ref. 163 with permission from Elsevier, copyright 2021.

Table 7 Summary of recent research on MXene-based nanomaterials for other applications

MXene composition	Synthesis strategy	Application	Animal models	Ref.
$Ti_3C_2T_x$	LiF/HCl etch-assisted sonication	Promoting angiogenesis and skeletal muscle regeneration	The tibial anterior muscle defects model in SD rats	17
Nb_2C MXene-functionalized hydrogel (OPTN)	HF etching and TPAOH intercalation	Promote skeletal muscle regeneration and functional restoration	A rat tibialis anterior muscle defect model	172
Sweat-stable MXene epidermal electrode ($Ti_3C_2T_x$)	LiF/HCl etch-assisted sonication	An all-in-one muscle theranostic platform	—	173
MOF-$Ti_3C_2T_x$	LiF/HCl etch-assisted sonication	Artificial muscles	—	174
ECM-Ti_3C_2 hydrogel	LiF/HCl etch-assisted sonication	Improve myocardial infarction and promote heart tissue regeneration	Mouse myocardial infarction model	175
Ti_2C-cryogel	10% HF etching	Repair of myocardial infarction	Myocardial infarction model in SD rats	186
MXene-functionalized collagen biomaterials ($Ti_3C_2T_x$)	LiF/HCl etch-assisted sonication	Cardiac tissue engineering	—	187
$Ti_3C_2T_x$-based artificial nerve guidance (MXPLT)	LiF/HCl etch-assisted sonication	Enhanced regeneration of peripheral nerve injury	A SD rat model with a 10 mm sciatic nerve defect	178
$Ti_3C_2T_x$-PLGA	LiF/HCl etch-assisted sonication	Neural stem cell engineering	—	179
Ti_3C_2-SP	HF etching and TPAOH intercalation	Drug delivery and tumor therapy	4T1 breast tumor-bearing mice model	180
DOX-$Ti_3C_2T_x$-DNA hydrogel	LiF/HCl etch-assisted sonication	Drug delivery and tumor therapy	The HeLa tumor-bearing animal model with BALB/c nude mice	181
G-MXene@F/C	—	Drug delivery and colon cancer treatment	CT26 colon tumor-bearing mice model	188
C-MOF/$Ti_3C_2T_x$	LiF/HCl etch-assisted sonication	Biosensor (uric acid (UA) and glucose (Glu) monitoring, muscle therapy)	—	184
$Ti_3C_2T_x$-based screen-printed electrode	HF etching, stirring and layering at 50 °C	Biosensor (continuous multi-component monitoring in whole blood)	—	185

fabrication of electrically conductive cardiac patches to facilitate the electrophysiological coupling of the cardiac patch to the host tissue. MXenes, with their excellent electrical conductivity, biocompatibility, antioxidant properties and hydrophilicity, are a promising candidate for the preparation of myocardial patches. Ren *et al.* developed an injectable antioxidant/conductive hydrogel (E-MXene) by combining MXene (Ti_3C_2) with cardiomyocyte extracellular matrix (ECM) hydrogels (Fig. 10B).[175] E-MXene hydrogel has high moisture and porosity, which enabled MXene to be uniformly distributed in the ECM to build a suitable conductive network that could fully utilize the antioxidant and conductive properties of MXene. After E-MXene was injected into the infarcted area of the mouse heart, the cardiac function of MI mice was improved by decreasing the excessive production of ROS to improve the tissue microenvironment, and enhancing the electrical signal conduction between the fibrotic scar tissues and the normal cardiac tissues.

Neuronal cells are electrically active and bioelectrical in nature, and adhesion-mediated signaling pathways are critical for regulating neuronal cell function and determining their fate, especially cell spreading, proliferation, and differentiation.[176] Therefore, the development of bioactive materials with both electrical conductivity and cell adhesion properties has great potential for promoting neural tissue regeneration. MXenes have excellent electrical conductivity, which will facilitate neurite growth and enhance neuronal development. Secondly, MXene's high hydrophilicity and rich surface functional groups facilitate the optimization of the bioadhesive properties and surface functionalization of the substrate, which can promote the adhesion of neural cells as well as modulate their behavior.[177] The above properties of MXene also mean it has unlimited potential in the field of neural tissue engineering. Wang *et al.* created a novel neural conduit with microchannel guidance (MXPLT) by 4D printing, which consisted of a monolayer of MXene $Ti_3C_2T_x$ nanosheets and poly(L-lactide-*co*-trimethylene carbonate) (PLATMC).[178] The printed nerve conduit had shape memory and automatically rolled into a tubular structure at 37 °C, firmly wrapping around the severed ends of the defective nerves. Its high ductility and elasticity could withstand nerve deformation caused by muscle movement. Micro-channels constructed through 4D printing accelerated cell migration during the nerve repair process, resulting in faster and better repair of long-distance nerve defects. The addition of MXenes improved the electrical conductivity of the nerve conduit, which created a complete electrical pathway during the nerve repair process and ultimately repaired peripheral nerve damage. In another study, $Ti_3C_2T_x$ MXene was used as a coating nanomaterial for aligned/randomly aligned poly (lactic acid) (PLLA) nanofibers, named M-ANF or M-RNF, respectively, and it was found that the addition of MXene promoted an increase in the number of neuromasts, their lengths, branching complexity, and synaptic densities (Fig. 10C).[179]

Drug delivery platforms can be used to improve the stability and specific targeting ability of drugs in biological environments, as well as to improve the stability of chemotherapy *in vivo*, by polymers or targeting functional agents. MXene-

based biomaterials offer numerous advantages in building drug delivery platforms. First, due to their unique lamellar structure, very large specific surface area, and nano-size, MXene-based biomaterials provide abundant anchor sites for efficient loading and delivery of therapeutic molecules and allow for easy distribution and accumulation of drugs at the therapeutic site. In addition, utilizing the physicochemical, electronic, and optical properties of MXene-based biomaterials

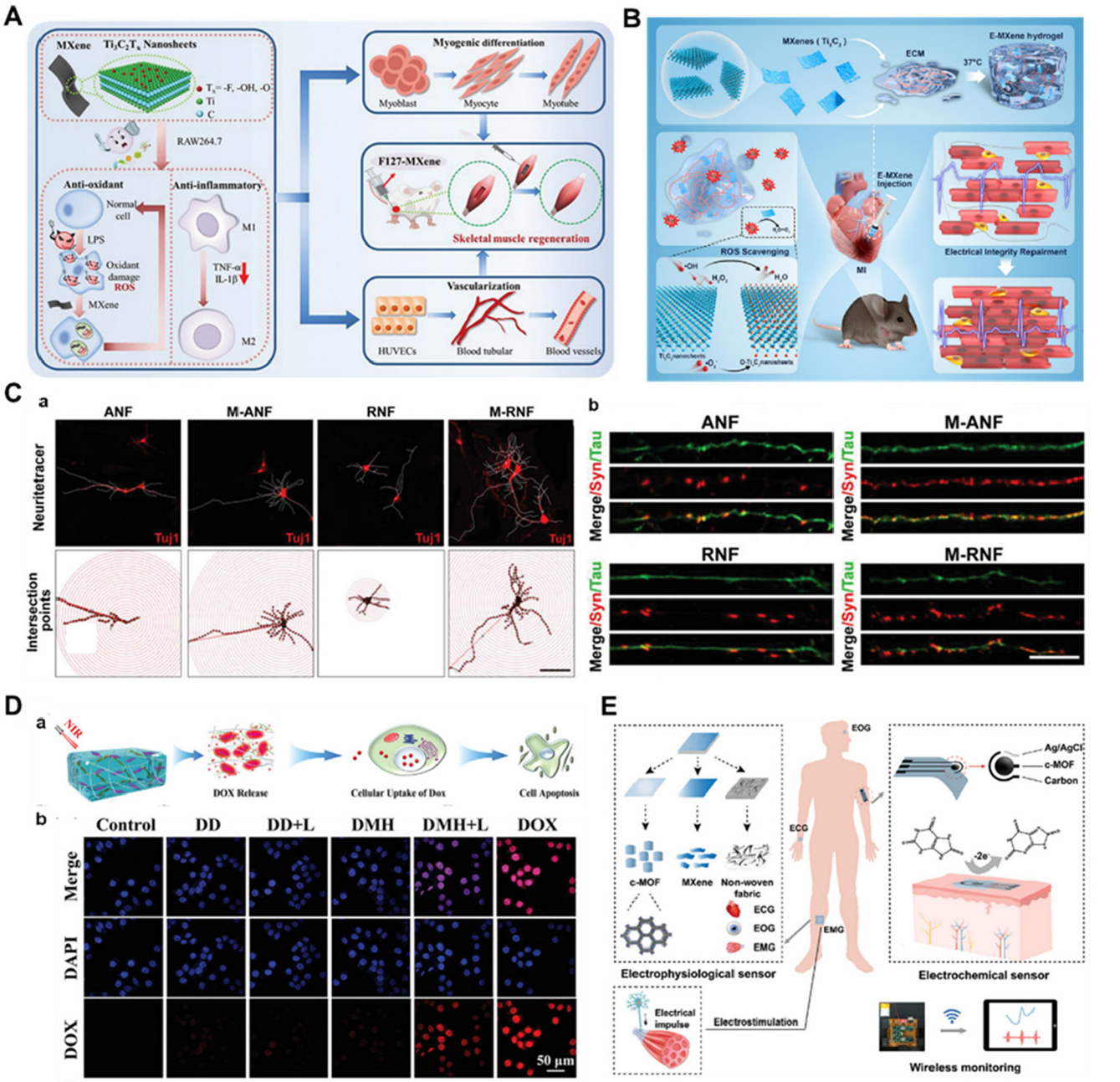

Fig. 10 MXene-based materials in other applications. (A) Schematic diagram of MXene regulating the myogenic differentiation and skeletal muscle regeneration.[17] Reproduced from ref. 17 with permission from Wiley-VCH, copyright 2023. (B) Schematic illustration of the preparation and application of E-MXene hydrogel in mice MI.[175] Reproduced from ref. 175 with permission from Elsevier, copyright 2024. (C) (a) The contours of 2D structures (top) and concentric rings for Sholl analysis (bottom) of NSC-derived neurons cultured on ANF, M-ANF, RNF, and M-RNF in differentiation medium for 7 days (scale bar, 100 μm) and (b) representative high-magnification fluorescence images of synaptophysin (red) and Tau (green) labeling after differentiation of NSCs for 14 days on the four substrates (scale bar, 10 μm).[179] Reproduced from ref. 179 with permission from Wiley-VCH, copyright 2023. (D) (a) Schematic diagram of the NIR irradiation-triggered DOX release from the DMH hydrogel to induce cancer cell apoptosis and (b) CLSM images of HeLa cells incubated with different buffer solution.[181] Reproduced from ref. 181 with permission from Wiley-VCH, copyright 2022. (E) Schematic diagram of an integrated biosensor for electrophysiological and electrochemical sensing. Data are transmitted wirelessly.[184] Reproduced from ref. 184 with permission from Wiley-VCH, copyright 2023.

will effectively integrate the drug delivery platforms with other bioimaging and therapeutic modalities (*e.g.*, PTT, PDT, CDT, SDT, *etc.*), which will facilitate the development of smart drug delivery platforms. Han *et al.* developed Ti_3C_2 MXene nanosheets with soybean phospholipid (SP) modification as effective drug carriers for loading and delivery of DOX and as synergistic therapeutic agents against cancer.[180] These Ti_3C_2 MXenes not only possessed a drug loading capacity of up to 211.8%, but also exhibited pH-responsive and NIR-triggered on-demand drug release properties. To improve therapeutic efficacy and reduce drug dosage, delivery efficiency can be further enhanced by using DNA, peptides or antibodies for surface functionalization or hydrogel encapsulation. He *et al.* established a promising and efficient photothermal-chemotherapeutic synergistic cancer treatment platform by integrating DNA hydrogels with $Ti_3C_2T_x$-based MXene as a photothermal agent and DOX as a loaded chemotherapeutic drug.[181] Under NIR irradiation, the temperature increase induced by the photothermal MXene nanosheets triggered a reversible transformation of the DOX-loaded MXene-DNA hydrogel from gel to solution, during which the DNA double-stranded cross-linking structure released DOX, resulting in highly efficient localized cancer therapy (Fig. 10D). Upon removal of NIR irradiation, the DNA double-stranded structure and hydrogel matrix were reformed, and recombination of free DOX and adaptive transformation of the hydrogel could be achieved. From the CLSM images of HeLa cells, it was observed that there was DOX release and uptake only in the cells of the material-treated group under NIR irradiation (Fig. 10D).

The lamellar structure of MXenes facilitates modification by various surface terminations, providing a rich variety of surface-active sites that can be used as a biosensing platform with high responsiveness to various external stimuli. In addition, MXenes have excellent conductivity, which facilitates low noise and high selectivity in biosensing reactions. Therefore, these unique properties make MXene a highly promising biosensor material. MXene-based wearable sensors with flexibility, gas sensors, glucose sensors and fluidic biosensors have been well-studied and demonstrated to have good specificity, selectivity, and sensitivity.[182,183] For example, Lin *et al.* designed an electrophysiological MOF/MXene electrode using highly conductive MXene and a porous conductive metal–organic framework (c-MOF, $Ni_3(HITP)_2$), which could realize a multifunctional biosensor integrating the electrochemical detection of uric acid (UA) and glucose (Glu) in sweat, electrophysiological signal acquisition, and electrical stimulation for treatment (Fig. 10E).[184] MOF/MXene electrodes enabled muscle therapy through electrical stimulation with lower electrode/skin interface impedance, higher stability and signal-to-noise ratio (SNR), and high charge storage capacity (CSC). In another study, an electrochemical microfluidic biosensor based on $Ti_3C_2T_x$ MXene was designed that can be applied to hemodialysis, enabling continuous detection of urea, uric acid and creatinine levels in human blood.[185] These efforts pave new paths for MXene applications in biomedical and sensing fields.

5. Conclusion and perspective

MXenes have attracted much attention in biomedicine and include many transition metal carbides and nitrides. Novel 2D MXene materials have been widely studied in the biomedical field due to their diverse chemical structures, tunable physicochemical properties, and desirable bioactivities. Despite the achievements of MXene-based biomaterials in biomedicine, research in this field is still in its infancy and there are many critical issues that need to be addressed.

MXene-based biomaterials used in the biomedical field face higher demands, requiring both good biosafety and corresponding biological functions *in vivo*, and at the same time their degradation efficiency *in vivo* needs to be considered to avoid negative impacts on the organism. Although many preliminary studies have demonstrated the generally low cytotoxicity of MXenes currently used in biomedicine, most of these studies have been conducted at *in vitro* levels or in small animals such as mice at low doses, and there is a lack of systematic evaluations of the long-term biosafety of MXenes in large animal models (*e.g.*, rabbits, dogs, pigs, and primates). In addition, there are fewer studies on the degradability of MXene-based biomaterials, and only some MXenes have been reported to be degradable. For biodegradable MXenes, the short-term toxicity *in vivo* and effects of their degradation products should be evaluated. For non-biodegradable MXenes, the long-term toxicity *in vivo* should be evaluated to understand their biodistribution and clearance rate in the body. More data on the safety and degradability of MXenes *in vivo* are needed in the future.

Putting aside the safety and degradability of MXenes *in vivo*, there are still many limitations for their translation from the laboratory to the clinic. On the one hand, the cellular uptake behavior, biological interactions, and the specific mechanism of action of MXenes on tissue regeneration are not yet clear. On the other hand, in order to cope with more complex physiological environments in the human body, it is necessary to establish different large-scale animal models or even clinical trials to evaluate the role played by MXene-based bioactive materials in the organism. In the future, more research is needed to investigate the mechanism of action of MXenes on cells and tissues by establishing more animal models to lay the foundation for clinical conversion. In addition, surface modification strategies can further enrich the biological functions of MXenes, and the current surface modification strategies for MXenes are classified as small-molecule modification, macromolecule modification, bioactive nanoparticle modification, and surface polymerization modification. The research on small-molecule modification of MXenes mainly focuses on the modification by silane agents, and more modification strategies of MXenes by other bioactive small molecules are expected to be explored in the future.

MXene-based biomaterials offer a new lease of life for tumor ablation as well as infection treatment, overcoming the limited therapeutic efficacy of certain therapies alone and the development of bacterial resistance. In addition, the fabrica-

tion of ultrasmall MXene-based QDs and their applications in therapy and regeneration require further attention. MXene QDs can be modified or coated on their surface with different materials or targeting tools to prolong the circulation and accumulate at the site of interest for imaging, enabling the diagnosis of diseases. The most promising future direction is to build multifunctional MXene-based therapeutic systems, using multiple therapeutic approaches to achieve diagnostic, combined therapeutic integration.

The unstable and highly oxidizable characteristics of MXenes limit their use in biomedical applications. The surface of MXenes is usually composed of –OH, –O or –F, making the surface hydrophilic, which together with the high surface charge leads to rapid aggregation and precipitation of few-layer MXenes in biological media, thus affecting their physicochemical properties and biological functions. In addition, although MXenes disperse very well in water, they are easily oxidized by oxygen in water and are very unfavorable for storage. Therefore, surface chemical modification of MXenes and surface engineering strategies could address the issues of stability, storage and sterilization, which are very important for clinical translation. Macromolecular modification for MXenes is mainly based on non-covalent interactions; *e.g.*, surface modification with macromolecules such as PEG, BSA, and HA can modulate the hydrophilicity and biocompatibility of MXene solutions but suffers from poor stability. In the modification of MXenes with bioactive nanoparticles (*e.g.*, Fe_3O_4, MnO_x, Au, Pt, *etc*.), although this can broaden their potential for therapeutic (PTT, PDT, CDT, *etc*.) and diagnostic imaging applications, the cytotoxicity of the metal ions needs to be considered. Surface polymerization modification methods (*e.g.*, modification by PDA, PLGA, Ppy, *etc*.) have the problems of difficult operation and complicated steps. In the future, optimization or development of new modification methods of MXenes in various ways to give them more stable properties and more comprehensive functions is expected.

Currently, the research on MXenes in the biomedical field is still focused on tumor therapy and antibacterial therapy, which mainly rely on PTT and PDT of MXenes, but most of the research on the photothermal performance of MXenes is focused on NIR-I. To cope with the treatment of deeper tissues, there is an urgent need for the development of MXene composites that can respond to NIR-II light. For the research of MXenes in tissue regeneration, there are more studies in the field of skin regeneration as well as bone regeneration, while there are fewer related reports in the field of muscle tissue engineering and nerve regeneration. In addition, most of the MXenes used in biomedical research are Ti/Nb-based carbons, mainly focusing on $Ti_3C_2T_x$, while there are fewer reports on other types of MXenes (*e.g.*, Ta_4C_3 and V_2C, *etc*.). In the future, the development of various types of different MXenes with broader applications in the biomedical field is expected.

MXene-based biomaterials offer new perspectives for biomedicine, and in the future, inexpensive mass production methods and new strategies for easy surface modification should be developed. We believe that as the scientific community continues to explore MXenes, these challenges will soon be solved, and the field of MXene composites will thrive in biomedicine with even more rational technological innovations.

Data availability

The data that support the findings of this study are available from the corresponding author upon reasonable request.

Conflicts of interest

There are no conflicts to declare.

Acknowledgements

This work was jointly supported by the National Natural Science Foundation of China (grant No. 52172288, 52302354), Funds for International Cooperation and Exchange of the National Natural Science Foundation of China (grant No. 52411540232), Natural Science Basic Research Project of Shaanxi Province of China (grant No. 2020JQ-564), Young Talent Support Plan of Xi'an Jiaotong University of China (grant No. QY6J003), and the Fundamental Research Funds for the Central Universities.

References

1 N. Zahin, R. Anwar, D. Tewari, *et al.*, Nanoparticles and its biomedical applications in health and diseases: special focus on drug delivery, *Environ. Sci. Pollut. Res.*, 2020, **27**(16), 19151–19168.
2 C. L. Tan, X. H. Cao, X. J. Wu, *et al.*, Recent Advances in Ultrathin Two-Dimensional Nanomaterials, *Chem. Rev.*, 2017, **117**(9), 6225–6331.
3 T. T. Hu, X. Mei, Y. J. Wang, *et al.*, Two-dimensional nanomaterials: fascinating materials in biomedical field, *Sci. Bull.*, 2019, **64**(22), 1707–1727.
4 M. Qiu, W. X. Ren, T. Jeong, *et al.*, Omnipotent phosphorene: a next-generation, two-dimensional nanoplatform for multidisciplinary biomedical applications, *Chem. Soc. Rev.*, 2018, **47**(15), 5588–5601.
5 Q. Wang and D. O'Hare, Recent Advances in the Synthesis and Application of Layered Double Hydroxide (LDH) Nanosheets, *Chem. Rev.*, 2012, **112**(7), 4124–4155.
6 C. H. Lui, L. Liu, K. F. Mak, *et al.*, Ultraflat graphene, *Nature*, 2009, **462**(7271), 339–341.
7 S. Liu, X. T. Pan and H. Y. Liu, Two-Dimensional Nanomaterials for Photothermal Therapy, *Angew. Chem., Int. Ed.*, 2020, **59**(15), 5890–5900.
8 Y. J. Chen, Y. K. Wu, B. B. Sun, *et al.*, Two-Dimensional Nanomaterials for Cancer Nanotheranostics, *Small*, 2017, **13**(10), 1603446.

9 M. Naguib, M. Kurtoglu, V. Presser, *et al.*, Two-Dimensional Nanocrystals Produced by Exfoliation of Ti_3AlC_2, *Adv. Mater.*, 2011, **23**(37), 4248–4253.
10 B. Soundiraraju and B. K. George, Two-Dimensional Titanium Nitride (Ti_2N) MXene: Synthesis, Characterization, and Potential Application as Surface-Enhanced Raman Scattering Substrate, *ACS Nano*, 2017, **11**(9), 8892–8900.
11 W. Feng, R. Y. Wang, Y. D. Zhou, *et al.*, Ultrathin Molybdenum Carbide MXene with Fast Biodegradability for Highly Efficient Theory-Oriented Photonic Tumor Hyperthermia, *Adv. Funct. Mater.*, 2019, **29**(22), 1901942.
12 H. Huang, C. H. Dong, W. Feng, *et al.*, Biomedical engineering of two-dimensional MXenes, *Adv. Drug Delivery Rev.*, 2022, **184**, 114178.
13 D. Saha, J. Dalmieda and V. Patel, Surface-Modified MXenes: Simulation to Potential Applications, *ACS Appl. Electron. Mater.*, 2023, **5**(6), 2933–2955.
14 A. P. Liu, Y. Liu, G. J. Liu, *et al.*, Engineering of surface modified $Ti_3C_2T_x$ MXene based dually controlled drug release system for synergistic multitherapies of cancer, *Chem. Eng. J.*, 2022, **448**, 137691.
15 J. P. Ma, L. Zhang and B. Lei, Multifunctional MXene-Based Bioactive Materials for Integrated Regeneration Therapy, *ACS Nano*, 2023, **17**(20), 19526–19549.
16 H. Lin, Y. Chen and J. L. Shi, Insights into 2D MXenes for Versatile Biomedical Applications: Current Advances and Challenges Ahead, *Adv. Sci.*, 2018, **5**(10), 1500518.
17 T. Li, J. P. Ma, W. S. Wang, *et al.*, Bioactive MXene Promoting Angiogenesis and Skeletal Muscle Regeneration through Regulating M2 Polarization and Oxidation Stress, *Adv. Healthcare Mater.*, 2023, **12**(4), 2201862.
18 X. Qu, Y. Guo, C. Xie, *et al.*, Photoactivated MXene Nanosheets for Integrated Bone–Soft Tissue Therapy: Effect and Potential Mechanism, *ACS Nano*, 2023, **17**(8), 7229–7240.
19 A. M. Jastrzebska, A. Szuplewska, T. Wojciechowski, *et al.*, Studies on cytotoxicity of delaminated Ti_3C_2 MXene, *J. Hazard. Mater.*, 2017, **339**, 1–8.
20 P. Ganguly, A. Breen and S. C. Pillai, Toxicity of Nanomaterials: Exposure, Pathways, Assessment, and Recent Advances, *ACS Biomater. Sci. Eng.*, 2018, **4**(7), 2237–2275.
21 T. Y. Wang, X. Y. Sun, X. Guo, *et al.*, Ultraefficiently Calming Cytokine Storm Using $Ti_3C_2T_x$ MXene, *Small Methods*, 2021, **5**(5), 2001108.
22 G. Y. Liu, J. H. Zou, Q. Y. Tang, *et al.*, Surface Modified Ti_3C_2 MXene Nanosheets for Tumor Targeting Photothermal/Photodynamic/Chemo Synergistic Therapy, *ACS Appl. Mater. Interfaces*, 2017, **9**(46), 40077–40086.
23 G. K. Nasrallah, M. Al-Asmakh, K. Rasool, *et al.*, Ecotoxicological assessment of $Ti_3C_2T_x$ (MXene) using a zebrafish embryo model, *Environ. Sci.: Nano*, 2018, **5**(4), 1002–1011.
24 H. Y. Huang, R. M. Jiang, Y. L. Feng, *et al.*, Recent development and prospects of surface modification and biomedical applications of MXenes, *Nanoscale*, 2020, **12**(3), 1325–1338.
25 J. Liu, W. Lu, X. F. Lu, *et al.*, Versatile $Ti_3C_2T_x$ MXene for free-radical scavenging, *Nano Res.*, 2022, **15**(3), 2558–2566.
26 S. Iravani and R. S. Varma, MXene-Based Composites as Nanozymes in Biomedicine: A Perspective, *Nano-Micro Lett.*, 2022, **14**, 213.
27 W. Feng, X. G. Han, H. Hu, *et al.*, 2D vanadium carbide MXenzyme to alleviate ROS-mediated inflammatory and neurodegenerative diseases, *Nat. Commun.*, 2021, **12**(1), 2203.
28 H. Hu, H. Huang, L. L. Xia, *et al.*, Engineering vanadium carbide MXene as multienzyme mimetics for efficient in ischemic stroke treatment, *Chem. Eng. J.*, 2022, **440**, 135810.
29 M. A. Tokmedash and J. H. Min, Designer Micro-/Nanocrumpled MXene Multilayer Coatings Accelerate Osteogenesis and Regulate Macrophage Polarization, *ACS Appl. Mater. Interfaces*, 2024, **16**(17), 21415–21426.
30 T. Liao, Z. Chen, Y. Kuang, *et al.*, Small-size $Ti_3C_2T_x$ MXene nanosheets coated with metal-polyphenol nanodots for enhanced cancer photothermal therapy and anti-inflammation, *Acta Biomater.*, 2023, **159**, 312–323.
31 Q. Q. Qiao, J. Y. Wang, B. J. Li, *et al.*, $Ti_3C_2T_x$ MXene nanosheet-based drug delivery/cascaded enzyme system for combination cancer therapy and anti-inflammation, *Appl. Mater. Today*, 2024, **38**, 102215.
32 Z. J. Li, W. Wei, M. M. Zhang, *et al.*, Cryptotanshinone-Doped Photothermal Synergistic MXene@PDA Nanosheets with Antibacterial and Anti-Inflammatory Properties for Wound Healing, *Adv. Healthcare Mater.*, 2023, **12**(28), 2301060.
33 D. X. Xu, Z. D. Li, L. S. Li, *et al.*, Insights into the Photothermal Conversion of 2D MXene Nanomaterials: Synthesis, Mechanism, and Applications, *Adv. Funct. Mater.*, 2020, **30**(47), 2000712.
34 K. Chaudhuri, M. Alhabeb, Z. X. Wang, *et al.*, Highly Broadband Absorber Using Plasmonic Titanium Carbide (MXene), *ACS Photonics*, 2018, **5**(3), 1115–1122.
35 X. T. Jiang, A. V. Kuklin, A. Baev, *et al.*, Two-dimensional MXenes: From morphological to optical, electric, and magnetic properties and applications, *Phys. Rep.*, 2020, **848**, 1–58.
36 J. Zeng, D. Goldfeld and Y. N. Xia, A Plasmon-Assisted Optofluidic (PAOF) System for Measuring the Photothermal Conversion Efficiencies of Gold Nanostructures and Controlling an Electrical Switch, *Angew. Chem., Int. Ed.*, 2013, **52**(15), 4169–4173.
37 J. T. Robinson, S. M. Tabakman, Y. Y. Liang, *et al.*, Ultrasmall Reduced Graphene Oxide with High Near-Infrared Absorbance for Photothermal Therapy, *J. Am. Chem. Soc.*, 2011, **133**(17), 6825–6831.
38 H. Lin, X. G. Wang, L. D. Yu, *et al.*, Two-Dimensional Ultrathin MXene Ceramic Nanosheets for Photothermal Conversion, *Nano Lett.*, 2017, **17**(1), 384–391.
39 Y. P. Wang, J. Yang, Y. H. Ma, *et al.*, Ta_3C_4 Nanosheets as a Novel Therapeutic Platform for Photothermal-Driven

ROS Scavenging and Immune Activation against Antibiotic-Resistant Infections in Diabetic Wounds, *Small*, 2024, **20**(36), 2400741.

40 H. Lin, S. S. Gao, C. Dai, *et al.*, A Two-Dimensional Biodegradable Niobium Carbide (MXene) for Photothermal Tumor Eradication in NIR-I and NIR-II Biowindows, *J. Am. Chem. Soc.*, 2020, **142**(23), 10567–10567.

41 Q. Xue, H. J. Zhang, M. S. Zhu, *et al.*, Photoluminescent Ti_3C_2 MXene Quantum Dots for Multicolor Cellular Imaging, *Adv. Mater.*, 2017, **29**(15), 1604847.

42 A. S. Sharbirin, S. Roy, T. T. Tran, *et al.*, Light-emitting Ti_2N (MXene) quantum dots: synthesis, characterization and theoretical calculations, *J. Mater. Chem. C*, 2022, **10**(16), 6508–6514.

43 S. Akhtar, J. Singh, T. T. Tran, *et al.*, Synthesis and optical properties of light-emitting V_2N MXene quantum dots, *Opt. Mater.*, 2023, **138**, 113660.

44 X. Yan, J. F. Ma, K. X. Yu, *et al.*, Highly green fluorescent Nb_2C MXene quantum dots for Cu^{2+} ion sensing and cell imaging, *Chin. Chem. Lett.*, 2020, **31**(12), 3173–3177.

45 S. Z. Li, J. F. Ma, X. L. Zhao, *et al.*, Highly fluorescence Ta_4C_3 MXene quantum dots as fluorescent nanoprobe for heavy ion detection and stress monitoring of fluorescent hydrogels, *Chin. Chem. Lett.*, 2022, **33**(4), 1850–1854.

46 A. V. Mohammadi, J. Rosen and Y. Gogotsi, The world of two-dimensional carbides and nitrides (MXenes), *Science*, 2021, **372**(6547), 1165–1179.

47 S. R. Ye, H. C. Zhang, H. Y. Lai, *et al.*, MXene: A wonderful nanomaterial in antibacterial, *Front. Bioeng. Biotechnol.*, 2024, **12**, 1338549.

48 K. Rasool, M. Helal, A. Ali, *et al.*, Antibacterial Activity of $Ti_3C_2T_x$ MXene, *ACS Nano*, 2016, **10**(3), 3674–3684.

49 R. P. Pandey, P. A. Rasheed, T. Gomez, *et al.*, Effect of Sheet Size and Atomic Structure on the Antibacterial Activity of Nb-MXene Nanosheets, *ACS Appl. Nano Mater.*, 2020, **3**(11), 11372–11382.

50 A. A. Shamsabadi, M. S. Gh, B. Anasori, *et al.*, Antimicrobial Mode-of-Action of Colloidal $Ti_3C_2T_x$ MXene Nanosheets, *ACS Sustainable Chem. Eng.*, 2018, **6**(12), 16586–16596.

51 K. Y. Zheng, S. Li, L. Jing, *et al.*, Synergistic Antimicrobial Titanium Carbide (MXene) Conjugated with Gold Nanoclusters, *Adv. Healthcare Mater.*, 2020, **9**(19), 2001007.

52 M. Rosales, A. Garcia, V. M. Fuenzalida, *et al.*, Unprecedented arsenic photo-oxidation behavior of few- and multi-layer $Ti_3C_2T_x$ nano-sheets, *Appl. Mater. Today*, 2020, **20**, 100769.

53 X. F. Liu, H. C. Xie, S. Zhuo, *et al.*, Ru(II) Complex Grafted $Ti_3C_2T_x$ MXene Nano Sheet with Photothermal/Photodynamic Synergistic Antibacterial Activity, *Nanomaterials*, 2023, **13**(6), 0958.

54 S. Iravani, E. N. Zare and P. Makvandi, Multifunctional MXene-Based Platforms for Soft and Bone Tissue Regeneration and Engineering, *ACS Biomater. Sci. Eng.*, 2024, **10**(4), 1892–1909.

55 Y. Fu, J. Zhang, H. Lin, *et al.*, 2D titanium carbide(MXene) nanosheets and 1D hydroxyapatite nanowires into free standing nanocomposite membrane: *in vitro* and *in vivo* evaluations for bone regeneration, *Mater. Sci. Eng., C*, 2021, **118**, 111367.

56 Z. C. Hu, J. Q. Lu, T. W. Zhang, *et al.*, Piezoresistive MXene/Silk fibroin nanocomposite hydrogel for accelerating bone regeneration by Re-establishing electrical microenvironment, *Bioact. Mater.*, 2023, **22**, 1–17.

57 L. P. Nan, Z. Lin, F. Wang, *et al.*, $Ti_3C_2T_x$ MXene-Coated Electrospun PCL Conduits for Enhancing Neurite Regeneration and Angiogenesis, *Front. Bioeng. Biotechnol.*, 2022, **10**, 850650.

58 M. Mozafari and M. Soroush, Surface functionalization of MXenes, *Mater. Adv.*, 2021, **2**(22), 7277–7307.

59 M. M. Ashebo, N. N. Liu, F. Yu, *et al.*, Surface functional modification of Nb_2CT_x MXene for high performance capacitive deionization, *Sep. Purif. Technol.*, 2024, **343**, 127125.

60 J. J. Ji, L. F. Zhao, Y. F. Shen, *et al.*, Covalent stabilization and functionalization of MXene via silylation reactions with improved surface properties, *FlatChem*, 2019, **17**, 100128.

61 H. Riazi, M. Anayee, K. Hantanasirisakul, *et al.*, Surface Modification of a MXene by an Aminosilane Coupling Agent, *Adv. Mater. Interfaces*, 2020, **7**(6), 1902008.

62 Y. Xia, T. Mathis, M. Q. Zhao, *et al.*, Thickness independent capacitance of vertically aligned liquid crystalline MXenes, *Abstr. Pap. Am. Chem. Soc.*, 2018, **256**, 409–412.

63 Y. Lei, Y. Cui, Q. Huang, *et al.*, Facile preparation of sulfonic groups functionalized Mxenes for efficient removal of methylene blue, *Ceram. Int.*, 2019, **45**(14), 17653–17661.

64 Z. Y. Jin, Y. F. Fang, X. X. Wang, *et al.*, Ultra-efficient electromagnetic wave absorption with ethanol-thermally treated two-dimensional Nb_2CT_x nanosheets, *J. Colloid Interface Sci.*, 2019, **537**, 306–315.

65 S. Kumar, Y. J. Lei, N. H. Alshareef, *et al.*, Biofunctionalized two-dimensional Ti_3C_2 MXenes for ultrasensitive detection of cancer biomarker, *Biosens. Bioelectron.*, 2018, **121**, 243–249.

66 W. Luo, H. X. Liu, X. Liu, *et al.*, Biocompatibility nanoprobe of MXene N-Ti_3C_2 quantum dot/Fe^{3+} for detection and fluorescence imaging of glutathione in living cells, *Colloids Surf., B*, 2021, **201**, 111631.

67 W. J. Zhang, S. W. Li, V. Vijayan, *et al.*, ROS- and pH-Responsive Polydopamine Functionalized $Ti_3C_2T_x$ MXene-Based Nanoparticles as Drug Delivery Nanocarriers with High Antibacterial Activity, *Nanomaterials*, 2022, **12**(24), 4392.

68 L. Chen, X. Y. Dai, W. Feng, *et al.*, Biomedical Applications of MXenes: From Nanomedicine to Biomaterials, *Acc. Mater. Res.*, 2022, **3**(8), 785–798.

69 J. Liu, H. B. Zhang, X. Xie, *et al.*, Multifunctional, Superelastic, and Lightweight MXene/Polyimide Aerogels, *Small*, 2018, **14**(45), 1802479.

70 Z. Ling, C. E. Ren, M. Q. Zhao, *et al.*, Flexible and conductive MXene films and nanocomposites with high capacitance, *Proc. Natl. Acad. Sci. U. S. A.*, 2014, **111**(47), 16676–16681.
71 F. Shahzad, M. Alhabeb, C. B. Hatter, *et al.*, Electromagnetic interference shielding with 2D transition metal carbides (MXenes), *Science*, 2016, **353**(6304), 1137–1140.
72 N. Li, X. L. Wang, Y. Liu, *et al.*, Ultrastretchable, Self-Adhesive and conductive MXene nanocomposite hydrogel for body-surface temperature distinguishing and electrophysiological signal monitoring, *Chem. Eng. J.*, 2024, **483**, 149303.
73 B. F. Guo, Y. J. Wang, C. F. Cao, *et al.*, Large-Scale, Mechanically Robust, Solvent-Resistant, and Antioxidant MXene-Based Composites for Reliable Long-Term Infrared Stealth, *Adv. Sci.*, 2024, **11**(17), 2309392.
74 B. Zhou, H. Yin, C. Dong, *et al.*, Biodegradable and Excretable 2D $W_{1.33}C_i$-MXene with Vacancy Ordering for Theory-Oriented Cancer Nanotheranostics in Near-Infrared Biowindow, *Adv. Sci.*, 2021, **8**(24), 2101043.
75 R. J. Liang, Y. S. Li, M. F. Huo, *et al.*, Triggering Sequential Catalytic Fenton Reaction on 2D MXenes for Hyperthermia-Augmented Synergistic Nanocatalytic Cancer Therapy, *ACS Appl. Mater. Interfaces*, 2019, **11**(46), 42917–42931.
76 Z. Liu, H. Lin, M. L. Zhao, *et al.*, 2D Superparamagnetic Tantalum Carbide Composite MXenes for Efficient Breast-Cancer Theranostics, *Theranostics*, 2018, **8**(6), 1648–1664.
77 C. Dai, H. Lin, G. Xu, *et al.*, Biocompatible 2D Titanium Carbide (MXenes) Composite Nanosheets for pH-Responsive MRI-Guided Tumor Hyperthermia, *Chem. Mater.*, 2017, **29**(20), 8637–8652.
78 C. Dai, Y. Chen, X. X. Jing, *et al.*, Two-Dimensional Tantalum Carbide (MXenes) Composite Nanosheets for Multiple Imaging-Guided Photothermal Tumor Ablation, *ACS Nano*, 2017, **11**(12), 12696–12712.
79 S. Q. Wen, Y. L. Xiong, S. F. Cai, *et al.*, Plasmon-enhanced photothermal properties of Au@$Ti_3C_2T_x$ nanosheets for antibacterial applications, *Nanoscale*, 2022, **14**(44), 16572–16580.
80 W. Tang, Z. Dong, R. Zhang, *et al.*, Multifunctional Two-Dimensional Core–Shell MXene@Gold Nanocomposites for Enhanced Photo–Radio Combined Therapy in the Second Biological Window, *ACS Nano*, 2019, **13**(1), 284–294.
81 J. Wang, X. Q. Wei, X. Y. Wang, *et al.*, Plasmonic Au Nanoparticle@$Ti_3C_2T_x$ Heterostructures for Improved Oxygen Evolution Performance, *Inorg. Chem.*, 2021, **60**(8), 5890–5897.
82 T. Wojciechowski, A. Rozmyslowska-Wojciechowska, G. Matyszczak, *et al.*, Ti_3C_2 MXene Modified with Ceramic Oxide and Noble Metal Nanoparticles: Synthesis, Morphostructural Properties, and High Photocatalytic Activity, *Inorg. Chem.*, 2019, **58**(11), 7602–7614.
83 H. Q. Geng, Z. J. Li, Q. Liu, *et al.*, Boosting the peroxidase-like activity of Pt nanozymes by a synergistic effect of Ti_3C_2 nanosheets for dual mechanism detection, *Dalton Trans.*, 2022, **51**(31), 11693–11702.
84 R. Yang, S. Q. Wen, S. F. Cai, *et al.*, MXene-based nanomaterials with enzyme-like properties for biomedical applications, *Nanoscale Horiz.*, 2023, **8**(10), 1333–1344.
85 L. Y. Zong, H. X. Wu, H. Lin, *et al.*, A polyoxometalate-functionalized two-dimensional titanium carbide composite MXene for effective cancer theranostics, *Nano Res.*, 2018, **11**(8), 4149–4168.
86 J. Li, Z. Li, X. Liu, *et al.*, Interfacial engineering of Bi_2S_3/$Ti_3C_2T_x$ MXene based on work function for rapid photo-excited bacteria-killing, *Nat. Commun.*, 2021, **12**(1), 1224.
87 H. Zheng, S. Q. Wang, F. Cheng, *et al.*, Bioactive anti-inflammatory, antibacterial, conductive multifunctional scaffold based on MXene@CeO_2 nanocomposites for infection-impaired skin multimodal therapy, *Chem. Eng. J.*, 2021, **424**, 130148.
88 Q. H. Yang, H. H. Yin, T. M. Xu, *et al.*, Engineering 2D Mesoporous Silica@MXene-Integrated 3D-Printing Scaffolds for Combinatory Osteosarcoma Therapy and NO-Augmented Bone Regeneration, *Small*, 2020, **16**(14), 1906814.
89 Q. Qing, X. Y. Shi, S. Z. Hu, *et al.*, Synchronously Enhanced Removal Ability and Stability of MXene through Biomimetic Modification, *Langmuir*, 2023, **39**(27), 9453–9467.
90 M. Steenackers, A. Küller, S. Stoycheva, *et al.*, Structured and Gradient Polymer Brushes from Biphenylthiol Self-Assembled Monolayers by Self-Initiated Photografting and Photopolymerization (SIPGP), *Langmuir*, 2009, **25**(4), 2225–2231.
91 P. Xiao, C. J. Wan, J. C. Gu, *et al.*, 2D Janus Hybrid Materials of Polymer-Grafted Carbon Nanotube/Graphene Oxide Thin Film as Flexible, Miniature Electric Carpet, *Adv. Funct. Mater.*, 2015, **25**(16), 2428–2435.
92 N. Tao, D. P. Zhang, X. L. Li, *et al.*, Near-infrared light-responsive hydrogels peroxide-decorated MXene-initiated polymerization, *Chem. Sci.*, 2019, **10**(46), 10765–10771.
93 J. Chen, K. Chen, D. Tong, *et al.*, CO_2 and temperature dual responsive "Smart" MXene phases, *Chem. Commun.*, 2015, **51**(2), 314–317.
94 C. Y. Ding, J. M. Liang, Z. Zhou, *et al.*, Photothermal enhanced enzymatic activity of lipase covalently immobilized on functionalized $Ti_3C_2T_x$ nanosheets, *Chem. Eng. J.*, 2019, **378**, 122205.
95 Q. Q. Qiao, J. Y. Wang, K. Long, *et al.*, A cascaded enzyme system based on the catalase-like activity of $Ti_3C_2T_x$ MXene nanosheets for the efficient combination cancer therapy, *Nano Today*, 2024, **54**, 102059.
96 J. F. Li, Z. Y. Li, X. M. Liu, *et al.*, Interfacial engineering of Bi_2S_3/$Ti_3C_2T_x$ MXene based on work function for rapid photo-excited bacteria-killing, *Nat. Commun.*, 2021, **12**(1), 1224.
97 M. Soleymaniha, M. A. Shahbazi, A. R. Rafieerad, *et al.*, Promoting Role of MXene Nanosheets in Biomedical

Sciences: Therapeutic and Biosensing Innovations, *Adv. Healthcare Mater.*, 2019, **8**(1), 1801137.

98 L. Zhou, F. M. Wu, J. H. Yu, *et al.*, Titanium carbide ($Ti_3C_2T_x$) MXene: A novel precursor to amphiphilic carbide-derived graphene quantum dots for fluorescent ink, light-emitting composite and bioimaging, *Carbon*, 2017, **118**, 50–57.

99 S. Y. Lu, L. Z. Sui, Y. Liu, *et al.*, White Photoluminescent Ti_3C_2 MXene Quantum Dots with Two-Photon Fluorescence, *Adv. Sci.*, 2019, **6**(9), 1801470.

100 Q. R. Fu, R. Zhu, J. B. Song, *et al.*, Photoacoustic Imaging: Contrast Agents and Their Biomedical Applications, *Adv. Mater.*, 2019, **31**(6), 1805875.

101 L. H. V. Wang and S. Hu, Photoacoustic Tomography: *In Vivo* Imaging from Organelles to Organs, *Science*, 2012, **335**(6075), 1458–1462.

102 V. K. Deb and U. Jain, Ti_3C_2 (MXene), an advanced carrier system: role in photothermal, photoacoustic, enhanced drugs delivery and biological activity in cancer therapy, *Drug Delivery Transl. Res.*, 2024, **14**, 3009–3031.

103 Y. L. Zhu, Z. Wang, R. X. Zhao, *et al.*, Pt Decorated $Ti_3C_2T_x$ MXene with NIR-II Light Amplified Nanozyme Catalytic Activity for Efficient Phototheranostics, *ACS Nano*, 2022, **16**(2), 3105–3118.

104 W. A. Kalender, X-ray computed tomography, *Phys. Med. Biol.*, 2006, **51**(13), R29–R43.

105 H. Lin, Y. W. Wang, S. S. Gao, *et al.*, Theranostic 2D Tantalum Carbide (MXene), *Adv. Mater.*, 2018, **30**(4), 1703284.

106 K. K. Feng, C. L. Li, R. Xiong, *et al.*, Multifunctional Theranostic 2D Vanadium Carbidel for Enhanced Cancer Immunotherapy, *Adv. Funct. Mater.*, 2024, 2406529.

107 E. Terreno, D. Delli Castelli, A. Viale, *et al.*, Challenges for Molecular Magnetic Resonance Imaging, *Chem. Rev.*, 2010, **110**(5), 3019–3042.

108 A. Sundaram, J. S. Ponraj, C. Wang, *et al.*, Engineering of 2D transition metal carbides and nitrides MXenes for cancer therapeutics and diagnostics, *J. Mater. Chem. B*, 2020, **8**(23), 4990–5013.

109 V. Neubertova, O. Guselnikova, Y. Yamauchi, *et al.*, Covalent functionalization of $Ti_3C_2T_x$ MXene flakes with Gd-DTPA complex for stable and biocompatible MRI contrast agent, *Chem. Eng. J.*, 2022, **446**, 136939.

110 G. H. Yang, J. L. Zhao, S. Z. Yi, *et al.*, Biodegradable and photostable Nb_2C MXene quantum dots as promising nanofluorophores for metal ions sensing and fluorescence imaging, *Sens. Actuators, B*, 2020, **309**, 127735.

111 Y. Zhu, Z. Wang, R. Zhao, *et al.*, Pt Decorated $Ti_3C_2T_x$ MXene with NIR-II Light Amplified Nanozyme Catalytic Activity for Efficient Phototheranostics, *ACS Nano*, 2022, **16**(2), 3105–3118.

112 B. Lu, S. Hu, D. Wu, *et al.*, Ionic liquid exfoliated $Ti_3C_2T_x$ MXene nanosheets for photoacoustic imaging and synergistic photothermal/chemotherapy of cancer, *J. Mater. Chem. B*, 2022, **10**(8), 1226–1235.

113 Z. C. Wang, H. M. Li, W. Y. She, *et al.*, 3-Bromopyruvate-Loaded Ti_3C_2 MXene/Cu_2O Nanosheets for Photoacoustic Imaging-Guided and Hypoxia-Relieving Enhanced Photothermal/Chemodynamic Therapy, *Anal. Chem.*, 2023, **95**(2), 1710–1720.

114 Y. Z. Wu, X. R. Song, W. Xu, *et al.*, NIR-Activated Multimodal Photothermal/Chemodynamic/Magnetic Resonance Imaging Nanoplatform for Anticancer Therapy by Fe(II) Ions Doped MXenes (Fe-Ti_3C_2), *Small*, 2021, **17**(33), 2101705.

115 S. Zada, W. H. Dai, Z. Kai, *et al.*, Algae Extraction Controllable Delamination of Vanadium Carbide Nanosheets with Enhanced Near-Infrared Photothermal Performance, *Angew. Chem., Int. Ed.*, 2020, **59**(16), 6601–6606.

116 X. F. Tang, Y. H. Zhu, D. L. Duan, *et al.*, Anionic Solid Solution MXene for Low-Dosage NIR-II Tumor Photothermal Therapy, *Adv. Funct. Mater.*, 2023, **33**(42), 2305965.

117 Y. H. Zhu, X. F. Tang, Q. Liu, *et al.*, Metallic Carbonitride MXene Based Photonic Hyperthermia for Tumor Therapy, *Small*, 2022, **18**(22), 2200646.

118 R. X. Zhao, Y. L. Zhu, L. L. Feng, *et al.*, Architecture of Vanadium-Based MXene Dysregulating Tumor Redox Homeostasis for Amplified Nanozyme Catalytic/Photothermal Therapy, *Adv. Mater.*, 2024, **36**(2), 2307115.

119 X. S. Li, F. Liu, D. P. Huang, *et al.*, Nonoxidized MXene Quantum Dots Prepared by Microexplosion Method for Cancer Catalytic Therapy, *Adv. Funct. Mater.*, 2020, **30**(24), 2000308.

120 P. Z. Xiong, X. D. Wei, L. Zhou, *et al.*, Near-Infrared Light-Triggered MXene Nanocomposite for Tumor-Specific Mild Photothermal-Enhanced Chemodynamic Therapy, *Adv. Funct. Mater.*, 2024, 2405124.

121 S. Zhang, L. N. Wu, W. Q. Shi, *et al.*, Nanoheterojunction Engineering Enables NIR-II-Triggered Photonic Hyperthermia and Pyroelectric Catalysis for Tumor-Synergistic Therapy, *Adv. Funct. Mater.*, 2023, **33**(29), 2302360.

122 G. Q. Li, X. Y. Zhong, X. W. Wang, *et al.*, Titanium carbide nanosheets with defect structure for photothermal-enhanced sonodynamic therapy, *Bioact. Mater.*, 2022, **8**, 409–419.

123 M. Zhang, D. Y. Yang, C. H. Dong, *et al.*, Two-Dimensional MXene-Originated Nanosonosensitizer Generation for Augmented and Synergistic Sonodynamic Tumor Nanotherapy, *ACS Nano*, 2022, **16**(6), 9938–9952.

124 G. Zhang, Y. Lu, J. Song, *et al.*, A multifunctional nano-hydroxyapatite/MXene scaffold for the photothermal/dynamic treatment of bone tumours and simultaneous tissue regeneration, *J. Colloid Interface Sci.*, 2023, **652**, 1673–1684.

125 X. K. Ju, J. Kong, G. H. Qi, *et al.*, A wearable electrostimulation-augmented ionic-gel photothermal patch doped with MXene for skin tumor treatment, *Nat. Commun.*, 2024, **15**(1), 762.

126 H.-Y. Xia, B.-Y. Li, Y.-T. Ye, *et al.*, Transition Metal Oxide-Decorated MXenes as Drugless Nanoarchitectonics for Enriched Nanocatalytic Chemodynamic Treatment, *Adv. Healthcare Mater.*, 2024, **13**(10), 2303582.

127 F. Duan, Q. Jia, G. Liang, *et al.*, Schottky Junction Nanozyme Based on Mn-Bridged Co-Phthalocyanines and $Ti_3C_2T_x$ Nanosheets Boosts Integrative Type I and II Photosensitization for Multimodal Cancer Therapy, *ACS Nano*, 2023, **17**(12), 11290–11308.

128 X. J. He, Y. Lv, Y. L. Lin, *et al.*, Platinum Nanoparticles Regulated V_2C MXene Nanoplatforms with NIR-II Enhanced Nanozyme Effect for Photothermal and Chemodynamic Anti-Infective Therapy, *Adv. Mater.*, 2024, **36**(25), 2400366.

129 X. P. Zhao, Y. Chen, R. X. Niu, *et al.*, NIR Plasmonic Nanozymes: Synergistic Enhancement Mechanism and Multi-Modal Anti-Infection Applications of MXene/MOFs, *Adv. Mater.*, 2024, **36**(8), 2307839.

130 H. C. Wang, N. Mu, Y. Q. He, *et al.*, Ultrasound-controlled MXene-based Schottky heterojunction improves anti-infection and osteogenesis properties, *Theranostics*, 2023, **13**(5), 1669–1683.

131 C. Yang, Y. Luo, H. Lin, *et al.*, Niobium Carbide MXene Augmented Medical Implant Elicits Bacterial Infection Elimination and Tissue Regeneration, *ACS Nano*, 2021, **15**(1), 1086–1099.

132 M. A. Unal, F. Bayrakdar, L. Fusco, *et al.*, 2D MXenes with antiviral and immunomodulatory properties: A pilot study against SARS-CoV-2, *Nano Today*, 2021, **38**, 101136.

133 X. A. Qiu, L. X. Nie, P. Liu, *et al.*, From hemostasis to proliferation: Accelerating the infected wound healing through a comprehensive repair strategy based on GA/OKGM hydrogel loaded with MXene@TiO_2 nanosheets, *Biomaterials*, 2024, **308**, 122548.

134 X. J. He, Y. A. Qian, C. L. Wu, *et al.*, Entropy-Mediated High-Entropy MXenes Nanotherapeutics: NIR-II-Enhanced Intrinsic Oxidase Mimic Activity to Combat Methicillin-Resistant Infection, *Adv. Mater.*, 2023, **35**(26), 2211432.

135 Y. Q. He, X. Liu, J. Lei, *et al.*, Bioactive VS_4-based sonosensitizer for robust chemodynamic, sonodynamic and osteogenic therapy of infected bone defects, *J. Nanobiotechnol.*, 2024, **22**, 31.

136 B. Li, W. Yang, R. Shu, *et al.*, Antibacterial and Angiogenic (2A) Bio-Heterojunctions Facilitate Infectious Ischemic Wound Regeneration via an Endogenous–Exogenous Bistimulatory Strategy, *Adv. Mater.*, 2024, **36**(6), 2307613.

137 X. S. Sun, X. J. He, Y. Zhu, *et al.*, Valence-switchable and biocatalytic vanadium-based MXene nanoplatform with photothermal-enhanced dual enzyme-like activities for anti-infective therapy, *Chem. Eng. J.*, 2023, **451**, 138985.

138 X. Zhou, Z. Y. Wang, Y. K. Chan, *et al.*, Infection Micromilieu-Activated Nanocatalytic Membrane for Orchestrating Rapid Sterilization and Stalled Chronic Wound Regeneration, *Adv. Funct. Mater.*, 2022, **32**(7), 2109469.

139 M. Kharaziha, A. Baidya and N. Annabi, Rational Design of Immunomodulatory Hydrogels for Chronic Wound Healing, *Adv. Mater.*, 2021, **33**(39), 2100176.

140 G. C. Gurtner, S. Werner, Y. Barrandon, *et al.*, Wound repair and regeneration, *Nature*, 2008, **453**(7193), 314–321.

141 Y. Li, J. Wang, Y. Wang, *et al.*, Advanced electrospun hydrogel fibers for wound healing, *Composites, Part B*, 2021, **223**, 109101.

142 J. Ma, S. Li, L. Zhang, *et al.*, Oxidativestress-scavenging thermo-activated MXene hydrogel for rapid repair of MRSA impaired wounds and burn wounds, *Mater. Today*, 2024, **80**, 139–155.

143 X. Q. Jiang, J. P. Ma, K. K. Xue, *et al.*, Highly Bioactive MXene-M2-Exosome Nanocomposites Promote Angiogenic Diabetic Wound Repair through Reconstructing High Glucose-Derived Immune Inhibition, *ACS Nano*, 2024, **18**(5), 4269–4286.

144 X. Yang, C. Q. Zhang, D. W. Deng, *et al.*, Multiple Stimuli-Responsive MXene-Based Hydrogel as Intelligent Drug Delivery Carriers for Deep Chronic Wound Healing, *Small*, 2022, **18**(5), 2104368.

145 Y. Li, R. Z. Fu, Z. G. Duan, *et al.*, Artificial Nonenzymatic Antioxidant MXene Nanosheet-Anchored Injectable Hydrogel as a Mild Photothermal-Controlled Oxygen Release Platform for Diabetic Wound Healing, *ACS Nano*, 2022, **16**(5), 7486–7502.

146 W. Y. Dai, R. Shu, F. Yang, *et al.*, Engineered Bio-Heterojunction Confers Extra- and Intracellular Bacterial Ferroptosis and Hunger-Triggered Cell Protection for Diabetic Wound Repair, *Adv. Mater.*, 2024, **36**(9), 2305277.

147 M. K. Li, Y. F. Zhang, L. S. Y. Lian, *et al.*, Flexible Accelerated-Wound-Healing Antibacterial MXene-Based Epidermic Sensor for Intelligent Wearable Human-Machine Interaction, *Adv. Funct. Mater.*, 2022, **32**(47), 2208141.

148 X. R. Kang, Y. Li, Z. G. Duan, *et al.*, A Mxene@TA/Fe dual-nanozyme composited antifouling hydrogel for burn wound repair, *Chem. Eng. J.*, 2023, **476**, 146420.

149 Z. T. Yang, H. Zheng, H. Y. Yin, *et al.*, Niobium carbide doped ROS/temperature dual-responsive multifunctional hydrogel for facilitating MRSA-infected wound healing, *Chem. Eng. J.*, 2023, **471**, 144634.

150 Y. N. Ding, L. Xu, S. N. Chen, *et al.*, Mxene composite fibers with advanced thermal management for inhibiting tumor recurrence and accelerating wound healing, *Chem. Eng. J.*, 2023, **459**, 141529.

151 Y. C. Gan, B. Liang, Y. Gong, *et al.*, Mxene-based mild hyperthemia microneedle patch for diabetic wound healing, *Chem. Eng. J.*, 2024, **481**, 148592.

152 X. K. Ju, J. Kong, G. H. Qi, *et al.*, Photoelectric-driven conductive composite ionogel patch for effective wound healing, *eScience*, 2024, **4**(2), 100223.

153 X. P. Chen, Y. P. Cheng and H. Wu, Recent trends in bone defect repair and bone tissue regeneration of the two-dimensional material MXene, *Ceram. Int.*, 2023, **49**(12), 19578–19594.

154 M. A. Khabisi, F. Shirini, K. Shirini, *et al.*, Additively manufactured MAX- and MXene-composite scaffolds for bone regeneration-recent advances and future perspectives, *Colloids Surf., B*, 2023, **225**, 113282.

155 H. Y. Wang, Y. C. Hsu, C. E. Wang, *et al.*, Conductive and Enhanced Mechanical Strength of $Mo_2Ti_2C_3$ MXene-Based Hydrogel Promotes Neurogenesis and Bone Regeneration in Bone Defect Repair, *ACS Appl. Mater. Interfaces*, 2024, **16**(14), 17208–17218.

156 B. Z. Huang, S. S. Li, S. M. Dai, *et al.*, $Ti_3C_2T_x$ MXene-Decorated 3D-Printed Ceramic Scaffolds for Enhancing Osteogenesis by Spatiotemporally Orchestrating Inflammatory and Bone Repair Responses, *Adv. Sci.*, 2024, 2400229.

157 K. Diedkova, A. D. Pogrebnjak, S. Kyrylenko, *et al.*, Polycaprolactone-MXene Nanofibrous Scaffolds for Tissue Engineering, *ACS Appl. Mater. Interfaces*, 2023, **15**(11), 14033–14047.

158 H. K. Pektas, Y. Demidov, A. Ahvan, *et al.*, MXene-Integrated Silk Fibroin-Based Self-Assembly-Driven 3D-Printed Theragenerative Scaffolds for Remotely Photothermal Anti-Osteosarcoma Ablation and Bone Regeneration, *ACS Mater. Au*, 2023, **3**(6), 711–726.

159 A. Maleki, M. Ghomi, N. Nikfarjam, *et al.*, Biomedical Applications of MXene-Integrated Composites: Regenerative Medicine, Infection Therapy, Cancer Treatment, and Biosensing, *Adv. Funct. Mater.*, 2022, **32**(34), 2203430.

160 Y. Chen, W. W. Liu, S. J. Wan, *et al.*, Superior Synergistic Osteogenesis of MXene-Based Hydrogel through Supersensitive Drug Release at Mild Heat, *Adv. Funct. Mater.*, 2024, **34**(2), 2309191.

161 K. Chen, Y. H. Chen, Q. H. Deng, *et al.*, Strong and biocompatible poly(lactic acid) membrane enhanced by $Ti_3C_2T_x$ (MXene) nanosheets for Guided bone regeneration, *Mater. Lett.*, 2018, **229**, 114–117.

162 J. B. Zhang, Y. Fu and A. C. Mo, Multilayered Titanium Carbide MXene Film for Guided Bone Regeneration, *Int. J. Nanomed.*, 2019, **14**, 10091–10102.

163 Y. Fu, J. B. Zhang, H. Lin, *et al.*, 2D titanium carbide (MXene) nanosheets and 1D hydroxyapatite nanowires into free standing nanocomposite membrane: *in vitro* and *in viv*o, evaluations for bone regeneration, *Mater. Sci. Eng., C*, 2021, **118**, 111367.

164 Z. M. Xu, Y. X. Zhang, H. Y. Dai, *et al.*, 3D printed MXene (Ti_2AlN)/polycaprolactone composite scaffolds for maxillofacial bone defect repair, *J. Ind. Eng. Chem.*, 2022, **114**, 536–548.

165 J. H. Yin, S. S. Pan, X. Guo, *et al.*, Nb_2C MXene-Functionalized Scaffolds Enables Osteosarcoma Phototherapy and Angiogenesis/Osteogenesis of Bone Defects (vol 13, 30, 2021), *Nano-Micro Lett.*, 2022, **14**, 30.

166 K. Diedkova, A. D. Pogrebnjak, S. Kyrylenko, *et al.*, Polycaprolactone–MXene Nanofibrous Scaffolds for Tissue Engineering, *ACS Appl. Mater. Interfaces*, 2023, **15**(11), 14033–14047.

167 G. N. Zhang, Y. Lu, J. B. Song, *et al.*, A multifunctional nano-hydroxyapatite/MXene scaffold for the photothermal/dynamic treatment of bone tumours and simultaneous tissue regeneration, *J. Colloid Interface Sci.*, 2023, **652**, 1673–1684.

168 S. S. Pan, J. H. Yin, L. D. Yu, *et al.*, 2D MXene-Integrated 3D-Printing Scaffolds for Augmented Osteosarcoma Phototherapy and Accelerated Tissue Reconstruction, *Adv. Sci.*, 2020, **7**(2), 1901511.

169 X. Mi, Z. Y. Su, Y. Fu, *et al.*, 3D printing of Ti_3C_2-MXene-incorporated composite scaffolds for accelerated bone regeneration, *Biomed. Mater.*, 2022, **17**(3), 035002.

170 R. Nie, Y. Sun, H. X. Lv, *et al.*, 3D printing of MXene composite hydrogel scaffolds for photothermal antibacterial activity and bone regeneration in infected bone defect models, *Nanoscale*, 2022, **14**(22), 8112–8129.

171 J. Zhao, T. H. Wang, Y. C. Zhu, *et al.*, Enhanced osteogenic and ROS-scavenging MXene nanosheets incorporated gelatin-based nanocomposite hydrogels for critical-sized calvarial defect repair, *Int. J. Biol. Macromol.*, 2024, **269**, 131914.

172 H. Zheng, Z. T. Yang, L. Zhou, *et al.*, Bioactive Nb_2C MXene-Functionalized Hydrogel with Microenvironment Remodeling and Enhanced Neurogenesis to Promote Skeletal Muscle Regeneration and Functional Restoration, *Small*, 2024, 2310483.

173 D. K. Song, G. Ye, Y. Zhao, *et al.*, An All-in-One, Bioderived, Air-Permeable, and Sweat-Stable MXene Epidermal Electrode for Muscle Theranostics, *ACS Nano*, 2022, **16**(10), 17168–17178.

174 M. Garai, M. Mahato, S. Nam, *et al.*, Metal Organic Framework-MXene Nanoarchitecture for Fast Responsive and Ultra-Stable Electro-Ionic Artificial Muscles, *Adv. Funct. Mater.*, 2023, **33**(10), 2212252.

175 X. Y. Ren, M. Xiao, J. Yang, *et al.*, Injectable MXene conductive hydrogel improves myocardial infarction through scavenging ROS and repairing myocardium electrical integrity, *Chem. Eng. J.*, 2024, **481**, 148791.

176 W. H. Chooi and S. Y. Chew, Modulation of cell-cell interactions for neural tissue engineering: Potential therapeutic applications of cell adhesion molecules in nerve regeneration, *Biomaterials*, 2019, **197**, 327–344.

177 J. Zou, J. Wu, Y. Z. Wang, *et al.*, Additive-mediated intercalation and surface modification of MXene, *Chem. Soc. Rev.*, 2022, **51**(8), 3314–3314.

178 Z. L. Wang, Y. Zheng, L. Qiao, *et al.*, 4D-Printed MXene-Based Artificial Nerve Guidance Conduit for Enhanced Regeneration of Peripheral Nerve Injuries, *Adv. Healthcare Mater.*, 2024, 2401093.

179 Y. D. Zhu, X. Y. Ma, L. P. Li, *et al.*, Surface Functional Modification by $Ti_3C_2T_x$ MXene on PLLA Nanofibers for Optimizing Neural Stem Cell Engineering, *Adv. Healthcare Mater.*, 2023, **12**(25), 2370149.

180 X. X. Han, J. Huang, H. Lin, *et al.*, 2D Ultrathin MXene-Based Drug-Delivery Nanoplatform for Synergistic

Photothermal Ablation and Chemotherapy of Cancer, *Adv. Healthcare Mater.*, 2018, **7**(9), 1701394.
181 P. P. He, X. X. Du, Y. Cheng, *et al.*, Thermal-Responsive MXene-DNA Hydrogel for Near-Infrared Light Triggered Localized Photothermal-Chemo Synergistic Cancer Therapy, *Small*, 2022, **18**(40), 2200263.
182 Q. U. Zahra, S. Ullah, F. Shahzad, *et al.*, MXene-based aptasensors: Advances, challenges, and prospects, *Prog. Mater. Sci.*, 2022, **129**, 100967.
183 U. Amara, I. Hussain, M. Ahmad, *et al.*, 2D MXene-Based Biosensing: A Review, *Small*, 2023, **19**(2), 2205249.
184 X. Lin, D. Song, T. Shao, *et al.*, A Multifunctional Biosensor via MXene Assisted by Conductive Metal–Organic Framework for Healthcare Monitoring, *Adv. Funct. Mater.*, 2024, **34**(11), 2311637.
185 J. Liu, X. T. Jiang, R. Y. Zhang, *et al.*, MXene-Enabled Electrochemical Microfluidic Biosensor: Applications toward Multicomponent Continuous Monitoring in Whole Blood, *Adv. Funct. Mater.*, 2019, **29**(6), 1807326.
186 G. L. Ye, Z. B. Wen, F. Wen, *et al.*, Mussel-inspired conductive Ti_2C-cryogel promotes functional maturation of cardiomyocytes and enhances repair of myocardial infarction, *Theranostics*, 2020, **10**(5), 2047–2066.
187 G. A. Asaro, M. Solazzo, M. Suku, *et al.*, MXene functionalized collagen biomaterials for cardiac tissue engineering driving iPSC-derived cardiomyocyte maturation, *npj 2D Mater. Appl.*, 2023, **7**, 44.
188 W. Yang, L. Wang, L. Fan, *et al.*, Photothermal Responsive Microcarriers Encapsulated With Cangrelor and 5-Fu for Colorectal Cancer Treatment, *Small Methods*, 2024, **8**(7), 2301002.